Impact de l'IRM multimodale dans la prise en charge des AVC ischémiques à la phase aigüe

Alexandre Bani-Sadr

THESE de DOCTORAT DE
L'UNIVERSITE CLAUDE BERNARD LYON 1

Ecole Doctorale N° accréditation 205
École Doctorale Interdisciplinaire Science-Santé

Discipline : Sciences de la vie, biologie, santé

Soutenue publiquement le 19/09/2023, par :
Alexandre Bani-Sadr

Impact de l'IRM multimodale dans la prise en charge des AVC ischémiques à la phase aigüe

---

Devant le jury composé de :

Wiart, Marlène	Directrice de Recherche CNRS / Université Claude Bernard Lyon I	Présidente
Boutet, Claire	Professeure des Universités - Praticienne Hospitalière / Université Jean Monnet	Rapporteure
Edjlali-Goujon, Myriam	Professeure des Universités - Praticienne Hospitalière / Université Paris Saclay	Rapporteure
Cotton, François	Professeur des Universités - Praticien Hospitalier / Université Claude Bernard Lyon I	Examinateur
Cuenod, Charles-André	Professeur des Universités - Praticien Hospitalier / Université Paris Cité	Examinateur
Nighoghossian, Norbert	Professeur Émérite des Universités / Université Claude Bernard Lyon I	Examinateur
Oppenheim, Catherine	Professeure des Universités- Praticienne Hospitalière / Université Paris Cité	Examinatrice
Berthezène, Yves	Professeur des Universités - Praticien Hospitalier / Université Claude Bernard Lyon I	Directeur de thèse

UNIVERSITE CLAUDE BERNARD LYON I

Président de l'Université	Frédéric FLEURY
Président du Conseil Académique et de la Commission Recherche	Hamda BEN HADID
Vice-Président du Conseil d'Administration	Didier REVEL
Vice-Présidente de la Commission Formation	Céline BROCHIER
Vice-Président Relations Hospitalo-Universitaires	Jean François MORNEX
Directeur général des services	Pierre ROLLAND

SECTEUR SANTE

Doyen de l'UFR de Médecine Lyon-Est	Gilles RODE
Doyen de l'UFR de Médecine et de Maïeutique Lyon Sud - Charles Mérieux	Philippe PAPAREL
Doyen de l'Institut des Sciences Pharmaceutiques et Biologiques (ISPB)	Claude DUSSART
Doyen de l'UFR d'Odontologie	Jean-Christophe MAURIN
Directeur de l'Institut des Sciences & Techniques de Réadaptation (ISTR)	Jacques LUAUTÉ
Présidente du Comité de Coordination des Études Médicales	Carole BURILLON

SECTEUR SCIENCES ET TECHNOLOGIE

Directrice de l'UFR Biosciences	Kathrin GIESELER
Directeur de l'UFR Faculté des Sciences	Bruno ANDRIOLETTI
Directeur de l'UFR Sciences & Techniques des Activités Physiques et Sportives (STAPS)	Guillaume BODET
Directeur de Polytech Lyon	Emmanuel PERRIN
Directeur de l'Institut Universitaire de Technologie Lyon 1 (IUT)	Michel MASSENZIO
Directeur de l'Institut des Science Financière & Assurances (ISFA)	Nicolas LEBOISNE

30 septembre 2022

REMERCIEMENTS

Aux rapporteures de ce travail,

Madame le Professeur Claire Boutet, nous vous remercions d'avoir accepté d'être rapporteure de ce travail ciblé sur l'apport de l'IRM à la phase aigüe de l'AVC ischémique. Soyez assurée de notre respectueuse considération.

Madame le Professeur Myriam Edjlali-Goujon, nous sommes très honorés de vous compter parmi nos juges et de soumettre ce travail à votre analyse. Avec nos sentiments les plus respectueux.

Aux examinateurs de ce travail,

Monsieur le Professeur François Cotton, nous sommes très honorés de vous compter parmi nos juges. Cette thèse sur l'imagerie de l'AVC ischémique à la phase aigüe témoigne de notre intérêt commun pour la neuroradiologie.

Monsieur le Professeur Charles-André Cuenod, nous vous remercions sincèrement d'avoir accepté d'être membre de ce jury. Votre expertise en imagerie de perfusion est reconnue par tous.

Monsieur le Professeur Norbert Nighoghossian, nous sommes ravis de vous compter parmi nos juges. Vous nous avez fourni le matériel et avez suivi de près l'avancement de notre travail de thèse. Votre rigueur scientifique, vos encouragements et vos conseils ont permis à ce travail d'aboutir. Soyez assuré de notre profonde gratitude.

Madame le Professeur Catherine Oppenheim, nous sommes très honorés que vous ayez accepté d'être membre de notre jury. Vos travaux sur l'imagerie de l'AVC ischémique sont une référence pour nous.

Madame le Docteur Marlène Wiart, nous vous remercions vivement d'avoir accepté d'être membre sur ce jury. Vos encouragements pendant les comités de suivi de thèse ont été très utiles.

Au directeur de ce travail,

Monsieur le Professeur Yves Berthezène, nous vous remercions vivement pour votre encadrement et vos encouragements notamment lors des multiples obstacles qui ont émaillés ce travail de thèse. Soyez assuré de notre profonde gratitude.

A mes collègues de Neuroradiologie (Marc Hermier, Roxana Ameli, Omer Eker, Matteo Cappucci, Roberto Riva, Morgane Laubacher) et aux équipes de Neurologie Vasculaire des Professeurs Nighoghossian et Cho (Laura Mechtouff que je remercie particulièrement pour avoir fourni les données biologiques, Laurent Derex pour ses précieux conseils et son esprit de camaraderie, Elodie Ong, Lucie Rascle et Julia Fontaine pour leur bonne humeur). C'est un plaisir de travailler avec vous. Ce travail n'aurait pas pu être possible sans vous.

A toute ma famille et mes amis pour leur soutien, leur patience et leur exemplarité. Vous êtes une source d'inspiration quotidienne.

RESUME

L'imagerie cérébrale joue un rôle crucial chez les patients victimes d'un accident vasculaire cérébral (AVC). L'avènement de la thrombectomie mécanique a bouleversé la prise en charge des patients atteints d'AVC ischémique et par conséquent la place de l'IRM à la phase aigüe. Notre travail de thèse se propose d'étudier l'apport de l'IRM multimodale dans la prise en charge de l'AVC ischémique à la phase aigüe.

Dans cette perspective, nous avons couplé l'analyse des IRM d'admission de la cohorte HIBISCUS-STROKE (CoHort of Patients to Identify Biological and Imaging markerS of CardiovascUlar Outcomes in Stroke) au devenir fonctionnel, au volume final de l'infarctus et à la dynamique des marqueurs sériques de l'inflammation.

Dans la première partie de notre travail, nous avons examiné l'apport de l'IRM dans la sélection des patients éligibles à une thrombectomie mécanique. Nous avons observé que les techniques d'angio-IRM étaient inférieures à l'artériographie cérébrale dans la localisation de l'occlusion intracrânienne malgré la prise en compte du caractère migratoire du thrombus. Nous avons montré que l'estimation du volume de la pénombre ischémique variait substantiellement selon le logiciel de post-traitement utilisé et que ces différences pouvaient impacter la sélection des patients éligibles à une thrombectomie mécanique. Dans une étude pilote, nous avons observé que les paramètres optimaux définissant le trouble de perfusion variaient selon le logiciel utilisé.

Dans la deuxième partie de notre travail, nous avons évalué l'apport pronostic de l'IRM chez les patients ayant bénéficié d'une recanalisation efficace après thrombectomie mécanique. Nous avons observé que le « brush sign » était associé à une croissance >11.6mL du volume de l'infarctus et que des hypersignaux FLAIR vasculaires peu étendus étaient associés à un moins bon résultat fonctionnel à 3 mois.

Dans la troisième partie de notre travail, nous avons examiné les relations entre la perméabilité de la barrière hémato-encéphalique sur l'IRM d'admission et la réponse neuroinflammatoire. Sur la population totale, nous avons montré qu'une perméabilité accrue de la barrière hémato-encéphalique était associée à un volume plus important de l'infarctus sur la population totale. Chez les patients à moins de 6h du début des symptômes, nous avons observé qu'une perméabilité accrue était associée à un volume plus important de l'infarctus et à des taux sériques plus importants de métalloprotéase matricielle 9.

La cohorte HIBISCUS-STROKE nous a donc permis de préciser l'apport de l'IRM dans la sélection et le pronostic des patients et d'identifier les facteurs associés à une augmentation de la perméabilité de la barrière hémato-encéphalique à la phase aigüe.

Mots-clés : IRM ; angio-IRM ; IRM de perfusion ; Infarctus cérébral ; Thrombectomie mécanique ; Lésions d'ischémie-reperfusion ; métalloprotéase matricielle 9

ABSTRACT

Cerebral imaging plays a crucial role in stroke patients. The advent of mechanical thrombectomy has transformed the management of acute ischemic stroke (AIS) patients, and consequently the role of MRI in the acute phase. Here, we propose to study the contribution of multimodal MRI to the management of AIS.

To this end, we have coupled the analysis of admission MRI from the HIBISCUS-STROKE (CoHort of Patients to Identify Biological and Imaging markerS of CardiovascUlar Outcomes in Stroke) cohort with functional outcome, final infarct volume and the dynamics of serum markers of inflammation.

In the first part of our work, we examined the contribution of MRI to the selection of patients eligible for mechanical thrombectomy. We observed that MRI angiography techniques were inferior to cerebral arteriography in localizing intracranial occlusion, despite taking into account the migratory nature of the thrombus. We showed that the estimation of the volume of the ischemic penumbra varied substantially according to the post-processing software used, and that these differences could have an impact on the selection of patients eligible for mechanical thrombectomy. In a pilot study, we observed that the optimal parameters defining the volumes of perfusion defect varied according to the software used.

In the second part of our work, we assessed the prognostic contribution of MRI in patients who had achieved successful recanalization after mechanical thrombectomy. We observed that “brush sign” was associated with >11.6mL growth in infarct volume, and that mild vascular FLAIR hypersignals were associated with poorer functional outcome at 3 months.

In the third part of our work, we examined the relationships between blood-brain barrier permeability on admission MRI and neuroinflammatory response. In the total population, we showed that increased blood-brain barrier permeability was associated with greater infarct volume. In patients within 6 hours of the onset of symptoms, we observed that increased permeability was associated with larger infarct volume and higher serum levels of matrix metalloprotease 9.

The HIBISCUS-STROKE cohort gave us the opportunity to assess the contribution of MRI to patient selection and prognosis, and to identify factors associated with increased blood-brain barrier permeability in the acute phase.

Keywords: MRI; angio-MRI; perfusion MRI; cerebral infarction; mechanical thrombectomy; ischemia-reperfusion lesions; matrix metalloprotease 9

TABLES DES MATIERES

LISTE DES ABBREVIATIONS

ADC : Apparent Diffusion Coefficient
ARM-CE : Angio-IRM des troncs supra-aortiques avec injection
ARM-TOF: Angio-IRM Time-of-Flight
AVC: Accident Vasculaire Cérébral
ASPECTS: Alberta Stroke Program Early CT Score
BHE : Barrière Hémato-Encéphalique
CBF : Cerebral Blood Flow
CBV: Cerebral Blood Volume
CRP: C Reactive Protein
IRM-DCE: Dynamic Contrast-Enhanced IRM
IRM-DSC: Dynamic Susceptibility-Contrast IRM
DWI: Diffusion Weighted-Imaging
FLAIR: Fluid-Attenuated Inversion Recovery
HARM: HyperAcute Reperfusion Marker
HIBISCUS-STROKE: Cohort of Patients to Identify Biological and Imaging markerS of CardiovascUlar Outcomes in Stroke
IL : Interleukine
IRM : Imagerie par Résonance Magnétique
MCP-1 : Monocyte Chemoattractant Protein-1
MMP : Matrix Metalloprotéase
mRS: modified Rankin Scale
mTICI: modified Treatment in Cerebral Infarction
NIHSS: National Institutes of Health Stroke Scale
sST2: soluble form of suppression of tumorigenicity 3
Tmax: Time-To-Maximum
TNF-R1: Tumor Necrosis Factor Receptor 1
VCAM-1 : Vascular Cell Adhesion Protein 1

PREAMBULE

Ce travail s'inscrit dans le projet de recherche hospitalo-universitaire MARVELOUS (ANR-16-RHUS-0009) de l'Université de Lyon. L'ensemble des données analysées sont issues de la cohorte HIBISCUS-STROKE (Cohort of Patients to Identify Biological and Imaging markerS of CardiovascUlar Outcomes in Stroke ; NCT : 05263804) qui a inclus des patients hospitalisés dans l'unité de soins intensifs neurovasculaires de l'hôpital Neurologique et Neurochirurgical Pierre Wertheimer (Hospices Civils de Lyon) pour un AVC ischémique traité par thrombectomie mécanique. Les patients inclus dans cette cohorte bénéficiaient d'une IRM multimodale d'admission, d'une analyse dynamique des marqueurs biologiques de l'inflammatoire et d'une IRM de suivi permettant de quantifier la lésion ischémique finale. L'objectif de la cohorte était de déterminer les valeurs pronostiques de l'IRM multimodale, des marqueurs biologiques et de caractériser leurs relations.

INTRODUCTION : ELEMENTS BIBLIOGRAPHIQUES

CHAPITRE 1 : L'infarctus cérébral.

1.1 Généralités.

Les accidents vasculaires cérébraux (AVC) constituent un problème majeur de santé publique. En 2019, les AVC demeuraient la seconde cause de mortalité dans le monde après les cardiopathies ischémiques avec 12.22 millions de cas incidents et représentaient la troisième cause combinée de handicap acquis chez l'adulte et de mortalité [1]. L'infarctus cérébral ou AVC ischémique représentait la principale cause d'AVC avec 7.63 millions de cas incidents [1]. L'infarctus cérébral est défini comme une dysfonction neurologique persistante pendant au moins 24 heures avec des preuves d'ischémie cérébrale aigue sur l'imagerie ou l'anatomopathologie [2]. Les principales étiologies de l'infarctus cérébral regroupent l'athérosclérose des artères cervicales, l'athérosclérose des artères intracrâniennes, la microangiopathie et les dissections artérielles. Les facteurs de risque d'AVC ischémique sont principalement l'hypertension artérielle, la dyslipidémie et les cardiopathies tel que la fibrillation atriale [1].

1.2 Physiopathologie de l'AVC ischémique

1.2.1 L'occlusion artérielle intracrânienne et ses conséquences hémodynamiques :

L'occlusion artérielle est responsable d'une réduction de la perfusion du parenchyme cérébral conduisant à l'infarctus cérébral. A la fin des années 70, des études électrophysiologiques ont permis de démontrer la coexistence de trois compartiments tissulaires distincts [3,4] :

- **Le noyau ischémique** correspondant à un tissu cérébral irréversiblement nécrosé et survenant suite à une réduction très sévère du débit sanguin cérébral.
- **La pénombre ischémique** correspondant à un tissu cérébral en état de sidération fonctionnelle mais non nécrosé et potentiellement viable en cas reperfusion. Ce tissu est le siège d'une réduction plus modéré du débit sanguin cérébral.
- **L'oligémie** correspondant un tissu cérébral hypoperfusé mais fonctionnel et non à risque de nécrose en l'absence de reperfusion.

Historiquement, la tomographie par émission de positons à l'^{15}O a été la première technique d'imagerie à imager la pénombre ischémique et à définir son profil hémodynamique par [5-7] :

- Un débit sanguin cérébral abaissé entre 7-8.5mL/100g/min et 17-22mL/100g/min
- Une consommation d'oxygène relativement préservée
- Une augmentation de la fraction d'extraction de l'oxygène (>70%)

1.2.2 Les collatérales, le temps et le devenir du tissu cérébral :

En l'absence de reperfusion, la pénombre ischémique est « consommée » et rejoint le noyau ischémique. La vitesse de propagation du noyau ischémique vers la pénombre est hautement variable d'un sujet à un autre [8]. Près de 25% des sujets présentant un AVC ischémique par occlusion proximale de la circulation antérieure sont dits « progresseurs rapides » et se présentent avec un noyau ischémique très étendu malgré une prise en charge hospitalière précoce [9]. A l'inverse, d'autres patients dit « progresseurs lents » peuvent conserver une pénombre ischémique substantielle jusqu'à 48h [10,11]. L'élément déterminant supposé de cette hétérogénéité inter-individuelle est la qualité de la circulation collatérale cérébrale c'est-à-dire un réseau vasculaire ancillaire stabilisant le débit sanguin cérébral lorsque l'artère principale est occluse [12]. Une circulation collatérale adéquate peut contribuer à maintenir la viabilité de la pénombre ischémique en l'absence de reperfusion [13]. Le recrutement et le maintien de ces réseaux anastomotiques notamment leptoméningés dépend de l'âge, du sexe, de la glycémie et du siège de l'occlusion artérielle [14]. D'autre facteurs comme les comorbidités cardio-pulmonaires, la configuration anatomique vasculaire cérébrale et la génétique entrent également en jeu [15,16].

1.2.3 Les conséquences de l'infarctus sur l'unité neurovasculaire :

La barrière hémato-encéphalique (BHE) est une interface dynamique importante entre le système vasculaire et le système nerveux centrale. Elle régule l'homéostasie ionique du système nerveux central et protège les tissus neuronaux de substances potentiellement toxiques et d'agents pathogènes en contrôlant l'entrée des nutriments et la sortie des déchets [17]. En règle générale, la BHE se réfère principalement à l'endothélium du système vasculaire. Son développement et son maintien impliquent, outre les jonctions intercellulaires endothéliales et les jonctions serrées, les péricytes, les astrocytes, les neurones et la matrice extracellulaire. Ce groupement cellulaire fonctionnel est appelé l'unité neurovasculaire [18].

Le parenchyme cérébral est un important consommateur d'oxygène et de glucose. Suite à la baisse du débit sanguin cérébral, il existe un défaut d'apport en oxygène et de glucose qui se traduit, à l'échelle cellulaire, en un arrêt des pompes sodium-potassium ($Na+/K^+$ ATPase) et calcium (Ca^{2+} ATPase). Une accumulation intracellulaire de sodium survient et provoque un gonflement osmotique des cellules ou œdème cytotoxique [19]. Ce phénomène peut être détecté par la diminution du coefficient de diffusion apparent (ADC) de l'eau qui se traduit par une augmentation du signal tissulaire en IRM de diffusion (DWI) [20]. A ce stade, la BHE est principalement intacte [21]. Sur le versant vasculaire, les troubles ioniques induisent un gonflement des cellules endothéliales qui est responsable d'une altération des jonctions serrées puis d'une une rupture [21]. Le dysfonctionnement des mitochondries conduit au relargage d'espèces réactives de l'oxygène comme les anions superoxydes dégradant également la BHE [21]. Conséquence de la lésion ischémique, la rupture de la BHE contribue à son extension en autorisant le passage de macromolécules du système vasculaire vers le système nerveux central [22]. Elle est associée à la survenue d'un œdème vasogénique, d'une transformation hémorragique et à un pronostic fonctionnel péjoratif [23-27]. En outre, il est supposé qu'elle joue un rôle déterminant dans la survenue des lésions d'ischémie-reperfusion après traitement de reperfusion [28,29].

1.2.4 L'évolution de la barrière hémato-encéphalique :

Historiquement, on pensait que la rupture de la BHE survenait à la phase subaigüe de l'AVC ischémique. Sur l'imagerie, elle était le plus souvent objectivée sous la forme d'un réhaussement gyriforme [30]. Dès 2004, Warach et Latour ont démontré que la rupture de la BHE survenait, chez certains patients, quelques heures après l'administration d'une thrombolyse intraveineuse, sous la forme d'un réhaussement des espaces sous-arachnoïdiens sur l'IRM en pondération Fluid-Attenuated Inversion Recovery (FLAIR) [29]. Ces observations ont conduit à proposer un modèle perméabilité de la BHE biphasique avec une première ouverture à 6h, une fermeture et une deuxième ouverture entre 72 et 96h [21]. Actuellement, la littérature suggère plutôt une dynamique plus continue avec deux pics de perméabilité sans fermeture intermédiaire [21,28,31-34]. Une première ouverture a été documentée chez l'homme dans les 6 heures après l'occlusion artérielle [35-37]. Durant les 72h suivantes, la réponse neuroinflammatoire participe à l'augmentation de la perméabilité et le second pic est observé [28,31,33,38].

Figure 1 : Dynamique présumée de la perméabilité de la BHE au cours de l'AVC ischémique

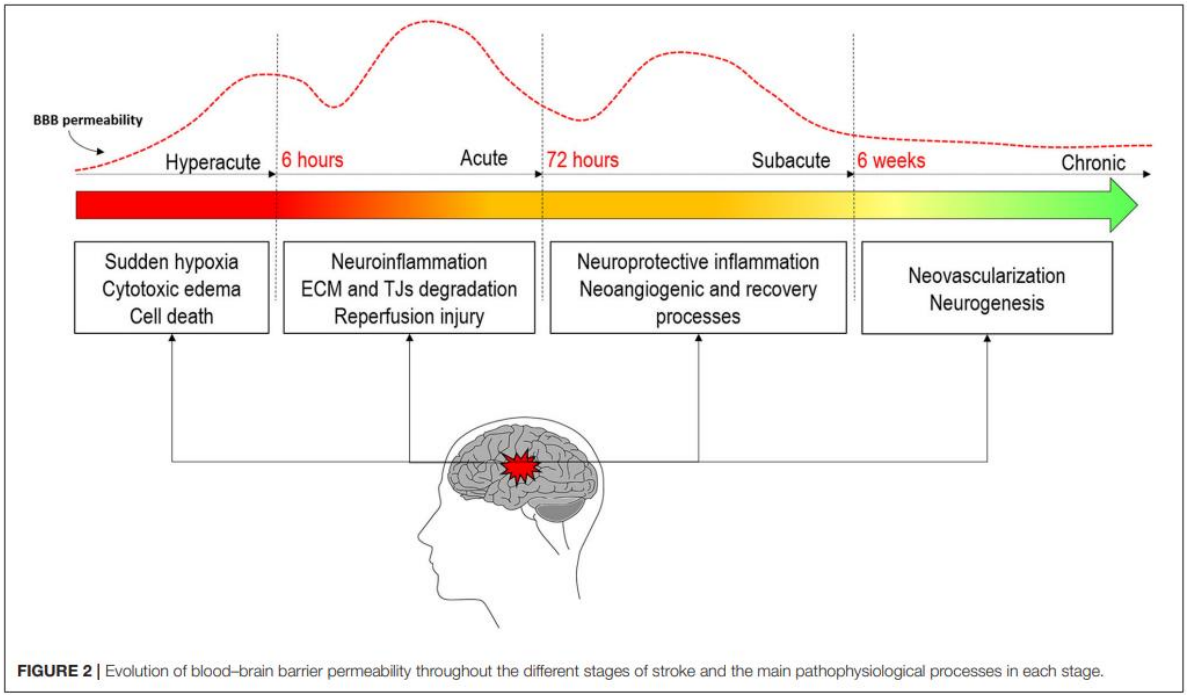

FIGURE 2 | Evolution of blood–brain barrier permeability throughout the different stages of stroke and the main pathophysiological processes in each stage.

Cette figure illustre la dynamique présumée de la perméabilité de la BHE au cours l'AVC ischémique, d'après Bernardo-Castro et al [21].

1.2.5 Les mécanismes impliqués dans la rupture de la barrière hémato-encéphalique :

Outre les troubles ioniques, la rupture de la BHE obéit à un processus physiopathologique complexe qui implique d'autres facteurs dont :

- **Le stress oxydatif** : le dysfonctionnement mitochondrial survient peu après l'occlusion vasculaire et induit un excès de production d'espèces réactives de l'oxygène lésant directement les cellules endothéliales et participant ainsi à la formation de l'œdème vasogénique [39].
- **Les métalloprotéases matricielles (MMP)** : cette famille enzymatique regroupe des protéases dépendantes du zinc qui sont rapidement exprimées par la microglie, les astrocytes et les leucocytes au décours de l'accident ischémique. Elles dégradent directement la membrane basale et les protéines constitutives des jonctions serrées [39].
- **Les médiateurs inflammatoires relargués par la microglie et les cellules immunitaires périphérique** : la nécrose cellulaire induit de la libération de multiples molécules déclenchant une cascade neuroinflammatoire qui implique notamment des cytokines pro-inflammatoires dont la famille des interleukines et du TNF-α. Cette cascade

conduit à une activation de la microglie et au recrutement de cellules immunitaires périphériques dont les polynucléaires neutrophiles et les lymphocytes T [39].

1.3 Stratégies thérapeutiques actuelles dans l'infarctus cérébral

Outre une hospitalisation en unité de soins intensifs neurovasculaires, la stratégie thérapeutique actuelle repose sur les traitements de reperfusion.

1.3.1 La thrombolyse intraveineuse

L'efficacité clinique de la thrombolyse intraveineuse par alteplase a été démontrée en 1995 dans l'essai contrôlé randomisé du « National Institute of Neurological Disorders and stroke rt-PA » chez des patients sélectionnés par scanner cérébral sans injection et dans un délai de 3 heures après l'apparition des symptômes [40]. En 2008, l'essai contrôlé randomisé ECASS 3 a démontré l'efficacité clinique de la thrombolyse intraveineuse jusqu'à 4h30 après le début des symptômes [41]. L'étude WAKE-UP a ensuite permis d'élargir les indications de thrombolyse intraveineuse aux patients présentant un déficit neurologique d'horaire inconnu si l'IRM n'objectivait pas d'œdème vasogénique (mismatch DWI-FLAIR) [42]. Plus récemment, la notion de fenêtre tissulaire s'est substituée à la notion de fenêtre temporelle. L'étude EXTEND a démontré un bénéfice à la thrombolyse intraveineuse jusqu'à 9h après le début des symptômes chez des patients présentant, sur l'imagerie, une pénombre ischémique substantielle définie par un rapport entre le volume d'hypoperfusion et le volume du noyau ischémique d'au moins à 1,2, une différence d'au moins 10mL et un volume du noyau ischémique inférieur à 70mL [43]. Néanmoins, l'apport de la thrombolyse intraveineuse est limité par la survenue de complications hémorragiques dans 6 à 8% des cas et une efficacité moindre pour les occlusions proximales [44,45].

1.3.2 La thrombectomie mécanique

En complément de la thrombolyse intraveineuse, la thrombectomie mécanique a été proposée pour lever les occlusions artérielles intracrâniennes proximales. Cette procédure consiste à naviguer par voie endovasculaire jusqu'au site d'occlusion artérielle puis de réaliser une ablation du thrombus au moyen d'un stent retriever et/ou d'une thromboaspiration sous contrôle radiologique. Les premiers essais cliniques randomisés ont démontré l'efficacité de la thrombectomie mécanique jusqu'à 6 heures après le début des symptômes chez les patients présentant une occlusion artérielle proximale [46-48]. Une méta-analyse démontrait que la thrombectomie mécanique évitait la perte d'autonomie pour un patient sur cinq [49]. Par la suite, le bénéfice de la thrombectomie mécanique a été démontré pour les AVC ischémiques à présentation tardive jusqu'à 24 heures après le début des symptômes lorsque l'imagerie

objectivait une pénombre ischémique substantielle [50,51]. De même que la thrombolyse intraveineuse, la thrombectomie mécanique est limitée par des complications hémorragiques avec un taux estimé entre 2 et 7% [52]. En outre, près de 25 à 54% des patients présentent une recanalisation dite futile c'est-à-dire une évolution clinique défavorable définie par un score modifié de Rankin (mRS) ≥ 2 malgré une thrombectomie réussie (score de reperfusion de thrombolyse modifié dans l'infarctus cérébral (mTICI) ≥ 2B) [49,53,54]. Le rôle des lésions d'ischémie-reperfusion est suspecté [55,56].

CHAPITRE 2 : L'apport de l'imagerie dans l'infarctus cérébral à la phase aigüe.

Bien que la tomographie par émission de positons à l'^{15}O soit toujours l'examen de référence pour l'imagerie de la pénombre ischémique, sa faible accessibilité en urgence et la logistique requise ont conduit au développement de l'IRM multimodale et du scanner multimodal.

2.1 L'IRM multimodale :

L'IRM T2* permet d'exclure le diagnostic d'hémorragie cérébrale avec une sensibilité similaire au scanner proche de 100% [57,58]. L'IRM de diffusion est considérée comme la méthode la plus fiable pour identifier le noyau ischémique avec un sensibilité de 83% contre 26% pour le scanner [58]. Chez les patients présentant un horaire de début des symptômes inconnu, la séquence FLAIR conditionne l'administration de la thrombolyse intraveineuse en objectivant ou non l'œdème vasogénique [42]. L'angio-IRM (angio-IRM Time-of-Flight (ARM-TOF) et/ou l'angio-IRM des troncs supra-aortiques avec injection (ARM-CE) permettent de documenter une occlusion artérielle intracrânienne conditionnant une thrombectomie mécanique. Pour les AVC de présentation tardive, l'IRM de perfusion donne une estimation du débit sanguin cérébral dont le mismatch avec l'IRM de diffusion permet d'estimer le volume de la pénombre ischémique [59]. Néanmoins, l'évaluation de la pénombre ischémique en IRM est dépendante de l'exploitation des données natives de l'IRM de perfusion. L'estimation des volumes du trouble de perfusion présente des variations substantielles en fonction de la méthode de calcul et du paramètre hémodynamique choisi [60]. Enfin, l'IRM multimodale est la technique de référence dans le diagnostic des autres pathologies cérébrales de révélation pseudo-vasculaire (stroke-mimics) [58,61].

2.2 Le scanner :

Le scanner est une alternative à l'IRM et présente certains avantages dont une plus large disponibilité et des temps d'acquisitions plus courts. Pour les AVC de moins de 4h30, le scanner permet d'éliminer l'hémorragie cérébrale et de documenter le siège de l'occlusion artérielle conditionnant ainsi les traitements de reperfusion [62]. Pour les AVC de présentation tardive, le scanner de perfusion permet de quantifier la pénombre ischémique [63]. Plus récemment, une étude a même suggéré que pour les AVC de présentation tardive avec un score de tomodensitométrie précoce du programme d'accident vasculaire cérébral de l'Alberta (ASPECTS) élevé, une sélection par scanner sans perfusion avant thrombectomie mécanique n'était pas inférieure à inférieure à une sélection par scanner avec perfusion [64]. Pour certains auteurs, le scanner est ainsi une méthode à privilégier car de réalisation plus rapide et plus pratique. Récemment, Kim et al ont conduit une étude observationnelle de grande taille comparant la sélection des patients avant traitement endovasculaire et n'ont pas montré de différence entre une sélection par IRM et une sélection par scanner sur le devenir fonctionnel à 3 mois [65]. Néanmoins, les auteurs indiquaient qu'une sélection par IRM pouvait réduire le risque d'hémorragie intracrânienne symptomatique [65]. En outre, une analyse post-hoc de l'étude THRACE a conclu qu'une sélection par IRM ne différait pas significativement les traitements de reperfusion et n'impactait pas l'issue clinique à 3 mois [66]. Enfin, une étude observationnelle a signalé un taux plus important de recanalisation futile en cas de sélection par scanner avant thrombectomie par rapport à une sélection par IRM [67].

2.3 L'apport pronostic de l'IRM :

L'organisation de la thrombectomie mécanique pose des défis logistiques et économiques aux systèmes de soins [68]. En dépit de son efficacité, le taux de recanalisation futile après thrombectomie mécanique est estimé à environ 25% dans les essais cliniques randomisés et jusqu'à 54% en pratique clinique [49,53,54]. Outre le délai, le score du National Institutes of Health Stroke Scale (NIHSS) et l'étendue des lésions ischémiques, peu de facteurs prédictifs préalables aux traitements sont rapportés [69,70]. Ainsi, l'identification de biomarqueurs prédictifs est jugée crucial pour certains auteurs afin d'assurer une meilleure sélection des patients [68].

2.4 Imagerie de la barrière hémato-encéphalique en IRM :

Les deux méthodes d'imagerie de la BHE les plus couramment utilisées reposent sur l'administration d'un agent de contraste [71] :

- **L'IRM dynamique de réhaussement du contraste (IRM-DCE)** basée sur modification du signal T1 induite par l'agent de contraste
- **L'IRM dynamique de susceptibilité du contraste (IRM-DSC)** basée sur les modifications du signal T2 ou T2* induites par l'agent de contraste.

2.4.1 Les bases biophysiques de l'IRM-DSC et DCE :

Contrairement au scanner, l'IRM détecte les modifications des temps de relaxation locaux de l'eau induites par l'agent de contraste et non directement sa présence. L'administration de l'agent de contraste induit deux effets principaux distincts [72]:

- L'interaction directe, à l'échelle moléculaire, entre l'agent de contraste et l'eau
- L'effet mésoscopique induit par la compartimentalisation de l'agent de contraste, à l'échelle cellulaire et/ou vasculaire.

Ainsi, les raccourcissements des temps de relaxation T1, T2 et T2* reflètent une combinaison entre la concentration de l'agent de contraste, ses propriétés magnétiques, sa distribution au sein des compartiments tissulaires, la microstructure locale (l'architecture vasculaire et tissulaire), la diffusion de l'eau et les échanges d'eau au travers des membranes cellules [72].

2.4.2 Bio-distribution de l'agent de contraste :

La bio-distribution de l'agent de contraste dans les tissus détermine en grande partie les modifications des temps de relaxation tissulaires. La plupart des agents de contraste IRM utilisés en pratiques cliniques sont des molécules de bas poids moléculaire qui diffusent librement après injection, traversent le système vasculaire et passent dans l'espace inter-cellulaire [71]. Le tissu cérébral normal constitue une exception car la BHE empêche quasiment toute extravasation de l'agent de contraste [72]. En cas de rupture de la BHE, la compartimentalisation de l'agent de contraste au sein du système vasculaire n'est plus respectée et l'agent de contraste peut diffuser dans l'espace extravasculaire extracellulaire affectant ainsi les temps de relaxation tissulaires T1 pour l'IRM-DCE et T2* pour l'IRM-DSC [72].

2.4.3 La quantification de la perméabilité de la barrière hémato-encéphalique en IRM-DCE :

L'analyse quantitative des données d'IRM-DCE repose classiquement sur un modèle pharmacocinétique à deux compartiments, qui comprend la fraction de volume du plasma sanguin (vp) et la fraction de volume de l'espace extracellulaire extravasculaire (ve) [72]. Une fois l'agent de contraste injecté dans le flux sanguin, il peut diffuser de manière réversible dans l'espace extracellulaire extravasculaire avec des constantes de vitesse qui reflètent l'influx (K^{trans}) et l'efflux (k_{ep}) de l'agent de contraste à travers l'endothélium vasculaire [72]. En appliquant des modèles pharmacocinétiques bi-compartimentaux tels que ceux développés par Tofts et Kéty [73,74], la détermination du K^{trans} au sein revient à résoudre l'équation suivante:

$$C_t(t) = K^{trans} \int_0^t Cp(t)\exp\left(-k_{ep}(T-t)\right)dt$$

Avec :

- $C_t(t)$: la concentration de l'agent de contraste dans le plasma
- $k_{ep} = K^{trans} \,/\, ve$

La résolution de cette équation fait habituellement appel à une méthode d'ajustement linéaire des moindres carrés [72].

Figure 2 : Modèle de Tofts-Kéty.

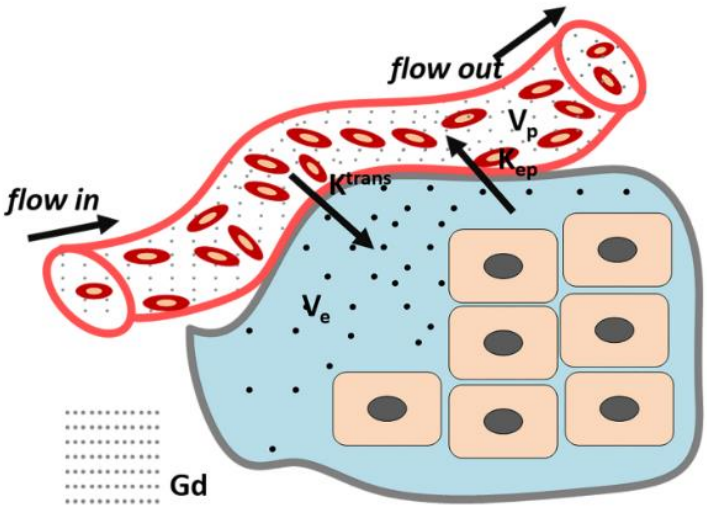

Figure 2: Tofts Model: classical DCE-MRI model. (K^{trans}: the transfer constant from vascular to extravascular extracellular space (EES); K_{ep}: Rate constant between the EES and the blood plasma; V_e: The fractional tissue EES (light green). V_p: The fractional plasma volume (white)

Cette figure illustre le modèle bi-compartimental de Tofts-Kety, d'après Yan et al [75].

2.4.4 La quantification de la perméabilité de la BHE en IRM-DSC.

En IRM-DSC, la quantification des paramètres hémodynamiques est dérivée de la théorie de la dilution des indicateurs [76,77]. En supposant que l'agent de contraste est compartimenté dans un vaisseau c'est-à-dire en cas d'intégrité de la BHE, un modèle pharmacocinétique unicompartimentale peut être appliqué et les paramètres hémodynamiques calculés à partir de la courbe de premier passage. La fonction d'entrée artérielle ($C_{AIF}(t)$) caractérise l'entrée du système et la fonction de résidu (R(t)) décrit la fraction d'agent de contraste restant dans le système vasculaire au temps t après l'injection [72]. Dans une étude IRM-DSC, le signal dans chaque voxel reflète la concentration de l'agent de contraste dans le tissu, C(t), qui est liée à $C_{AIF}(t)$ et R(t) selon l'équation de convolution suivante [72] :

$$C_t(t) = \frac{\rho}{Hf} CBF \int_0^t C_{AIF}(t)\mathrm{R}(\mathrm{t}-\tau)d\tau$$

Avec :

- $C_t(t)$: la concentration de l'agent de contraste dans le plasma
- ρ : la densité du tissu cérébral soit typiquement 1g/mL
- Hf: le facteur d'hématocrite rendant compte de la différence d'hématocrite entre la fonction d'entrée artériel et le système capillaire [78]
- *CBF*: Cerebral Blood Flow (Flux Sanguin Cérébral)

A partir de l'évolution du signal IRM-DSC lors du premier passage de l'agent de contraste, $C_{AIF}(t)$ et C(t) sont mesurées. La fonction résidu R(t) est déterminée en déconvoluant les courbes $C_{AIF}(t)$ et C(t) et le CBF déterminé à partir de la hauteur initiale de la fonction de résidu. Les cartes du volume sanguin cérébral (CBV) sont ensuite dérivées en utilisant l'équation suivant [72]:

$$CBV = \frac{Hf}{\rho} \frac{\int_{-\infty}^{+\infty} C_{tissu}(t)dt}{\int_{-\infty}^{+\infty} C_{AIF}(t)dt}$$

En cas de rupture de la BHE, la compartimentalisation de l'agent de contraste au sein du secteur vasculaire n'est plus respectée. La fuite de l'agent de contraste réduit son effet T2* (effet T1 shine-through) car elle abaisse la différence de concentration entre l'espace intravasculaire et l'interstitium et induit une compartimentalisation de l'agent de contraste autour des cellules qui est responsable d'un gradient de champ magnétique mésoscopique [79]. De ce fait, l'effet de susceptibilité magnétique de l'agent de contraste devient variable dans le temps et contamine le signal prévu en particulier aux points temporels ultérieurs au pic de premier passage [79-81]. Ces effets influencent la dynamique temporelle du signal IRM-DSC et perturbent le comportement linéaire de l'agent de contraste par rapport à la vitesse de relaxation et entraînent une surestimation du CBF et du CBV [82,83]. Des méthodes de post-traitement des images ont été proposées pour compenser les effets de la fuite de l'agent de contraste sur le signal, dont la méthode de Weisskoff est la plus couramment utilisée [80]. Cette méthode traite l'effet T1 shine-through par un modèle d'ajustement linéaire estimant la différence entre l'effet de susceptibilité magnétique induit par l'agent de contraste mesuré et l'effet de susceptibilité magnétique attendu en l'absence d'extravasation de produit de contraste. Ce modèle fait appel à une constante d'extravasation du produit de contraste, le K2 [80]. Pour certains auteurs, le paramètre K2 a été interprété comme une mesure de la perméabilité de la BHE [24,25,84,85].

Figure 2 : Effet de la correction de l'extravasation de l'agent de contraste sur la courbe d'intensité du signal.

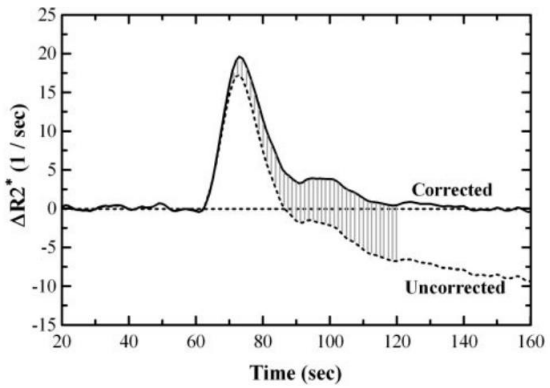

Fig 1. Typical corrected and uncorrected ΔR2* curves are shown. Note that even the first-pass curve is shifted to account for early leakage occurring during this segment. Without correction, the area under the curve (relative cerebral blood volume [rCBV]) is underestimated, even for integration techniques that stop at zero crossing or use gamma fitting.

Cette figure illustre l'effet de la correction de l'extravasation de l'agent de contraste par la méthode de Weisskoff et Boxermann sur la courbe intensité signal de l'IRM-DSC [80].

2.3.4 Évaluer la perméabilité de la barrière hémato-encéphalique dans l'infarctus cérébral :

Bien que les mesures de perméabilité vasculaire obtenus par K^{trans} soient considérées comme plus précises que celles obtenues par K2 [86], la détermination de la fraction de volume de l'espace extracellulaire extravasculaire ve nécessaire au calcul du K^{trans} nécessite un temps d'acquisition IRM long d'au moins 5min [87]. A ce jour, ce facteur limite l'intégration de l'IRM-DCE au protocole des IRM d'admission des patients présentant une suspicion d'infarctus cérébral. A l'inverse, l'IRM-DSC présente l'avantage d'un temps d'acquisition plus court et est déjà réalisée en routine clinique particulièrement en cas de présentation tardive. Néanmoins, la méthode de Weisskoff et Boxerman fait l'hypothèse d'une perfusion cérébrale symétrique [88]. En cas d'hypoperfusion, le retard d'arrivée de l'agent de contraste peut rendre le calcul K2 erroné [88]. R Leigh et al ont proposé une méthode permettant de corriger les cartes K2 du délai d'arrivée du produit de contraste [88]. Cette méthode a été implémentée par la société Olea Medical (La Ciotat, France), partenaire du projet de recherche hospitalo-universitaire MARVELOUS (ANR-16-RHUS-0009), pour générer des cartes K2 corrigées du délai d'arrivée du produit de contraste.

PROBLEMATIQUE – OBJECTIFS

Dans ce contexte, notre travail de thèse s'est réalisé en trois étapes :

Tout d'abord, le premier objectif a été de caractériser l'apport des techniques d'IRM dans la sélection des patients éligibles à un traitement de reperfusion à travers l'évaluation de l'apport respectif des techniques d'angio-IRM dans la localisation de l'occlusion artérielle intracrânienne et l'évaluation du post-traitement de l'IRM-DSC dans la quantification de la pénombre ischémique.

Le deuxième objectif a été d'identifier l'apport pronostic de l'IRM d'admission à travers l'identification de biomarqueurs radiologiques prédictifs de croissance des lésions ischémiques et/ou d'évolution clinique défavorable malgré une recanalisation après thrombectomie mécanique.

Enfin, le troisième objectif a été de caractériser les facteurs associés à une augmentation de perméabilité de la BHE sur l'IRM d'admission.

METHODES

La cohorte HIBISCUS- STROKE.

La cohorte HIBISCUS-STROKE est une étude observationnelle monocentrique qui a débuté en 2016 et s'est achevée en 2022. Elle a inclus des patients pris en charge dans l'unité de soins intensifs neurovasculaires de l'hôpital Neurologique et Neurochirurgical Pierre Wertheimer (Hospices Civils de Lyon) pour un AVC ischémique aigu par occlusion artérielle intracrânienne proximale de la circulation antérieure. Les patients inclus dans cette cohorte bénéficiaient d'une IRM d'admission multimodale et d'une thrombectomie mécanique. L'IRM d'admission comprenait des séquences DWI, T2*, FLAIR, ARM-TOF, ARM-CE et IRM-DSC. Au décours, les patients bénéficient d'une analyse séquentielle des marqueurs neuroinflammatoires sur sang veineux périphérique à l'admission, à 6, 24, 48 heures et à 3 mois. Ces marqueurs comprenaient la CRP (C reactive protein), les IL-6, IL-8, IL-10 (interleukins-6, -8 et -10), MCP-1 (monocyte chemoattractant protein-1), TNF-R1 (tumor necrosis factor eceptor-1), sST2 (soluble suppression of tumorigenecity 2), MMP-9, P-selectine et VCAM-1 (vascular cell adhesion molecule 1). Un scanner était réalisé à 24h afin de documenter une éventuelle complication hémorragique et une IRM de suivi à 6 jours comprenant une séquence FLAIR était effectuée afin de quantifier le volume final de la lésion ischémique. Les patients inclus avaient un suivi neurologique pour une évaluation clinique à 3 et 12 mois afin d'établir le score de mRS. Le consentement de l'ensemble des patients ou de leurs proches était recueilli pendant l'hospitalisation

Figure 3 : Parcours de recherche des patients inclus dans la cohorte HIBISCUS-STROKE.

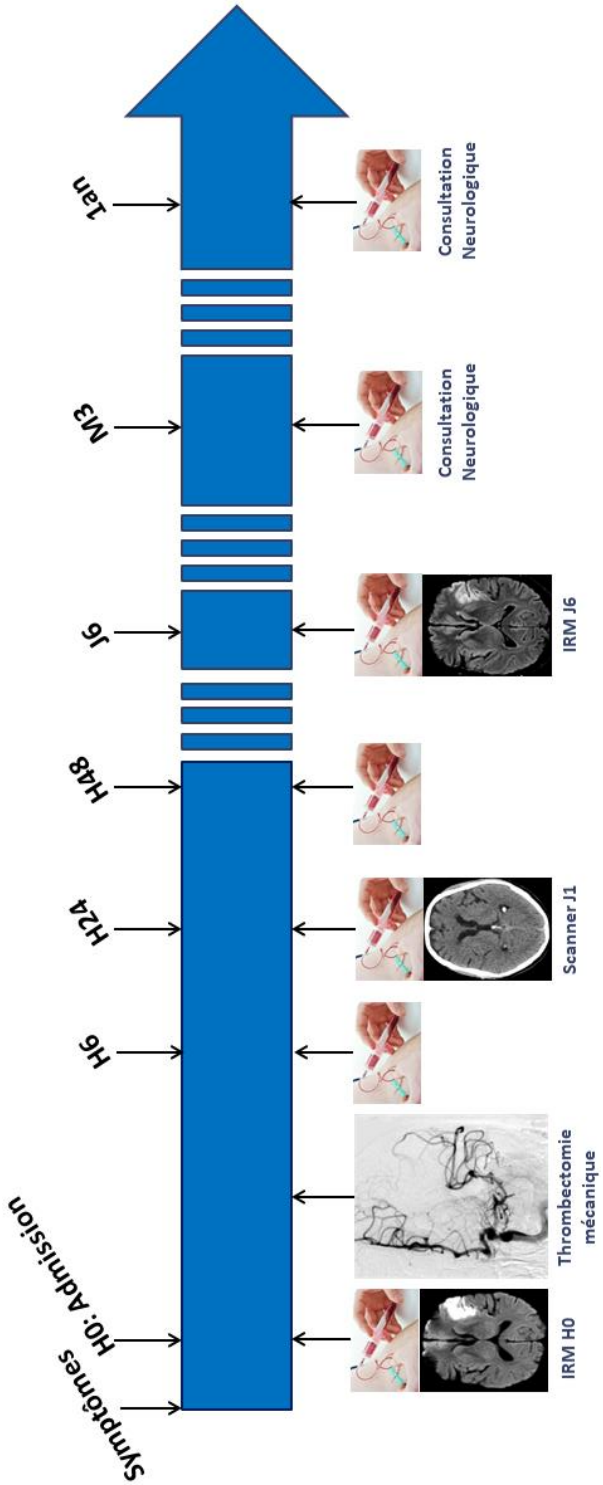

Cette figure illustre le parcours de recherche des patients ayant participé à la cohorte HIBISCUS-STROKE.

RESULTATS

La partie résultats est présentée selon les articles originaux ayant répondu aux trois objectifs de la thèse.

1. Apport de l'IRM multimodale dans la sélection des patients éligibles à un traitement de reperfusion :

1.1 Article n°1 publié dans *Revue Neurologique* :

Bani-Sadr A, Aguilera M, Cappucci M, Hermier M, Ameli R, Filip A, Riva R, Tuttle C, Cho TH, Mechtouff L, Nighoghossian N, Eker O, Berthezene Y. Comparison of magnetic resonance angiography techniques to brain digital subtraction arteriography in the setting of mechanical thrombectomy: A non-inferiority study. Rev Neurol (Paris), 2022;178(6):539-545

1.2 Article n°2 publié dans *Journal of Neurointerventional Surgery* :

Bani-Sadr A, Cho TH, Cappucci M, Hermier M, Ameli R, Filip A, Riva R, Derex L, De Bourguignon C, Mechtouff L, Eker OF, Nighoghossian N, Berthezene Y. Assessment of three MR perfusion software packages in predicting final infarct volume after mechanical thrombectomy. J Neurointerv Surg, 2023;15(4):393-398

1.3 Article n°3 publié *Magnetic Resonance Materials in Physics, Biology and Medicine :*

Bani-Sadr A, Trintignac M, Mechtouff L, Hermier M, Cappucci M, Ameli R, de Bourguignon C, Derex L, Cho TH, Nighoghossian N, Eker O, Berthezene Y. Is the optimal Tmax threshold identifying perfusion deficit volumes variable across MR perfusion software packages? A pilot study. MAGMA, 2023 (In Press).

2. Apport pronostic de l'IRM après recanalisation efficace

2.1 Article n°4 publié dans *European Radiology :*

Bani-Sadr A, Pavie D, Mechtouff L, Cappucci M, Hermier M, Ameli R, Derex L, De Bourguignon C, Cho TH, Eker O, Nighoghossian N, Berthezene Y. Brush sign and collateral supply as potential markers of large infarct growth after successful thrombectomy. Eur Radiol, 2023;33(6):4502-4509

Cet article a fait l'objet d'un éditorial :
Guenette JP. Brush strokes on MRI. Eur Radiol, 2023;33(6) :4500-4501

2.2 Article n°5 publié dans *Diagnostic and Interventional Imaging :*

Bani-Sadr A, Escande R, Mechtouff L, Pavie D, Hermier M, Derex L, Eker O, Cho TH, Nighoghossian N, Berthezene Y. Vascular hyperintensities on baseline FLAIR images are associated with functional outcome in stroke patients with successful recanalization after mechanical thrombectomy. Diag Interv Imaging, 2023;104(7-8):337-342

3. Facteurs associés à une augmentation de perméabilité de la BHE sur l'IRM d'admission.

3.1 Article n°6 publié dans *Neurology :*

Bani-Sadr A; Mechtouff L, De Bourguignon L, Mauffrey A, Boutelier T, Cho TH, Cappucci M, Ameli R, Hermier M, Derex L, Nighoghossian N, Berthezene Y. Brain-Blood Barrier Permeability and Kinetic of Inflammatory Markers in Acute Ischemic Stroke Patients Treated by Thrombectomy. Neurology, 2023 (In Press)

Étude n°1 : Comparaison des techniques d'angio-IRM et de l'artériographie cérébrale dans le cadre de la thrombectomie mécanique : une étude de non-infériorité

Contexte et état de la question.

En cas d'AVC ischémique aigu, l'identification et la localisation précise de l'occlusion artérielle est cruciale puisqu'une occlusion proximale peut justifier d'une thrombectomie mécanique [51]. Deux techniques d'angio-IRM (l'ARM-TOF et l'ARM-CE) sont habituellement utilisées et ont chacune des avantages et des inconvénients. Dans les études antérieures ayant évalué ces techniques, l'artériographie cérébrale était considérée comme la technique de référence [89,90]. Plus récemment, il a été rapporté que le thrombus changeait régulièrement de localisation entre l'imagerie initiale de l'artériographie cérébrale avec un taux moyen rapporté de 20 % [91-93]. Dans ce contexte, ce premier travail visait à réaliser une étude de non-infériorité comparant l'ARM-CE et l'ARM-TOF à l'artériographie cérébrale dans la localisation de l'occlusion artérielle et d'étudier les facteurs de divergence entre les techniques d'angio-IRM et l'artériographie cérébrale.

Principaux résultats.

Nous avons observé que l'ARM-CE et l'ARM-TOF étaient toutes deux inférieures à l'artériographie cérébrale dans la localisation des occlusions artérielles intracrâniennes malgré la prise en compte du caractère migratoire du thrombus. Par rapport à l'ARM-TOF, l'ARM-CE était plus précise pour les occlusions en tandem et les occlusions proximales du segment M1 de l'artère cérébrale moyenne. Les facteurs de discordance entre l'angio-IRM et l'artériographie cérébrale étaient identiques pour les deux techniques et incluaient les occlusions en tandem, les occlusions de l'artère carotide interne proximale et le délai entre l'IRM et la thrombectomie mécanique.

Available online at
ScienceDirect
www.sciencedirect.com

Elsevier Masson France
EM|consulte
www.em-consulte.com

Original article

Comparison of magnetic resonance angiography techniques to brain digital subtraction arteriography in the setting of mechanical thrombectomy: A non-inferiority study

A. Bani-Sadr [a,b,*,1], M. Aguilera [a,1], M. Cappucci [a], M. Hermier [a], R. Ameli [a], A. Filip [a], R. Riva [a], C. Tuttle [a], T.-H. Cho [c,d], L. Mechtouff [c,d], N. Nighoghossian [c,d], O. Eker [a,b], Y. Berthezene [a,b]

[a] Department of Neuroradiology, East Group Hospital, Hospices Civils de Lyon, 59, boulevard Pinel, 69500 Bron, France
[b] CREATIS Laboratory, CNRS UMR 5220, INSERM U1294, Claude-Bernard Lyon I University, 7, avenue Jean-Capelle O, 69100 Villeurbanne, France
[c] Stroke Department, East Group Hospital, Hospices Civils de Lyon, 59, boulevard Pinel, 69500 Bron, France
[d] CarMeN Laboratory, INSERM U1060, Claude-Bernard Lyon I University, 59, boulevard Pinel, 69500 Bron, France

INFO ARTICLE

Article history:
Received 29 August 2021
Received in revised form
1st December 2021
Accepted 6 December 2021
Available online 9 February 2022

Keywords:
Stroke
Thrombectomy
Magnetic resonance angiography

ABSTRACT

Introduction. – We performed a non-inferiority study comparing magnetic resonance angiography (MRA) techniques including contrast-enhanced (CE) and time-of-flight (TOF) with brain digital subtraction arteriography (DSA) in localizing occlusion sites in acute ischemic stroke (AIS) with a prespecified inferiority margin taking into account thrombus migration.

Materials and methods. – HIBISCUS-STROKE (CoHort of Patients to Identify Biological and Imaging markerS of CardiovascUlar Outcomes in Stroke) includes large-vessel-occlusion (LVO) AIS treated with mechanical thrombectomy (MT) following brain magnetic resonance imaging (MRI) including both CE-MRA and TOF-MRA. Locations of arterial occlusions were assessed independently for both MRA techniques and compared to brain DSA findings. Number of patients needed was 48 patients to exclude a difference of more than 20%. Discrepancy factors were assessed using univariate general linear models analysis.

Results. – The study included 151 patients with a mean age of 67.6 ± 15.9 years. In all included patients, TOF-MRA and CE-MRA detected arterial occlusions, which were confirmed by brain DSA. For CE-MRA, 38 (25.17%) patients had discordant findings compared with brain DSA and 50 patients (33.11%) with TOF-MRA. The discordance factors were identical for both MRA techniques namely, tandem occlusions (OR = 1.29, $P = 0.004$ for CE-MRA and OR = 1.61, $P < 0.001$ for TOF-MRA), proximal internal carotid artery occlusions

* *Corresponding author at*: Department of Neuroradiology, East Group Hospital, Hospices Civils de Lyon. 59, boulevard Pinel, 69500 Bron, France.
E-mail addresses: alexandre.bani-sadr@chu-lyon.fr (A. Bani-Sadr).
[1] Both authors contribute equally to this work.
https://doi.org/10.1016/j.neurol.2021.12.009

(OR = 1.30, $P = 0.002$ for CE-MRA and OR = 1.47, $P < 0.001$ for TOF-MRA) and time from MRI to MT (OR = 1.01, $P = 0.01$ for CE-MRA and OR = 1.01, $P = 0.02$ for TOF-MRA).
Conclusion. – Both MRA techniques are inferior to brain DSA in localizing arterial occlusions in LVO-AIS patients despite addressing the migratory nature of the thrombus.

1. Introduction

Identification and precise localization of arterial occlusions are paramount in patients with acute ischemic stroke (AIS) who may require mechanical thrombectomy (MT) in case of large-vessel-occlusion (LVO) [1,2].

In clinical practice, most centers favor computed tomography (CT) scans with almost systematic cervical and intracranial vessel exploration. However, some centers prefer magnetic resonance imaging (MRI) for which the magnetic resonance angiography (MRA) protocol is variable. A recent multi-centric study comparing the effect on workflow and functional outcome of CT and MRI reported that only 28% of patients had had a contrast-enhanced MRA (CE-MRA) of the supra-aortic vessels and that all patients included underwent time-of-flight MRA (TOF-MRA) of the intracranial arteries [3]. Both MRA techniques have advantages and drawbacks. TOF-MRA is reported to have high sensitivity (85–100%) and specificity (91–100%) in identifying arterial occlusion and does not require the use of a contrast media [4,5]. However, TOF-MRA has a small field-of-view, longer acquisition duration and may overestimate the degree of stenosis [6,7]. Conversely, CE-MRA has shorter acquisition time, a larger field-of-view allowing complete evaluation of cervical arteries, and is less sensitive to blood flow artifacts [8].

Previous studies that compared the performance of CE-MRA and TOF-MRA in locating arterial occlusions in LVO-AIS patients considered brain digital subtraction arteriography (DSA) as the reference [9,10]. However, recent studies have reported that thrombus regularly changes location between initial imaging and MT with an average reported rate of 20% [11–13]. This raises the question of the comparability of MRA techniques and brain DSA because the migratory nature of the thrombus was not addressed in previous studies [9,10].

In this setting, we aimed to perform a non-inferiority study comparing CE-MRA and TOF-MRA to brain DSA for locating arterial occlusions in LVO-AIS patients and to investigate factors of discrepancies between MRA techniques and brain DSA.

2. Material and methods

2.1. Patient population

We performed a retrospective cohort study including patients from the HIBISCUS-STROKE cohort (CoHort of Patients to Identify Biological and Imaging markerS of CardiovascUlar Outcomes in Stroke; NCT03149705).

This cohort is an ongoing observational cohort conducted since October 2016 that includes patients referred to our stroke center for LVO-AIS of the anterior circulation and candidates for MT [9]. Patients were included in this study if they underwent an initial MRI with TOF-MRA and CE-MRA followed by a brain DSA performed during MT. We excluded patients with posterior circulation AIS and those for whom one of the angiographic modalities was not available.

Baseline data on demographics characteristics were collected at hospital admission. In line with international guidelines, patients were additionally treated with intravenous thrombolysis immediately after brain MRI [14].

2.2. Brain MRI

Brain MRI was performed on a 3T scanner (Philips Achieva, Philips Healthcare, Best, The Netherlands) and included parenchymal brain imaging sequences (axial DWI, T2 FLAIR, T2*), angiographic sequences (3D TOF-MRA and CE-MRA). The total acquisition time was 15 minutes.

CE-MRA required the administration a bolus of gadoterate meglumine (Dotarem; Guerbet, Aulnay-sous-Bois, France) at a standard dose (0.1 mmol/kg) via a peripheral venous catheter at 2 mL/s. The arrival of the bolus in the arterial circulation required fast serial 2D images. The MRA acquisition parameters are presented in Supplemental material 1.

2.3. DSA imaging

Brain DSA was performed immediately prior to MT by experienced neurointerventionalists using a biplanar system (Siemens Axiom Artis). Angiographic images acquired at two images per second with manual injection of iodinated contrast media. These images were further considered as the reference for extra- and intracranial artery analysis.

2.4. Image analysis

MRA images were reviewed, in random order, independently by two neuroradiologists blinded from clinical data, other MR sequences, and DSA. In case of discrepancy, a third neuroradiologist evaluated the images. Brain DSAs were also evaluated by two operators blinded from clinical data and MRIs, and a consensus was reached in case of discrepancy between them. All readings assessed the presence of an occlusion and its location according to the following classification: common carotid artery (CCA), internal carotid artery (ICA) including proximal ICA and distal ICA, proximal middle cerebral artery (MCA) including proximal M1 segment and distal M1 segment, and proximal M2 segment of MCA. In case of tandem occlusions, both levels were reported. Image quality was assessed using a three-point subjective score: 0 = poor quality resulting in impossible interpretation; 1 = moderate

quality with rare artifacts; 2 = good image quality with no artifacts.

2.5. Statistical analysis

Data were summarized as mean (± standard-deviation), median (IQR) or counts (%) as appropriate. The accuracy, sensitivity, specificity, and predictive values of each MRA technique were calculated using brain DSA as reference and compared using McNemar's test. Inter-rater agreement for TOF-MRA, CE-MRA and brain DSA were assessed using the kappa coefficient [15].

This study was designated as a non-inferiority study to assess TOF-MRA and CE-MRA in locating arterial occlusion in AIS patients compared to brain DSA. The prespecified non-inferiority margin for discrepancy rate was chosen at 20% because this is the average reported rate of thrombus migration [11–13]. Assuming 100% accuracy for brain DSA, 48 patients were needed to be 90% sure that a 95% one-sided confidence interval would exclude a difference of $> 20\%$. Univariate analyses using general linear models were performed to assess potential factors of discrepancies namely time between MRI and MT, tandem occlusion, intravenous thrombolysis and image quality. A two-sided P-value < 0.05 was considered as statistically significant. All statistical analyses were performed with the R software, version 3.2.1 (R foundation for Statistical Computing, Vienna, Austria).

3. Results

3.1. Demographics and image characteristics of included patients

During the study period, 151 patients (on a base of 174 patients) met the inclusion criteria. Twenty-three patients were excluded because of incomplete MRI protocol ($n = 5$) or poor image quality either for TOF-MRA ($n = 2$), CE-MRA ($n = 2$) or brain DSA ($n = 5$). Nine patients with posterior site occlusion were also excluded.

The population included 85 males (56.29%) and 66 females (43.71%) with a mean age of 67.6 ± 15.9 years (range: 27–94). All patients underwent MT and 79 (52.31%) of them received intravenous thrombolysis. The mean delay between brain MRI and DSA was 67.22 ± 58.53 min. The distribution of arterial occlusion sites documented by brain DSA and both MRA techniques is presented in Supplemental material 2 and image quality is reported in Supplemental material 3.

3.2. Comparison of CE-MRA and brain DSA

In all included patients, CE-MRA detected at least one arterial occlusion. The location of occlusion site was discordant with brain DSA findings in 38 (25.17%) patients. Inter-rater agreement was almost perfect CE-MRA ($\kappa = 0.92$, 95% CI [0.86–0.97], $P \leq 0.01$). As presented in Table 1, CE-MRA exhibited excellent diagnostic performance except for moderate specificity for the distal ICA and the proximal M1 segment of the MCA. Fig. 1 presents an example of a pseudo-occlusion of the proximal ICA, which illustrates the limitation of CE-MRA in assessing proximal ICA patency.

In univariate analysis, discrepancies between CE-MRA and brain DSA were associated with tandem occlusion (OR = 1.29, $P = 0.004$), proximal ICA occlusion (OR = 1.30, $P = 0.002$) and time from MRI to MT (OR = 1.01, $P = 0.01$) but not with intravenous thrombolysis ($P = 0.96$), nor with image quality ($P = 0.69$).

3.3. Comparison of TOF-MRA and brain DSA

TOF-MRA identified at least one arterial occlusion for each included patient. Occlusion site was discordant in 50 subjects (33.11%) compared with brain DSA. Inter-rater agreement was also almost perfect ($\kappa = 0.98$, 95% CI: 0.95–1.00, $P < 0.001$). As presented in Table 2, TOF-MRA had low sensitivity for tandem occlusions. Fig. 2 presents an example of tandem occlusions misdiagnosed with TOF-MRA.

Discrepancies between TOF-MRA and brain DSA were associated with tandem occlusion (OR = 1.61, $P < 0.001$), proximal ICA occlusion (OR = 1.47, $P < 0.001$) and time from MRI to MT (OR = 1.01, $P = 0.02$) but not with intravenous thrombolysis ($P = 0.97$), nor with image quality ($P = 0.68$). Supplemental material 3 presents an example of thrombus migration.

3.4. Comparison of CE-MRA and TOF-MRA

Compared to TOF-MRA, CE-MRA was statistically more accurate for proximal M1 occlusion ($P = 0.002$) and tandem occlusions ($P < 0.001$). An example of a tandem carotid-sylvian occlusion is shown in Fig. 2.

For all other locations, there was no statistically significant difference between the two MRA techniques (all $P > 0.68$).

Table 1 – Diagnostic performances of CE-MRA.

	Accuracy % [95% CI]	Sensitivity %	Specificity %	PPV %	NPV %
Tandem	90.73 [84.93–94.84]	95.00	74.19	93.44	79.31
Proximal ICA	94.04 [88.99–97.24]	93.22	96.97	99.10	80.00
Distal ICA	92.72 [87.34–96.31]	98.45	59.09	93.38	86.67
Proximal M1	86.09 [79.53–91.18]	87.36	84.38	83.08	83.08
Distal M1	86.75 [80.29–91.72]	90.68	72.73	92.24	68.57
Proximal M2	92.72 [87.34–96.31]	97.52	73.33	93.65	88.00

CE-MRA: contrast-enhanced magnetic resonance angiography; PPV: positive predictive value; NPV: negative predictive value; ICA: internal carotid artery; M1: first segment of the middle cerebral artery; M2: second segment of the middle cerebral artery; 95% CI: 95% confidence interval.

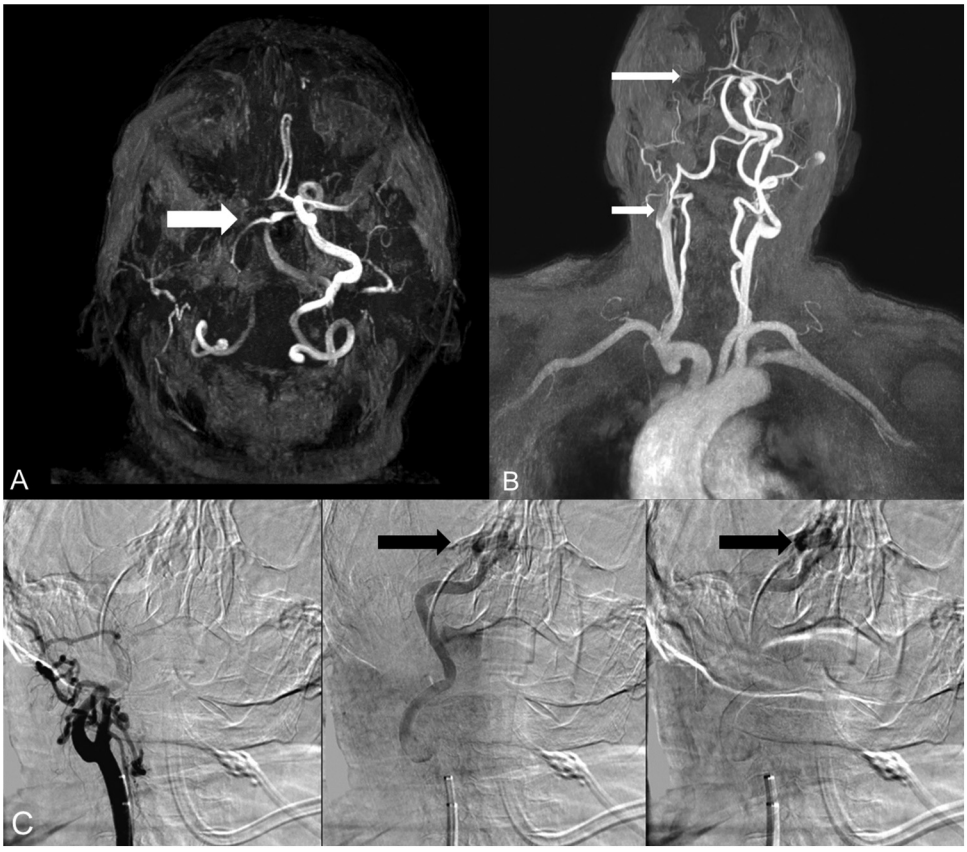

Fig. 1 – An example of pseudo-occlusion of proximal ICA. In this patient, TOF-MRA (Fig. 1A) revealed a signal void (white arrow) in the right proximal ICA suggesting an occlusion of the latter. CE-MRA (Fig. 1B) shows opacification defects of the proximal ICA and the proximal M1 segment of the MCA (white arrows) that suggest a tandem occlusion. Brain DSA findings (Fig. 1C) are discordant by showing an occlusion of the right carotid termination (black arrow) responsible for severe slowing of blood flow and explaining the abnormalities of proximal ICA found both for TOF-MRA and CE-MRA. TOF-MRA: time-of-flight magnetic resonance imaging; ICA: internal carotid artery; MCA: middle cerebral artery; CE-MRA: contrast-enhanced magnetic resonance imaging; DSA: digital subtraction angiography.

4. Discussion

The aim of this retrospective cohort study was to determine whether CE-MRA and TOF-MRA were non-inferior compared to brain DSA in localizing the arterial occlusion site in patients with LVO-AIS when addressing the migratory nature of the thrombus.

Our results demonstrated that both MRA are inferior to brain DSA and this might be explained by three main reasons.

First, thrombus location regularly changes between initial imaging and DSA with an average reported rate of 20% [11–13]. Occlusion site discrepancies between MRA techniques and brain DSA were associated with time from baseline MRI to brain DSA but not with intravenous thrombolysis. These findings are in disagreement with previous articles as several

Table 2 – Diagnostic performances of TOF-MRA.

	Accuracy % [95% CI]	Sensitivity %	Specificity %	PPV %	NPV %
Tandem	78.81 [71.42–85.03]	3.23	98.33	33.33	79.73
Proximal ICA	94.04 [88.99–97.24]	94.07	93.94	98.23	81.58
Distal ICA	92.05 [86.53–95.83]	98.45	54.55	92.70	85.71
Proximal M1	76.82 [69.27–83.29]	89.66	59.38	75.00	80.85
Distal M1	84.77 [78.03–90.09]	90.68	63.64	89.92	65.62
Proximal M2	91.39 [85.73–95.34]	97.52	66.67	92.19	86.96

TOF-MRA: time-of-flight magnetic resonance angiography; PPV: positive predictive value; NPV: negative predictive value; ICA: internal carotid artery; M1: first segment of the middle cerebral artery; M2: second segment of the middle cerebral artery; 95% CI: 95% confidence interval.

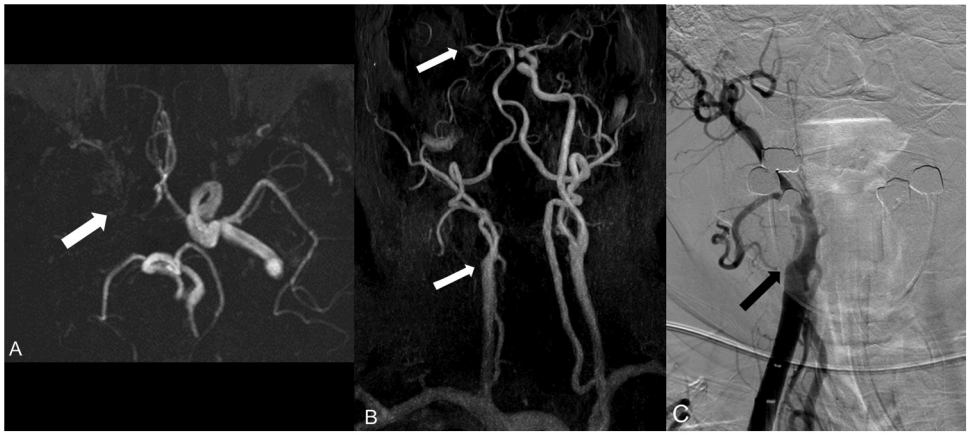

Fig. 2 – An example of tandem occlusion. In this example, TOF-MRA (Fig. 2A) revealed a signal void in the right proximal ICA (white arrow) and, CE-MRA (Fig. 2B) demonstrated a tandem occlusion including the proximal ICA and the proximal M1 segment of the MCA (white arrows). Brain DSA (Figs. 2C and D) confirms tandem occlusion by visualizing opacification defects at the original of the right proximal ICA and the proximal M1 segment of the MCA (black arrows). TOF-MRA: time-of-flight magnetic resonance imaging; CE-MRA: contrast-enhanced magnetic resonance imaging; MCA: middle cerebral artery.

authors reported that thrombus migration was associated with intravenous thrombolysis [11–13]. A possible explanation is a different definition of thrombus migration, with most authors defining it as any downstream migration of the clot. In our study, we only considered a different location according to the pre-established grid as a discrepancy. As a result, we may have misrecognized millimeter-scale migrations.

Second, both MRA techniques have impaired accuracies in case of tandem occlusions, i.e. 20.53% in our study population. As a blood-flow based technique, TOF-MRA does not allow precise assessment of intracranial vasculature in cases of occlusion and/or severe stenosis of the carotid bulb. Likewise, contrast flow can also be impeded by an extracranial ICA stenosis and/or obstruction of the proximal ICA that may also preclude precise assessment of intracranial vasculature with CE-MRA [8,16]. Third, an intracranial clot may lead to extracranial ICA pseudo-occlusions in about 11–46% of cases [17–19]. The underlying mechanism of pseudo-occlusion is a stagnant contrast flow proximal to an intracranial occlusion and has also been reported for CT angiography [20–22].

As a result, CE-MRA had excellent sensitivity but moderate specificity for tandem occlusions. In our study, the false positive rate of CE-MRA (20.69%) was lower than the reported rate for CT angiography (30.4%) by Rocha et al. [21]. A possible explanation is that CE-MRA acquisition is later than that of CT angiography because of a longer acquisition time. In addition, we found that CE-MRA was more accurate for tandem occlusions and the M1 proximal segment of the MCA, which is in agreement with previous studies [9,10]. The most likely explanation is that the CE-MRA field-of-view extends from the aortic arch to the distal intracranial arteries in contrast to TOF-MRA that only assesses intracranial vasculature. Since TOF-MRA is inferior to CE-MRA and time-consuming, our results suggest that TOF-MRA in the MRA protocol is superfluous for AIS suspicion.

Knowledge of the limitations of the MRA techniques is essential. Most importantly, misdiagnosis of tandem occlusions can lead to severe issues. It may directly impact the management of AIS patients since recent studies suggest that carotid stent placement with anti-platelet therapy may be the most effective therapy for tandem occlusions [23,24]. In addition, this might influence the indications for intravenous thrombolysis as its efficacy is reported to be weak for tandem occlusions [25].

This study has several limitations. First, this was a single-center retrospective cohort study. In addition, we only studied early CE-MRA. Recently, some authors compared early and delayed CE-MRA for the assessment proximal ICA patency [26]. They concluded that delayed CE-MRA may improve accuracy and reliability [26]. In addition, none of the included patients had severe arterial stenosis, which probably explains the absence of false positives for TOF-MRA. In clinical practice, it is difficult to distinguish severe intracranial stenosis from arterial occlusion with TOF-MRA, unlike CE-MRA [6,7].

5. Conclusion

Both CE-MRA and TOF-MRA are inferior to brain DSA in locating arterial occlusion in LVO-AIS patients despite addressing the migratory nature of the thrombus because both techniques have impaired accuracies for tandem occlusions and for assessing proximal ICA patency.

Disclosure of interest

The authors declare that they have no competing interest.

Acknowledgement

This work was supported by the RHU MARVELOUS (ANR-16-RHUS-0009) of Université de Lyon, within the program

''Investissements d'Avenir'' operated by the French National Research Agency.

Appendix A. Supplementary data

Supplementary data associated with this article can be found, in the online version, at https://doi.org/10.1016/j.neurol.2021.12.009.

REFERENCES

[1] Nogueira RG, Jadhav AP, Haussen DC, Bonafe A, Budzik RF, Bhuva P, et al. Thrombectomy 6 to 24 hours after stroke with a mismatch between deficit and infarct. N Engl J Med 2018;378:11–21. http://dx.doi.org/10.1056/NEJMoa1706442.

[2] Ma H, Campbell BCV, Parsons MW, Churilov L, Levi CR, Hsu C, et al. Thrombolysis guided by perfusion imaging up to 9 hours after onset of stroke. N Engl J Med 2019;380:1795–803. http://dx.doi.org/10.1056/NEJMoa1813046.

[3] Provost C, Soudant M, Legrand L, Ben Hassen W, Xie Y, Soize S, et al. Magnetic resonance imaging or computed tomography before treatment in acute ischemic stroke: effect on workflow and functional outcome. Stroke 2019;50:659–64. http://dx.doi.org/10.1161/STROKEAHA.118.023882.

[4] Stock KW, Radue EW, Jacob AL, Bao XS, Steinbrich W. Intracranial arteries: prospective blinded comparative study of MR angiography and DSA in 50 patients. Radiology 1995;195:451–6. http://dx.doi.org/10.1148/radiology.195.2.7724765.

[5] Korogi Y, Takahashi M, Mabuchi N, Miki H, Shiga H, Watabe T, et al. Intracranial vascular stenosis and occlusion: diagnostic accuracy of three-dimensional, Fourier transform, time-of-flight MR angiography. Radiology 1994;193:187–93. http://dx.doi.org/10.1148/radiology.193.1.8090890.

[6] Ishimaru H, Ochi M, Morikawa M, Takahata H, Matsuoka Y, Koshiishi T, et al. Accuracy of pre- and postcontrast 3D time-of-flight MR angiography in patients with acute ischemic stroke: correlation with catheter angiography. AJNR Am J Neuroradiol 2007;28:923–6.

[7] Sohn C-H, Sevick RJ, Frayne R. Contrast-enhanced MR angiography of the intracranial circulation. Magn Reson Imaging Clin N Am 2003;11:599–614. http://dx.doi.org/10.1016/s1064-9689(03)00064-3.

[8] Yang CW, Carr JC, Futterer SF, Morasch MD, Yang BP, Shors SM, et al. Contrast-enhanced MR angiography of the carotid and vertebrobasilar circulations. AJNR Am J Neuroradiol 2005;26:2095–101.

[9] Boujan XT, Neuberger XU, Pfaff XJ, Nagel XS, Herweh XC, Bendszus XM, et al. value of contrast-enhanced MRA versus time-of-flight MRA in acute ischemic stroke MRI n.d.:7.

[10] Dhundass S, Savatovsky J, Duron L, Fahed R, Escalard S, Obadia M, et al. Improved detection and characterization of arterial occlusion in acute ischemic stroke using contrast-enhanced MRA. J Neuroradiol 2020;47:278–83. http://dx.doi.org/10.1016/j.neurad.2019.02.011.

[11] Alves HC, Treurniet KM, Jansen IGH, Yoo AJ, Dutra BG, Zhang G, et al. Thrombus migration paradox in patients with acute ischemic stroke. Stroke 2019;50:3156–63. http://dx.doi.org/10.1161/STROKEAHA.119.026107.

[12] Lee S-J, Lee T-K, Kim B-T, Shin D-S. Clinical implications of preinterventional thrombus migration in patients with emergent large vessel occlusion. World Neurosurg 2020. http://dx.doi.org/10.1016/j.wneu.2020.11.080 [S1878875020324554].

[13] Lim JC, Churilov L, Bivard A, Ma H, Dowling RJ, Campbell BCV, et al. Does intravenous thrombolysis within 4.5 to 9 hours increase clot migration leading to endovascular inaccessibility? Stroke 2021;52:1083–6. http://dx.doi.org/10.1161/STROKEAHA.120.030661.

[14] Powers WJ, Rabinstein AA, Ackerson T, Adeoye OM, Bambakidis NC, Becker K, et al. Guidelines for the early management of patients with acute ischemic stroke: 2019 update to the 2018 Guidelines for the Early Management of Acute Ischemic Stroke: a guideline for healthcare professionals from the American Heart Association/American Stroke Association. Stroke 2019;50:e344–418. http://dx.doi.org/10.1161/STR.0000000000000211.

[15] Landis JR, Koch GG. The measurement of observer agreement for categorical data. Biometrics 1977;33:159–74.

[16] Korn A, Bender B, Brodoefel H, Hauser T-K, Danz S, Ernemann U, et al. Grading of carotid artery stenosis in the presence of extensive calcifications: dual-energy CT angiography in comparison with contrast-enhanced MR angiography. Clin Neuroradiol 2015;25:33–40. http://dx.doi.org/10.1007/s00062-013-0276-0.

[17] Grossberg JA, Haussen DC, Cardoso FB, Rebello LC, Bouslama M, Anderson AM, et al. Cervical carotid pseudo-occlusions and false dissections: intracranial occlusions masquerading as extracranial occlusions. Stroke 2017;48:774–7. http://dx.doi.org/10.1161/STROKEAHA.116.015427.

[18] Chen Z, Zhang M, Shi F, Gong X, Liebeskind D, Ding X, et al. Pseudo-occlusion of the internal carotid artery predicts poor outcome after reperfusion therapy. Stroke 2018;49:1204–9. http://dx.doi.org/10.1161/STROKEAHA.118.021229.

[19] Poppe AY, Jacquin G, Roy D, Stapf C, Derex L. Tandem carotid lesions in acute ischemic stroke: mechanisms, therapeutic challenges, and future directions. AJNR Am J Neuroradiol 2020;41:1142–8. http://dx.doi.org/10.3174/ajnr.A6582.

[20] Diouf A, Fahed R, Gaha M, Chagnon M, Khoury N, Kotowski M, et al. Cervical internal carotid occlusion versus pseudo-occlusion at CT angiography in the context of acute stroke: an accuracy, interobserver, and intraobserver agreement study. Radiology 2018;286:1008–15. http://dx.doi.org/10.1148/radiol.2017170681.

[21] Rocha M, Delfyett WT, Agarwal V, Aghaebrahim A, Jadhav A, Jovin TG. Diagnostic accuracy of emergency CT angiography for presumed tandem internal carotid artery occlusion before acute endovascular therapy. J Neurointerventional Surg 2018;10:653–6. http://dx.doi.org/10.1136/neurintsurg-2017-013169.

[22] Kappelhof M, Marquering HA, Berkhemer OA, Borst J, van der Lugt A, van Zwam WH, et al. Accuracy of CT angiography for differentiating pseudo-occlusion from true occlusion or high-grade stenosis of the extracranial ICA in acute ischemic stroke: a retrospective MR CLEAN Substudy. AJNR Am J Neuroradiol 2018;39:892–8. http://dx.doi.org/10.3174/ajnr.A5601.

[23] Zhu F, Bracard S, Anxionnat R, Derelle A-L, Tonnelet R, Liao L, et al. Impact of emergent cervical carotid stenting in tandem occlusion strokes treated by thrombectomy: a review of the TITAN Collaboration. Front Neurol 2019;10:206. http://dx.doi.org/10.3389/fneur.2019.00206.

[24] Sadeh-Gonik U, Tau N, Friehmann T, Bracard S, Anxionnat R, Derelle A-L, et al. Thrombectomy outcomes for acute stroke patients with anterior circulation tandem lesions: a

clinical registry and an update of a systematic review with meta-analysis. Eur J Neurol 2018;25:693–700. http://dx.doi.org/10.1111/ene.13577.

[25] Tsivgoulis G, Katsanos AH, Schellinger PD, Köhrmann M, Varelas P, Magoufis G, et al. Successful reperfusion with intravenous thrombolysis preceding mechanical thrombectomy in large-vessel occlusions. Stroke 2018;49:232–5. http://dx.doi.org/10.1161/STROKEAHA.117.019261.

[26] Boisseau W, Benaissa A, Fahed R, Amegnizin J-L, Smajda S, Benadjaoud S, et al. Delayed contrast-enhanced MR angiography for the assessment of internal carotid bulb patency in the context of acute ischemic stroke: an accuracy, interrater, and intrarater agreement study. AJNR Am J Neuroradiol 2021. http://dx.doi.org/10.3174/ajnr.A7054.

Étude n°2 : Comparaison des logiciels de perfusion IRM dans la prédiction du volume final de l'infarctus cérébral après thrombectomie mécanique.

Contexte et état de la question.

Certaines données indiquent que la quantification du noyau ischémique et de la pénombre ischémique a une valeur ajoutée en assurant une meilleure sélection des patients éligibles à un traitement de reperfusion, en particulier cas de présentation tardive [94-97]. Dans les essais cliniques multicentriques randomisés sur la thrombectomie mécanique, le logiciel RAPID® (IschemiaView, Menlo Park, Californie) a été utilisé pour analyser les séquences de perfusion en scanner et en IRM afin de sélectionner les indications de reperfusion [43,48,50,51,98]. Cependant, d'autres logiciels de perfusion sont utilisés en pratique clinique. Pour le scanner, il a été démontré que les volumes présumés du noyau ischémique et de la pénombre ischémique peuvent varier de manière significative entre les logiciels et que ces variations peuvent influencer la sélection des patients [99-101]. L'objectif principal de cette deuxième étude était d'évaluer les performances de 3 logiciels de perfusion IRM (RAPID® ; OleaSphere® et ; Philips ®) dans la prédiction du volume de la lésion ischémique finale chez les patients traités par thrombectomie mécanique. L'objectif secondaire était de déterminer si une correction des volumes calculés automatiquement par un expert pouvait améliorer la prédiction.

Principaux résultats.

Dans cette étude, nous avons observé que la quantification du noyau ischémique, à l'aide d'un seuil d'ADC ≤620 × 10^{-6} m^2/s, était reproductible d'un logiciel à l'autre. Ce seuil prédisait correctement le volume final de la lésion ischémique en cas de recanalisation. A l'inverse, l'étendue du trouble de perfusion variait substantiellement d'un logiciel à l'autre. En cas d'échec de recanalisation, la précision de la prédiction du volume final était plus importante pour les logiciels RAPID® et OleaSphere®. En cas d'AVC de présentation tardive, l'application des critères volumétriques tels que ceux de DEFUSE 3 aurait conduit à une sélection différente selon le logiciel utilisé [50]. La correction des volumes automatiquement générés par un expert permettait d'améliorer la reproductibilité et la qualité de prédiction du volume final de la lésion ischémique.

Original research

Assessment of three MR perfusion software packages in predicting final infarct volume after mechanical thrombectomy

Alexandre Bani-Sadr ,[1,2] Tae-Hee Cho,[3] Matteo Cappucci ,[1] Marc Hermier,[1] Roxana Ameli,[1] Andrea Filip,[1] Roberto Riva,[1] Laurent Derex,[3] Charles De Bourguignon,[4] Laura Mechtouff ,[3] Omer F Eker,[1,2] Norbert Nighoghossian,[3] Yves Berthezene[1,2]

► Additional supplemental material is published online only. To view, please visit the journal online (http://dx.doi.org/10.1136/neurintsurg-2022-018674).

[1]Neuroradiology, Hospices Civils de Lyon, Bron, France
[2]MYRIAD, CREATIS, Villeurbanne, France
[3]Stroke Department, Hospices Civils de Lyon, Lyon, France
[4]Centre d'Investigations Cliniques, Hospices Civils de Lyon, Lyon, France

Correspondence to
Dr Alexandre Bani-Sadr, Neuroradiology, Hospices Civils de Lyon, Bron, France; apbanisadr@gmail.com

Received 20 January 2022
Accepted 28 February 2022
Published Online First 22 March 2022

ABSTRACT

Aims To evaluate the performance of three MR perfusion software packages (A: RAPID; B: OleaSphere; and C: Philips) in predicting final infarct volume (FIV).

Methods This cohort study included patients treated with mechanical thrombectomy following an admission MRI and undergoing a follow-up MRI. Admission MRIs were post-processed by three packages to quantify ischemic core and perfusion deficit volume (PDV). Automatic package outputs (uncorrected volumes) were collected and corrected by an expert. Successful revascularization was defined as a modified Thrombolysis in Cerebral Infarction (mTICI) score ≥2B. Uncorrected and corrected volumes were compared between each package and with FIV according to mTICI score.

Results Ninety-four patients were included, of whom 67 (71.28%) had a mTICI score ≥2B. In patients with successful revascularization, ischemic core volumes did not differ significantly from FIV regardless of the package used for uncorrected and corrected volumes (p>0.15). Conversely, assessment of PDV showed significant differences for uncorrected volumes. In patients with unsuccessful revascularization, the uncorrected PDV of packages A (median absolute difference −40.9 mL) and B (median absolute difference −67.0 mL) overestimated FIV to a lesser degree than package C (median absolute difference −118.7 mL; p=0.03 and p=0.12, respectively). After correction, PDV did not differ significantly from FIV for all three packages (p≥0.99).

Conclusions Automated MRI perfusion software packages estimate FIV with high variability in measurement despite using the same dataset. This highlights the need for routine expert evaluation and correction of automated package output data for appropriate patient management.

INTRODUCTION

The efficacy of mechanical thrombectomy (MT) and intravenous thrombolysis has been demonstrated up to 24 hours and 9 hours after symptom onset, respectively, in selected patients with acute ischemic stroke (AIS).[1–5] A growing body of evidence indicates that quantification of ischemic core and salvageable brain tissue using advanced neuroimaging may have a major added value by ensuring better patient selection, especially in late-presenting AIS.[6–9]

In landmark trials, RAPID software has been used for CT and MR perfusion analysis and for patient selection.[1–5] However, other CT and MR perfusion packages are used in other centers around the world.

Studies have shown that the presumed volumes of ischemic core and salvageable brain tissue can vary significantly between CT perfusion software packages, which may influence patient selection for reperfusion therapy.[10–12] Indeed, post-processing of perfusion images is not standardized and suppliers of imaging software use different algorithms for data processing including de-noising, correction of motion artifacts, and calculation of perfusion maps.[13] It is therefore important to use validated software packages to decide on reperfusion therapy based on reliable data. In this context, few comparative data are available for MR perfusion software packages. Although two recent studies have reported substantial differences in ischemic core volume and the extent of ischemic penumbra,[14 15] these studies did not include the final infarct volume (FIV).[14 15] As a result, the accuracy of MR perfusion software packages in predicting FIV remains poorly explored.

We aimed to asses three MR perfusion packages (RAPID, OleaSphere, and Philips) used in clinical practice in predicting FIV in patients with AIS treated with MT and to determine whether correction of the outputs of the packages may improve FIV prediction.

METHODS

The local ethics committee approved the study and all subjects or their relatives signed an informed consent form (IRB number: 00009118).

Study design and patient cohort

The HIBISCUS-STROKE Cohort (CoHort of Patients to Identify Biological and Imaging markerS of CardiovascUlar Outcomes in Stroke; NCT: 03149705) is an ongoing observational study including all patients admitted to our stroke center since October 2016 for AIS due to large vessel occlusion of the anterior circulation (ie, occlusions of the internal carotid artery, M1 or M2 proximal segments of the middle cerebral artery). These patients were treated by MT following admission

To cite: Bani-Sadr A, Cho T-H, Cappucci M, *et al*. *J NeuroIntervent Surg* 2023;**15**:393–398.

MRI and had a follow-up MRI at day 6 to assess FIV. In accordance with international guidelines, eligible patients were additionally treated with intravenous thrombolysis.[16] We collected baseline data on demographic characteristics and National Institutes of Health Stroke Scale (NIHSS) scores at admission. Successful revascularization was defined as achieving a modified Thrombolysis in Cerebral Infarction (mTICI) score ≥2B.

The inclusion criteria for this study cohort were (1) availability of perfusion-weighted imaging (PWI) on the admission MRI and (2) availability of follow-up MRI.

MR image acquisition

Brain MRI was performed with 1.5 Tesla or 3 Tesla Ingenia scanners (Philips Healthcare, Best, The Netherlands). Initial brain MRI included parenchymal brain imaging (axial diffusion-weighted imaging (DWI), axial fluid-attenuation inversion recovery (FLAIR), T2*), angiographic sequences (three-dimensional (3D) Time-Of-Flight and contrast-enhanced MR angiography) and PWI (dynamic susceptibility contrast-enhanced MR perfusion). For PWI, a bolus of gadoterate meglumine (Dotarem; Guerbet, Aulnay-sous-Bois, France) was administered at a standard rate (0.1 mmol/kg body weight) at 4 mL/s via a power injector followed by 20 mL saline solution at the same dose. Follow-up MRI was performed on day 6 and comprised axial FLAIR. The acquisition parameters for these sequences are summarized in online supplemental table 1.

Quantification of baseline ischemic core and perfusion deficit volumes (PDV)

Admission MRIs were post-processed by three MR perfusion software packages:

Package A

RAPID (iSchemaView Inc, Menlo Park, USA) is a fully automated post-processing software package using a delay-insensitive deconvolution algorithm.[17–19]

Package B

Olea Sphere version 3.0.22 (Olea Medical, La Ciotat, France) is a fully automated post-processing software package used for quantitative stroke analysis. This package offers three deconvolution models: standard singular value decomposition, circular singular value decomposition,[20] oscillating index singular value decomposition.[21] In this study we used circular singular value deconvolution, which is a delay-insensitive algorithm proposed by default.

Package C

T2* Perfusion MR Clinical application Package, IntelliSpace Portal 11 (Philips Healthcare, The Netherlands) is a semi-automated post-processing software package using a delay-insensitive algorithm.

All packages used the same criteria to define ischemic core (apparent diffusion coefficient (ADC) ≤620 × 10^{-6} m^2/s) and PDV (Time-to-Maximum (Tmax) ≥6 s).

Package outputs were retrieved and corrected for all studies, blinded to FIV, for both ischemic core and PDV to obtain corrected volumes.

For package A, these corrections were performed by the company because the package does not allow the user to correct its outputs. The corrections consisted of reprocessing the images over a shorter time frame avoiding motion artifacts in combination with manual correction of segmentation errors. For packages B and C, the corrections were performed by a single investigator (ABS) and consisted of a manual correction of segmentation errors. Examples of corrections applied on ADC and Tmax maps are shown in online supplemental figure 1).

FIV assessment

FIV was segmented using day 6 FLAIR images with a semi-automated 3D Slicer (https://www.slicer.org/) after co-registration of day 6 FLAIR images and initial DWI images.

According to the mismatch model, we hypothesized that ischemic core expansion would be minimal in patients with successful revascularization resulting in close volumes for FIV and ischemic core volume. Conversely, in patients with unsuccessful revascularization, we hypothesized that the ischemic core would expand throughout the ischemic penumbra resulting in close volumes for FIV and PDV.

Evaluation of the clinical impact of volumetric differences between packages

To assess the clinical impact of volumetric differences, we assumed that the study population included patients admitted between 6 and 16 hours after last known normal. We counted the number of patients who would have been eligible for MT by applying DEFUSE 3 trial criteria using corrected volumes.[4]

Statistical analysis

The normal or non-normal distributions of each dataset were verified using the Shapiro–Wilk test and appropriate parametric or non-parametric tests were subsequently used. Continuous variables were expressed as medians and interquartile ranges (IQR) because none of them assumed a normal distribution and categorical data were summarized as counts and proportions. Volumes were compared using the non-parametric Wilcoxon test for paired differences with Bonferroni correction for multiple tests and correlations were measured using Pearson's correlation coefficient (r). A two-sided p value <0.05 was considered statistically significant and all statistical analyses were performed with R software version 3.2.1 (R Foundation for Statistical Computing, Vienna, Austria).

RESULTS

Study population characteristics, clinical and procedural outcomes

Among the 223 patients included in the cohort, 129 were excluded because PWI (n=69) and day 6 FLAIR (n=60) were not performed. The remaining 94 patients constituted the study population, of whom 67 (71.3%) had successful revascularization. The clinical, radiological, and outcome characteristics of the study population are shown in table 1.

For the ischemic core, package C provided a significantly smaller volume than package A (p=0.03) and there were no significant differences after correction (all p≥0.24). For PDV, packages A and B provided significantly smaller volumes than package A (p=0.002 and p=0.03, respectively), and there were no significant differences after correction (all p≥0.98). The correction time required was 173.00 s for package B (IQR 150.75; 205.00) and 152.00 s (IQR 116.75; 199.75, p=0.06) for package C.

Comparison of FIV and ischemic core volumes in patients with successful revascularization

In patients achieving successful revascularization, ischemic core volumes did not differ significantly from FIV for all

Table 1 Clinical, radiological, and outcome characteristics of the study population

	Whole population (n=94)	Successful reperfusion (n=67)	Unsuccessful reperfusion (n=27)
Clinical characteristics			
Age (years), median (IQR)	71.0 (54.8; 81.8)	70.0 (57.0; 82.5)	72.0 (51.0; 80.5)
Male, n (%)	54 (57.4)	39 (58.2)	15 (55.6)
Baseline NIHSS, median (IQR)	14.0 (8.0; 18.0)	15.0 (9.5; 17.0)	13.0 (6.5; 19.0)
Time from symtpom onset to MRI (min), median (IQR)	120.0 (87.5; 257.0)	109.0 (80.0; 251.5)	167.0 (99.5; 357.5)
Right side, n (%)	49 (52.1)	36 (53.7)	13 (48.1)
Occlusion site			
Internal carotid artery, n (%)	20 (21.3)	14 (20.9)	6 (22.2)
M1 segment of MCA, n (%)	55 (58.5)	43 (64.1)	12 (44.5)
M2 segment of MCA, n (%)	19 (20.2)	10 (14.9)	9 (33.3)
Procedural characteristics			
Time from MRI to groin puncture (min), median (IQR)	105.0 (78.0; 124.0)	102.5 (74.0; 123.8)	110.0 (78.8; 129.8)
Recanalisation degree, n (%)			
mTICI 0	10 (10.6)	–	10 (37.0)
mTICI 1	2 (2.1)	–	2 (7.4)
mTICI 2A	15 (16.0)	–	15 (55.6)
mTICI 2B	27 (28.7)	27 (40.3)	–
mTICI 2C	16 (17.0)	16 (23.9)	–
mTICI 3	24 (25.6)	24 (35.8)	–
Perfusion software package characteristics			
Uncorrected ischemic core (mL), median (IQR)			
Package A	31.0 (8.3; 60.5)	28.0 (8.5; 60.0)	44.0 (6.0; 65.0)
Package B	20.1 (9.4; 40.2)	19.2 (10.7; 36.2)	24.0 (6.1; 41.8)
Package C	12.6 (3.3; 31.2)	13.5 (4.8; 29.7)	10.2 (1.0; 31.2)
Corrected ischemic core (mL), median (IQR)			
Package A	24 (1.8; 57.0)	28.0 (8.5; 54.5)	22.0 (0.0; 56.0)
Package B	12.6 (3.5; 29.0)	13.2 (5.4; 29.0)	9.6 (2.2; 28.6)
Package C	13.1 (3.3; 32.2)	14.0 (4.5; 31.8)	10.3 (1.4; 32.3)
Uncorrected perfusion deficit volume (mL), median (IQR)			
Package A	102.0 (56.3; 158.0)	100.0 (72.5; 149.5)	105.0 (41.0; 180.5)
Package B	127.2 (83.1; 183.3)	132.3 (90.8; 182.4)	116.4 (70.7; 194.3)
Package C	174.8 (112.7; 279.3)	172.3 (107.7; 273.4)	183.0 (128.3; 305.1)
Corrected perfusion deficit volume (mL), median (IQR)			
Package A	102.0 (56.3; 158.0)	100.0 (72.5; 149.5)	105.0 (36.5; 180.5)
Package B	110.4 (66.6; 159.1)	121.4 (75.9; 158.4)	101.4 (49.1; 177.1)
Package C	104.1 (60.4; 150.7)	110 (64.2; 145.7)	87.3 (41.4; 154.9)
Final infarct volume (mL), median (IQR)	25.1 (7.8; 60.2)	20.3 (8.0; 56.9)	34.7 (6.9; 83.7)

MCA, middle cerebral artery; mTICI, modified Thrombolysis in Cerebral Infarction score; NIHSS, National Institute of Health Stroke Scale.

packages either for uncorrected or corrected volumes (all p≥0.28, figure 1). The correlations of uncorrected volumes and FIV were moderate for packages A and B (r=0.65 and r=0.62, respectively) and weak for package C (r=0.45). Bland–Altman analyses (figure 2) showed that ischemic core provided by packages B and C underestimated FIV both for uncorrected volumes (mean difference −13.5 mL (limits of agreement −94.1; 67.1) and −16.9 mL (limits of agreement (−107.8; 74.0), respectively) and corrected volumes (mean difference −18.7 mL (limits of agreement −99.2; 61.7) and −16.8 mL (limits of agreement −107.5; 73.8), respectively) compared with package A (mean difference −0.9 mL (limits of agreement −78.9; 77.0) for uncorrected volumes and mean difference −2.1 mL (limits of agreement −78.3; 74.1) for corrected volumes).

Comparison of FIV and PDV in patients with unsuccessful revascularization

In patients with unsuccessful revascularization, PDV overestimated FIV regardless of the package used for both uncorrected and corrected volumes (all p<0.05). Bland–Altman analyses (figure 3) indicated that the uncorrected PDV provided by packages A and B overestimated FIV to a lesser extent (mean difference 60.6 mL (limits of agreement −129.7; 251.0) and mean difference 77.2 mL (limits of agreement −111.6; 266.1),

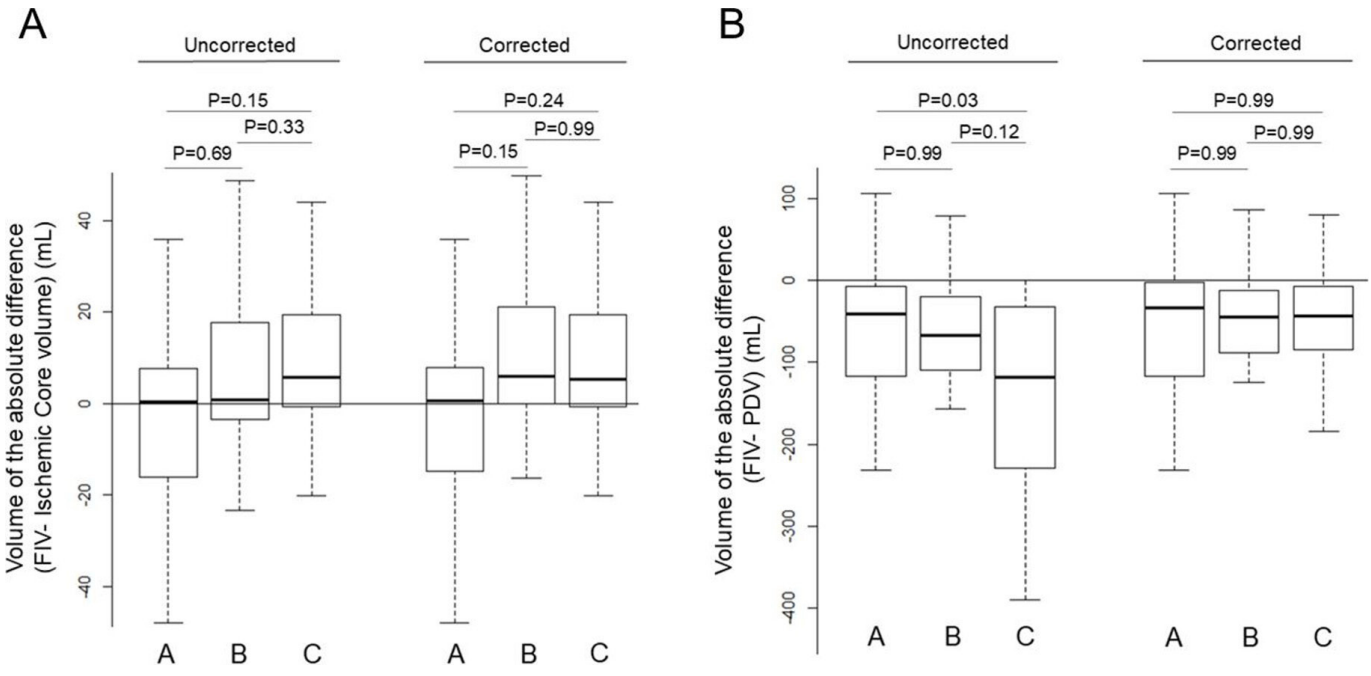

Figure 1 Boxplots of absolute difference (FIV – ischemic core volume or PDV). (A) Boxplots of absolute difference (FIV – ischemic core volume) in patients with successful revascularization. Before correction, medians of absolute differences (FIV – ischemic core volume) did not differ significantly between packages (all p>0.15); 0.32 mL (IQR −16.02; 7.57) for package A, 0.83 mL (IQR −3.47; 15.72) for package B, and 5.42 mL (IQR −0.67; 19.05) for package C. No significant difference was found after correction (all p>0.15). (B) Boxplots of absolute difference volumes (FIV – PDV) in patients with unsuccessful revascularization. Before correction, PDVs provided by package C (median of absolute difference −118.70 mL (IQR −228.83; −32.75)) overestimated FIV significantly compared with package A (median of absolute difference −40.93 mL (IQR −116.81; −7.81); p=0.03) and package B (median of absolute difference −67.51 mL (IQR −110.23; −20.49), p=0.12). After correction, the overestimation did not significantly differ between packages (all p=0.99). FIV, final infarct volume; PDV: perfusion deficit volume.

respectively) compared with package C (mean difference 182.0 mL (limits of agreement −196.8; 561.0)). The absolute differences (FIV – PDV) were significantly larger with package C compared with package A (p=0.03, figure 1). The correlations of uncorrected volumes and FIV were moderate for packages A and B (r=0.43 and 0.34, respectively), and negligible for package C (r=0.18). After correction, the overestimation of FIV was less with mean differences of 58.9 mL (limits of agreement −132.8; 251.0), 57.4 mL (limits of agreement −114.3; 229.2), and 40.5 mL (limits of agreement −95.0; 176.1) for packages A, B, and C, respectively. The absolute differences (FIV – PDV) were not significantly different between the three packages (all p≥0.99, figure 1).

Estimation of patients eligible for MT beyond 6 hours after last known normal

Assuming that the study population included patients admitted between 6 and 16 hours after last known normal, application of the DEFUSE 3 trial criteria would have led to MT in 51 patients (54.26%) with package A, 63 patients (67.02%) with package B, and 64 patients (65.96%) with package C when using corrected volumes. The number of patients eligible for MT and the detailed criteria when applying the thresholds of the DEFUSE 3 trial are shown in online supplemental table 2.

DISCUSSION

We aimed to assess the accuracy of three MR perfusion software packages in predicting FIV in patients with AIS treated by MT. Our primary findings are fourfold: (1) quantification of the ischemic core is reproducible among packages and correctly predicts FIV in patients with successful revascularization; (2) quantification of PDV differs significantly among packages, with packages A and B being more accurate in predicting FIV in patients with unsuccessful revascularization; (3) corrections to PDV outputs of packages may improve FIV prediction; and (4) volumetric differences of both ischemic core and PDV may lead to different treatment depending on the package used when applying strict volumetric criteria.

Regarding the volume of the ischemic core, package C provided significantly smaller uncorrected volumes compared with package A. After correction, no significant difference was found. Because these packages defined the ischemic core identically using the same threshold (ADC ≤620 × 10^{-6} m^2/s), our findings suggest that segmentation of DWI lesions is comparable. Based on the mismatch model, we hypothesized that ischemic core expansion would be minimal in patients with successful revascularization. Subgroup analysis of these patients indicated minor differences between FIV and uncorrected ischemic core volumes provided by the three packages. Some authors have argued that this method is limited because it does not distinguish pan-necrosis from incomplete necrosis within a voxel and does not account for the reversibility of DWI abnormalities.[22–24] Nevertheless, our results support that this is a clinically relevant method to quantify the ischemic core in current clinical practice.[25]

Uncorrected PDV, as used in clinical practice, differed significantly from one package to another whereas corrected PDV did not differ significantly. In patients with unsuccessful revascularization, PDV provided by package C overestimated FIV to a greater extent than packages A and B. The most likely explanation is a difference in the post-processing of PWI images including in motion artifact correction, perfusion map

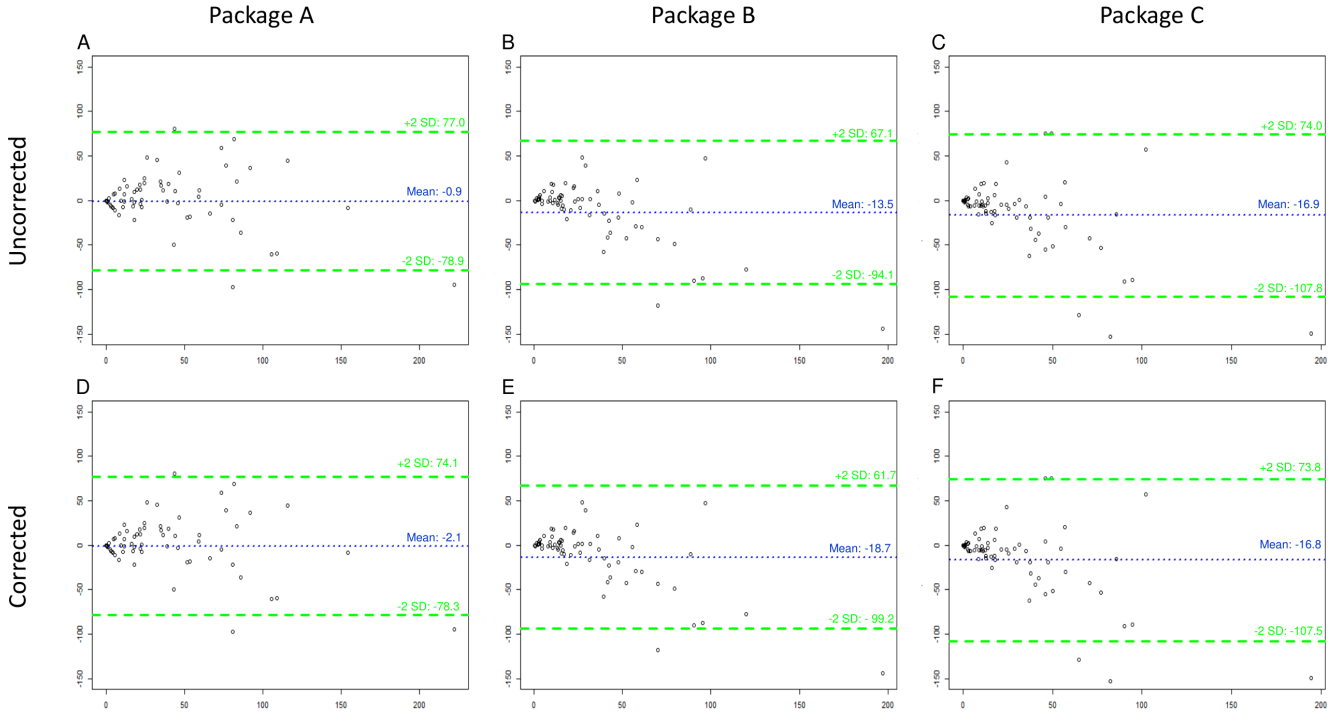

Figure 2 Bland–Altman plots comparing final infarct volume and ischemic core in patients with successful revascularization. The plots represent the absolute difference between the ischemic core and the final infarct volume (mL) as a function of the mean of two measurements before correction for packages A, B and C (A–C) and after correction for packages A, B and C (D–F). The blue line represents the mean difference and the green lines represent the limits of agreement (±2SD).

computation, and segmentation algorithms. These results are consistent with those of Deutschmann *et al* who compared PDV provided by RAPID and OleaSphere.[14] They reported a slightly larger ischemic core and smaller PDV for package A with a mean difference in presumed ischemic penumbra volume of almost 30 mL.[14] In the present study, we evaluated FIV using follow-up MRI on day 6 which allowed us to assess the accuracy of predictions.[26 27] After correction, overestimation was smaller and did not differ significantly among the three packages. This suggests that automatic segmentation of perfusion maps should be carefully checked and corrected, if necessary, before considering them in the reperfusion decision.

Accordingly, assuming that the study population included patients admitted between 6 and 16 hours after symptom onset and applying DEFUSE 3 trial criteria, the use of corrected volumes provided by package A would have led to more

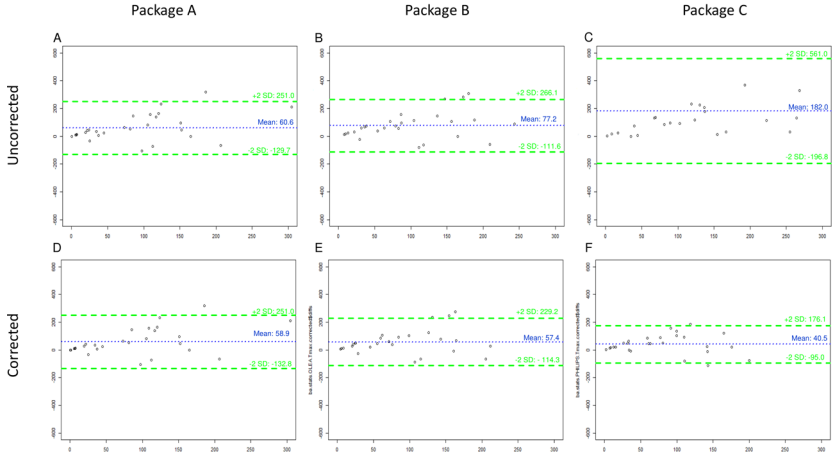

Figure 3 Bland–Altman plots comparing final infarct volume and perfusion deficit volumes in patients with successful revascularization. The plots represent the absolute difference between the perfusion deficit volume and the final infarct volume as a function of the mean of two before correction for packages A, B and C (A–C) and after correction for packages A, B and C (D–F). The blue line represents the mean difference and the green lines represent the limits of agreement (±2SD).

restricted indications for MT (n=51/94) compared with packages B (n=63/94) and C (n=64/94). In our study population, the critical explanatory factor is the difference of patients with an estimated ischemic core >70 mL (difference of n=12 between packages A and B and n=11 between packages B and C). These results are consistent with those of Deutschmann *et al* who found RAPID to be more restrictive in MT indications when applying DEFUSE 3 criteria.[14] In the context of ongoing studies intended to treat patients with larger core,[28 29] the results of the packages should be assessed with caution in the MT decision-making process.

Several possible limitations should be considered in this study. In addition to the single-center nature of this cohort, the major limitation of this study is the small number of patients with unsuccessful revascularization (n=26). This might limit statistical power, especially for the comparison of PDV provided by packages A and B. This also prevented us from performing other analyses that took into account critical factors such as the degree of revascularization (ie, TICI score 0 vs 1 and 2A) and the time elapsed from admission MRI to revascularization. Finally, corrections have been made by an expert for packages B and C. These additional corrections may have a limited value in clinical practice as this approach is time consuming, especially in non-expert centers. This argues for automatic correction as performed by RAPID in the setting of AIS.

CONCLUSIONS

Automated MR perfusion software packages estimate FIV with high variability in measurement despite using the same dataset. This highlights the need for routine expert evaluation and correction of automated package output data for appropriate patient management.

Contributors ABS, THC, NN and YB conceived and designed the project. YB and NN supervised the project. ABS, LM and OFE performed the measurements. THC, MC, MH, RA, AF, RR, LD, CDB, LM and OFE made substantial contributions to acquisition of data. ABS, LM, LD, NN and YB drafted the article and revised it critically and is the guarantor of the study. YB is the guarantor of this study. All authors approved the version to be published.

Funding This study was supported by the RHU MARVELOUS (Recherche Hospitalo-Universitaire MR Imaging to Prevent Cerebral and Myocardial Injury, ANR-16-RHUS-0009) of Claude Bernard University, Lyon I within the program "Investissements d'Avenir" operated by the French National Research Agency (ANR).

Competing interests None declared.

Patient consent for publication Consent obtained directly from patient(s)

Ethics approval This study involves human participants. Institutional Review Board (Hospices Civils de Lyon, Lyon, France) approval was obtained (IRB number: 00009118). Participants gave informed consent to participate in the study before taking part.

Provenance and peer review Not commissioned; externally peer reviewed.

Data availability statement Data are available upon reasonable request. Data are available upon reasonable request from the corresponding author.

ORCID iDs
Alexandre Bani-Sadr http://orcid.org/0000-0002-1808-2484
Matteo Cappucci http://orcid.org/0000-0002-4198-1410
Laura Mechtouff http://orcid.org/0000-0001-9165-5763

REFERENCES

1 Campbell BCV, Mitchell PJ, Kleinig TJ, *et al*. Endovascular therapy for ischemic stroke with perfusion-imaging selection. *N Engl J Med* 2015;372:1009–18.
2 Saver JL, Goyal M, Bonafe A, *et al*. Stent-retriever thrombectomy after intravenous t-PA vs. t-PA alone in stroke. *N Engl J Med* 2015;372:2285–95.
3 Nogueira RG, Jadhav AP, Haussen DC, *et al*. Thrombectomy 6 to 24 hours after stroke with a mismatch between deficit and infarct. *N Engl J Med* 2018;378:11–21.
4 Albers GW, Marks MP, Kemp S, *et al*. Thrombectomy for stroke at 6 to 16 hours with selection by perfusion imaging. *N Engl J Med* 2018;378:708–18.
5 Ma H, Campbell BCV, Parsons MW, *et al*. Thrombolysis guided by perfusion imaging up to 9 hours after onset of stroke. *N Engl J Med* 2019;380:1795–803.
6 Campbell BC, Parsons MW. Imaging selection for acute stroke intervention. *Int J Stroke* 2018;13:554–67.
7 Bivard A, Parsons M. Tissue is more important than time: insights into acute ischemic stroke from modern brain imaging. *Curr Opin Neurol* 2018;31:23–7.
8 Tsivgoulis G, Katsanos AH, Schellinger PD. Advanced neuroimaging in stroke patient selection for mechanical thrombectomy: a systematic review and meta-analysis. *Stroke* 2018;49:3067–70.
9 Campbell BCV, Khatri P. Stroke. *The Lancet* 2020;396:129–42.
10 Austein F, Riedel C, Kerby T, *et al*. Comparison of perfusion CT software to predict the final infarct volume after thrombectomy. *Stroke* 2016;47:2311–7.
11 Koopman MS, Berkhemer OA, Geuskens RREG, *et al*. Comparison of three commonly used CT perfusion software packages in patients with acute ischemic stroke. *J Neurointerv Surg* 2019;11:1249–56.
12 Rava RA, Snyder KV, Mokin M, *et al*. Assessment of computed tomography perfusion software in predicting spatial location and volume of infarct in acute ischemic stroke patients: a comparison of Sphere, Vitrea, and RAPID. *J Neurointerv Surg* 2021;13:130–5.
13 Demeestere J, Wouters A, Christensen S, *et al*. Review of perfusion imaging in acute ischemic stroke: from time to tissue. *Stroke* 2020;51:1017–24.
14 Deutschmann H, Hinteregger N, Wießpeiner U, *et al*. Automated MRI perfusion-diffusion mismatch estimation may be significantly different in individual patients when using different software packages. *Eur Radiol* 2021;31:658–65.
15 Pistocchi S, Strambo D, Bartolini B, *et al*. MRI software for diffusion-perfusion mismatch analysis may impact on patients' selection and clinical outcome. *Eur Radiol* 2022;32:1144–53.
16 Powers WJ, Rabinstein AA, Ackerson T, *et al*. Guidelines for the early management of patients with acute ischemic stroke: 2019 update to the 2018 guidelines for the early management of acute ischemic stroke: a guideline for healthcare professionals from the American Heart Association/American Stroke Association. *Stroke* 2019;50.
17 Albers GW, Goyal M, Jahan R, *et al*. Ischemic core and hypoperfusion volumes predict infarct size in SWIFT PRIME. *Ann Neurol* 2016;79:76–89.
18 Wheeler HM, Mlynash M, Inoue M, *et al*. Early diffusion-weighted imaging and perfusion-weighted imaging lesion volumes forecast final infarct size in DEFUSE 2. *Stroke* 2013;44:681–5.
19 Rao V, Christensen S, Yennu A, *et al*. Ischemic core and hypoperfusion volumes correlate with infarct size 24 hours after randomization in DEFUSE 3. *Stroke* 2019;50:626–31.
20 Ostergaard L, Weisskoff RM, Chesler DA, *et al*. High resolution measurement of cerebral blood flow using intravascular tracer bolus passages. Part I: Mathematical approach and statistical analysis. *Magn Reson Med* 1996;36:715–25.
21 Wu O, Østergaard L, Weisskoff RM, *et al*. Tracer arrival timing-insensitive technique for estimating flow in MR perfusion-weighted imaging using singular value decomposition with a block-circulant deconvolution matrix. *Magn Reson Med* 2003;50:164–74.
22 Garcia JH, Lassen NA, Weiller C, *et al*. Ischemic stroke and incomplete infarction. *Stroke* 1996;27:761–5.
23 Labeyrie M-A, Turc G, Hess A, *et al*. Diffusion lesion reversal after thrombolysis: a MR correlate of early neurological improvement. *Stroke* 2012;43:2986–91.
24 Goyal M, Ospel JM, Menon B, *et al*. Challenging the ischemic core concept in acute ischemic stroke imaging. *Stroke* 2020;51:3147–55.
25 Røhl L, Østergaard L, Simonsen CZ, *et al*. Viability thresholds of ischemic penumbra of hyperacute stroke defined by perfusion-weighted MRI and apparent diffusion coefficient. *Stroke* 2001;32:1140–6.
26 Tourdias T, Renou P, Sibon I, *et al*. Final cerebral infarct volume is predictable by MR imaging at 1 week. *AJNR Am J Neuroradiol* 2011;32:352–8.
27 Krongold M, Almekhlafi MA, Demchuk AM, *et al*. Final infarct volume estimation on 1-week follow-up MR imaging is feasible and is dependent on recanalization status. *Neuroimage Clin* 2015;7:1–6.
28 Sarraj A, Hassan AE, Savitz S, *et al*. Outcomes of endovascular thrombectomy vs medical management alone in patients with large ischemic cores: a secondary analysis of the Optimizing Patient's Selection for Endovascular Treatment in Acute Ischemic Stroke (SELECT) study. *JAMA Neurol* 2019;76:1147.
29 Panni P, Gory B, Xie Y. Acute stroke with large ischemic core treated by thrombectomy: predictors of good outcome and mortality. *Stroke* 2019;50:1164–71.

Étude n°3 : Le seuil optimal de Tmax identifiant le volume du trouble de perfusion est-il variable selon les logiciels de perfusion IRM ? Une étude pilote.

Contexte et état de la question.

Dans l'étude n°2, nous avions constaté que le logiciel OleaSphere® fournissait des volumes d'hypoperfusion plus étendus que le logiciel RAPID®. Cette observation était concordante avec les résultats de Deutschmann et al [102]. Nous avons donc fait l'hypothèse que le seuil de Time-To-Maximum (Tmax) optimal dans la prédiction du volume final de la lésion ischémique était variable d'un logiciel à l'autre. Ce troisième travail visait à déterminer le seuil de Tmax optimal pour prédire le volume final de la lésion ischémique pour les logiciels RAPID® et OleaSphere® chez des patients en échec de thrombectomie mécanique (score mTICI=0).

Principaux résultats.

Nos résultats ont indiqué que les meilleures prédictions des volumes finaux étaient obtenues pour RAPID® avec un seuil de Tmax ≥6s et pour OleaSphere® avec un seuil de Tmax ≥10s. Ces résultats impliquent que le seuil de Tmax ≥ 6s utilisé par défaut pour la plupart des logiciels de perfusion IRM pourrait ne pas être optimal pour tous les logiciels.

Magnetic Resonance Materials in Physics, Biology and Medicine
https://doi.org/10.1007/s10334-023-01068-0

RESEARCH ARTICLE

Is the optimal Tmax threshold identifying perfusion deficit volumes variable across MR perfusion software packages? A pilot study

Alexandre Bani-Sadr[1,2] · Mathilde Trintignac[1] · Laura Mechtouff[3,4] · Marc Hermier[1] · Matteo Cappucci[1] · Roxana Ameli[1] · Charles de Bourguignon[5] · Laurent Derex[3] · Tae-Hee Cho[3,4] · Norbert Nighoghossian[3,4] · Omer Faruk Eker[1,2] · Yves Berthezene[1,2]

Received: 23 October 2022 / Revised: 6 February 2023 / Accepted: 7 February 2023

Abstract

Purpose Accurate quantification of ischemic core and ischemic penumbra is mandatory for late-presenting acute ischemic stroke. Substantial differences between MR perfusion software packages have been reported, suggesting that the optimal Time-to-Maximum (Tmax) threshold may be variable. We performed a pilot study to assess the optimal Tmax threshold of two MR perfusion software packages (A: RAPID®; B: OleaSphere®) by comparing perfusion deficit volumes to final infarct volumes as ground truth.

Methods The HIBISCUS-STROKE cohort includes acute ischemic stroke patients treated by mechanical thrombectomy after MRI triage. Mechanical thrombectomy failure was defined as a modified thrombolysis in cerebral infarction score of 0. Admission MR perfusion were post-processed using two packages with increasing Tmax thresholds (≥ 6 s, ≥ 8 s and ≥ 10 s) and compared to final infarct volume evaluated with day-6 MRI.

Results Eighteen patients were included. Lengthening the threshold from ≥ 6 s to ≥ 10 s led to significantly smaller perfusion deficit volumes for both packages. For package A, Tmax ≥ 6 s and ≥ 8 s moderately overestimated final infarct volume (median absolute difference: – 9.5 mL, interquartile range (IQR) [– 17.5; 0.9] and 0.2 mL, IQR [– 8.1; 4.8], respectively). Bland–Altman analysis indicated that they were closer to final infarct volume and had narrower ranges of agreement compared with Tmax ≥ 10 s. For package B, Tmax ≥ 10 s was closer to final infarct volume (median absolute difference: – 10.1 mL, IQR: [– 17.7; – 2.9]) versus – 21.8 mL (IQR: [– 36.7; – 9.5]) for Tmax ≥ 6 s. Bland–Altman plots confirmed these findings (mean absolute difference: 2.2 mL versus 31.5 mL, respectively).

Conclusions The optimal Tmax threshold for defining the ischemic penumbra appeared to be most accurate at ≥ 6 s for package A and ≥ 10 s for package B. This implies that the widely recommended Tmax threshold ≥ 6 s may not be optimal for all available MRP software package. Future validation studies are required to define the optimal Tmax threshold to use for each package.

Keywords Stroke · Thrombectomy · Perfusion MR · Image processing

✉ Alexandre Bani-Sadr
apbanisadr@gmail.com; alexandre.bani-sadr@chu-lyon.fr

[1] Department of Neuroradiology, East Group Hospital, Hospices Civils de Lyon, 59 Bd Pinel, 69500 Bron, France

[2] CREATIS Laboratory, CNRS UMR 5220, INSERM U 5220, Claude Bernard Lyon I University, 7 Avenue Jean Capelle O, 69100 Villeurbanne, France

[3] Stroke Department, East Group Hospital, Hospices Civils de Lyon, 59 Bd Pinel, 69500 Bron, France

[4] CarMeN Laboratory, INSERM U1060, Claude Bernard Lyon I University, 59 Bd Pinel, 69500 Bron, France

[5] Clinical Investigation Center, INSERM, 1407. 59 Bd Pinel, 69500 Bron, France

Introduction

Mechanical thrombectomy (MT) has dramatically improved the treatment of large-vessel-occlusion acute ischemic stroke (AIS) [1, 2]. It has been demonstrated to be effective up to 24 h after symptoms onset in patients selected by perfusion imaging [3, 4]. Therefore, accurate quantification of the ischemic core and salvageable brain tissue is mandatory.

In imaging, the concept of mismatch is a surrogate marker for quantifying the volume of salvageable brain tissue (i.e., the ischemic penumbra, a critically perfused tissue at risk of infarction if no reperfusion is established to maintain

Published online: 22 February 2023

viability [5]). It is the difference between the perfusion deficit and the ischemic core. In clinical practice, multiple CT perfusion and MR perfusion (MRP) software packages are routinely used to quantify the ischemic penumbra. Comparative studies of CT perfusion software packages have indicated significant differences in ischemic core and perfusion deficit volumes (PDV) which may influence patient selection for reperfusion therapy [6, 7]. Recently, authors have compared two commonly used MRP software packages and reported a mean difference in presumed penumbra volume of almost 30 mL despite using the same parameter and the same threshold to delineate the ischemic core [8] (Apparent Diffusion Coefficient $\leq 620 \times 10^{-6}$ m^2/s) and the perfusion deficit (Time-to-Maximum (Tmax) ≥ 6 s). These authors have indicated that the differences in penumbral volumes were mainly related to different PDV [8]. Therefore, we hypothesized that the optimal Tmax threshold delineating perfusion deficit volumes was variable across MRP software packages.

We performed a pilot study comparing the final infarct volume (FIV) to PDV obtained from two commonly used MRP software packages (A: RAPID®; B: OleaSphere®) with various Tmax threshold in AIS patients with failed reperfusion after MT.

Materials and methods

Study population

HIBISCUS-STROKE Cohort (CoHort of Patients to Identify Biological and Imaging markerS of CardiovascUlar Outcomes in Stroke; NCT: 03149705) is an ongoing observational study since October, 2016 that included anterior circulation AIS patients due to large vessel occlusions (i.e., occlusions of internal carotid artery, and M1 or M2 proximal segments of middle cerebral artery) treated with MT after multimodal brain MRI. In accordance with international guidelines, eligible patients were additionally treated with intravenous thrombolysis [9]. They underwent a brain CT scan at day 1 to rule out any hemorrhagic transformation and a follow-up MRI at day 6 to assess FIV.

We defined failed reperfusion after MT as achieving a modified thrombolysis in cerebral infarction reperfusion (mTICI) score = 0.

Inclusion criteria in this retrospective study were: (1) available MRP, (2) available follow-up MRI, and 3) mTICI score = 0.

Neuroimaging

Brain MRIs were performed with 1.5-Tesla or 3-Tesla *Ingenia* scanners (*Philips Healthcare, Best, The Netherlands)*. The admission brain MRI protocol included axial diffusion-weighted imaging (DWI), axial T2 fluid-attenuated inversion recovery (T2-FLAIR), axial T2-gradient echo, 3D time-of-flight MRA, dynamic-susceptibility-contrast MRI, and contrast-enhanced MRA. For MRP, a bolus of gadoterate meglumine (*Dotarem; Guerbet, Aulnay-sous-Bois, France*) was administered at a standard dose (0.1 mmol/kg weight body) at 4 mL/s via a power injector followed by 20 mL of saline solution at a same dose. Follow-up MRI was performed at day 6 and comprised axial T2-FLAIR. Supplemental Table 1 summarizes the acquisitions parameters of these sequences.

Quantification of PDV

PDV were calculated automatically using the following MRP software packages.

Package A

RAPID® (iSchemaView Inc, Menlo Park, USA) is a fully automated post-processing software package using a delay-insensitive deconvolution algorithm [10–12].

Package B

OleaSphere® version 3.0.22 (Olea Medical, La Ciotat, France) is a fully automated post-processing software package. This package offers three deconvolutions' models: standard singular value decomposition, circular singular value decomposition [13], and oscillating index singular value decomposition [14]. In this study, we used the circular singular value deconvolution which is a delay-insensitive algorithm proposed by default.

Both packages recommend a threshold of Tmax ≥ 6 s to define ischemic penumbra.

Table 1 Baseline characteristics of study population

Study Population (*n*)	18
Age (years), median [IQR]	70.6 [59.8–81.5]
Males, *n* (%)	7 (44.4)
Tobacco, *n* (%)	4 (22.2)
Hypertension, *n* (%)	10 (55.6)
Diabetes mellitus, *n* (%)	6 (42.9)
Dyslipidemia, *n* (%)	4 (22.2)
Intravenous thrombolysis, *n* (%)	13 (72.2)
Time from symptom onset to MRI (min), median [IQR]	106.5 [97.5–1726.5]
ASPECTS-DWI score, median [IQR]	8.0 [7.0–9.0]

IQR Interquartile Range, *ASPECTS-DWI* Diffusion-Weighted Imaging Alberta Stroke Program Early Computed Tomography Scores

For PDV, we assessed three increasing Tmax thresholds (Tmax ≥ 6 s, ≥ 8 s, and ≥ 10 s), since a previous report indicated that package B overestimated PDV compared to package A [8]. In addition, package A defaults PDV defaults PDV for Tmax thresholds of ≥ 4 s, ≥ 6 s, ≥ 8 s, and ≥ 10 s.

According to the perfusion–diffusion mismatch model, we assumed that the optimal Tmax threshold would provide PDV that would be close to FIV in non-reperfused patients (mTICI score = 0).

FIV assessment

FIV was segmented using day-6 T2-FLAIR images by a stroke neurologist (THC) with expertise in neurovascular imaging (> 15 years) using a semi-automated (3D Slicer: https://www.slicer.org/) after co-registration of day-6 T2-FLAIR images and baseline DWI images.

Statistical analysis

The normal or non-normal distributions of each dataset were verified using the Shapiro–Wilk test, and appropriate parametric or non-parametric tests were subsequently used. Continuous variables were expressed as means and standard deviations or medians and interquartile ranges (IQR) according to the normality of their distribution, and categorical data were summarized as counts and proportions. Volumes were compared using non-parametric Wilcoxon test for paired differences. Descriptive statistics, Spearman's correlation coefficient, and linear regression analysis were used to compare FIV and hypoperfused tissue volume. Spearman's correlation coefficients were compared for the three different Tmax threshold from *t* tests [25]. Bland–Altman analyses were performed to assess volumetric agreement between FIV and hypoperfusion tissue volume for each MR perfusion software package, and for each Tmax threshold. A two-sided p value < 0.05 was considered as statistically significant, and all statistical analyses were performed with R software, version 3.2.1 (*R foundation for Statistical Computing, Vienna, Austria*).

Results

Study population

Since October 2016, 239 subjects were included in the HIBISCUS-STROKE cohort. Among them, 101 patients were excluded, because MRP and/or day-6 T2-FLAIR were not performed. Among the 138 remaining patients, 19 patients (13.8%) had failed MT with an mTICI score of 0. One patient was excluded because of excessive motion artifacts leading to unexploitable MRP for both MRP software packages. The remaining 18 patients constituted the study population. Median age was 70.6 years (IQR: [59.8–81.5]) and seven (44.4%) were males. Median National Institute of Health Stroke score was 6.0 (IQR: [3.5–8.5]) and, mean FIV was 25.6 (± 47.6) mL. Table 1 summarizes baseline clinical and radiological characteristics of study population.

Effect of lengthening the Tmax threshold

Table 2 presents PDV and FIV obtained for each patient.

Lengthening the Tmax threshold from ≥ 6 to ≥ 8 s and ≥ 10 s led to smaller PDV with medians of 13.5 mL (IQR: [9.0; 35.3]), 5.5 mL (IQR: [0.0; 23.5]), and 3.5 mL (IQR: [0.0; 11.8]), respectively, for package A and of 35.2 mL (IQR: [18.7; 67.5]), 24.2 mL (IQR: [12.1; 44.6]), and 20.2 mL (IQR: [10.6; 36.3]), respectively, for package B. Volumes obtained using Tmax ≥ 10 s were significantly smaller than those obtained with Tmax ≥ 6 s ($p = 0.01$ for package A and, $p = 0.05$ for package B). Figure 1 illustrates the impact of lengthening the Tmax threshold on PDV for both MRP software packages.

Figure 2 presents boxplots of absolute difference between FIV and PDV. For package A, Tmax ≥ 6 s moderately overestimated FIV (median absolute difference: – 9.5 mL, IQR: [– 17.5; 0.9]) compared with Tmax ≥ 8 s (median absolute difference: 0.2 mL, [– 8.1; 4.5]), but the difference was not statistically significant ($p = 0.10$). As presented in Fig. 3, Bland–Altman analysis indicated that Tmax thresholds ≥ 6 s and ≥ 8 s were closer to FIV (mean absolute differences 4.8 and – 8.4 mL) compared to the Tmax threshold ≥ 10 s (mean absolute difference – 17.4 mL). The ranges of agreement were also narrower for thresholds ≥ 6 s and ≥ 8 s.

For package B, PDV overestimated FIV regardless of the Tmax threshold used. The threshold of Tmax ≥ 10 s provided volumes closer to FIV with a median absolute difference of – 10.1 mL (IQR: [– 17.7; – 2.9]) versus – 21.8 mL (IQR: [– 36.7; – 9.5]) with Tmax ≥ 6 s. Bland–Altman plots indicated the threshold of Tmax ≥ 10 s was closer to FIV compared to Tmax ≥ 6 s (mean absolute difference: 2.2 mL versus 31.5 mL). The ranges of agreements were also narrower. As presented in Table 3, correlation coefficients tended to be higher for Tmax ≥ 10 s, but this was not statistically significant (all $p > 0.34$).

Discussion

Our results indicate that Tmax threshold ≥ 6 s is optimal for package A, while a Tmax threshold ≥ 10 s is more appropriate for package B to forecast FIV in patients with failed MT. These findings suggest that optimal Tmax threshold varies depending on the MRP software package used. This may

Table 2 Detailed volumes obtained for included patients

Patient	Sex	Age	Thrombolysis	Final infarct volume (mL)	Package A			Package B			Significant visual overlap		
					PDV Tmax ≥ 10 s (mL)	PDV Tmax ≥ 8 s (mL)	PDV Tmax ≥ 6 s (mL)	PDV Tmax ≥ 10 s (mL)	PDV Tmax ≥ 8 s (mL)	PDV Tmax ≥ 6 s (mL)	Between FIV and PDV of Package A	Between FIV and PDV of Package B	Between PDV of Packages A and B
1	F	94	Yes	129.9	30.0	91.0	175.0	114.8	154.5	246.3	Yes	Yes	Yes
2	M	70	No	10.8	15.0	24.0	37.0	22.9	30.1	45.0	Yes	Yes	Yes
3	F	82	Yes	96.3	37.0	52.0	73.0	34.3	44.9	61.0	Yes	Yes	Yes
4	M	60	Yes	0.2	0.0	0.0	4.0	20.3	23.6	33.3	Yes	Yes	Yes
5	F	55	No	0.3	0.0	18.0	30.0	16.0	24.8	37.1	Yes	Yes	Yes
6	F	72	Yes	2.3	0.0	0.0	0.0	61.1	62.2	69.7	No	Yes	No
7	M	83	Yes	1.2	0.0	0.0	0.0	10.5	11.1	14.6	No	Yes	No
8	F	80	Yes	41.1	0.0	0.0	9.0	1.2	4.5	17.0	Yes	Yes	Yes
9	M	78	No	5.4	5.0	16.0	49.0	90.5	118.5	191.6	Yes	Yes	Yes
10	F	80	No	11.3	14.0	22.0	30.0	25.4	31.2	47.8	Yes	Yes	Yes
11	F	62	No	0.3	4.0	6.0	9.0	9.1	11.6	16.1	Yes	Yes	Yes
12	F	37	Yes	10.6	3.0	5.0	12.0	14.4	15.2	18.8	Yes	Yes	Yes
13	M	50	Yes	0.2	0.0	3.0	15.0	4.0	5.7	18.7	Yes	Yes	Yes
14	M	66	Yes	0.7	4.0	4.0	11.0	37.0	43.9	75.9	Yes	Yes	Yes
15	F	91	No	0.2	0.0	0.0	0.0	2.7	2.9	3.8	No	No	No
16	M	60	Yes	0.1	5.0	9.0	17.0	11.0	13.6	21.3	Yes	Yes	Yes
17	F	50	No	148.5	30.0	48.0	76.0	43.0	58.7	86.7	Yes	Yes	Yes
18	F	88	Yes	1.7	0.0	0.0	12.0	20.1	21.6	24.0	No	Yes	No

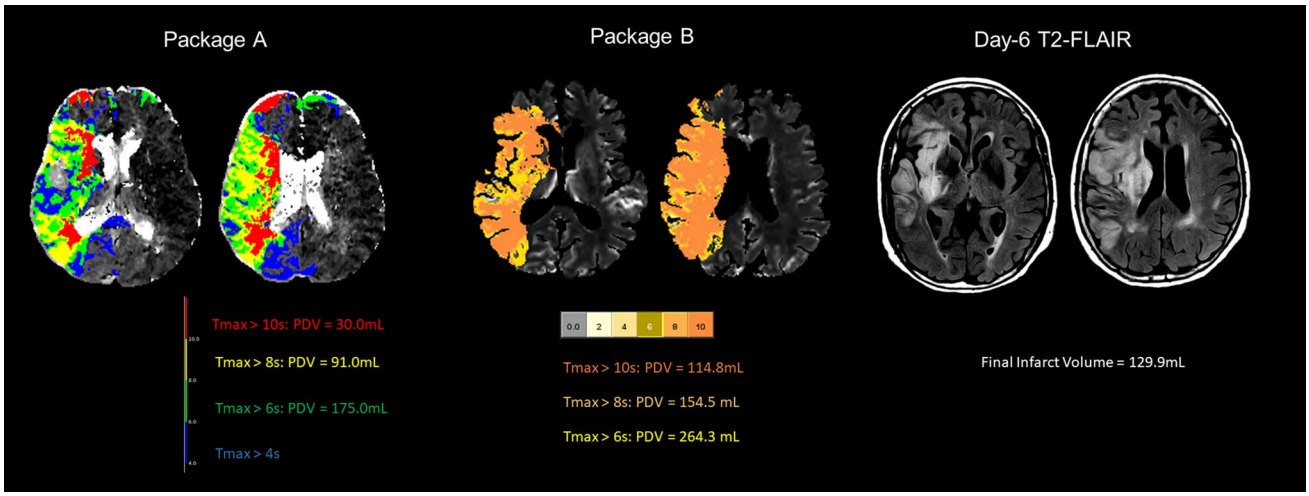

Fig. 1 Effect of Tmax threshold lengthening on perfusion deficit volume. This figure illustrates the difference of perfusion deficits volumes depending on the MR perfusion package used. For package A, volumes using Tmax thresholds ≥ 6 s and ≥ 8 s were closer to the final infarct volume. Conversely, for package B, the best prediction of final infarct volume was found using a Tmax threshold ≥ 10 s. *Tmax* Time-to-Maximum, *T2-FLAIR* T2-Fluid-Attenuated Inversion Recovery

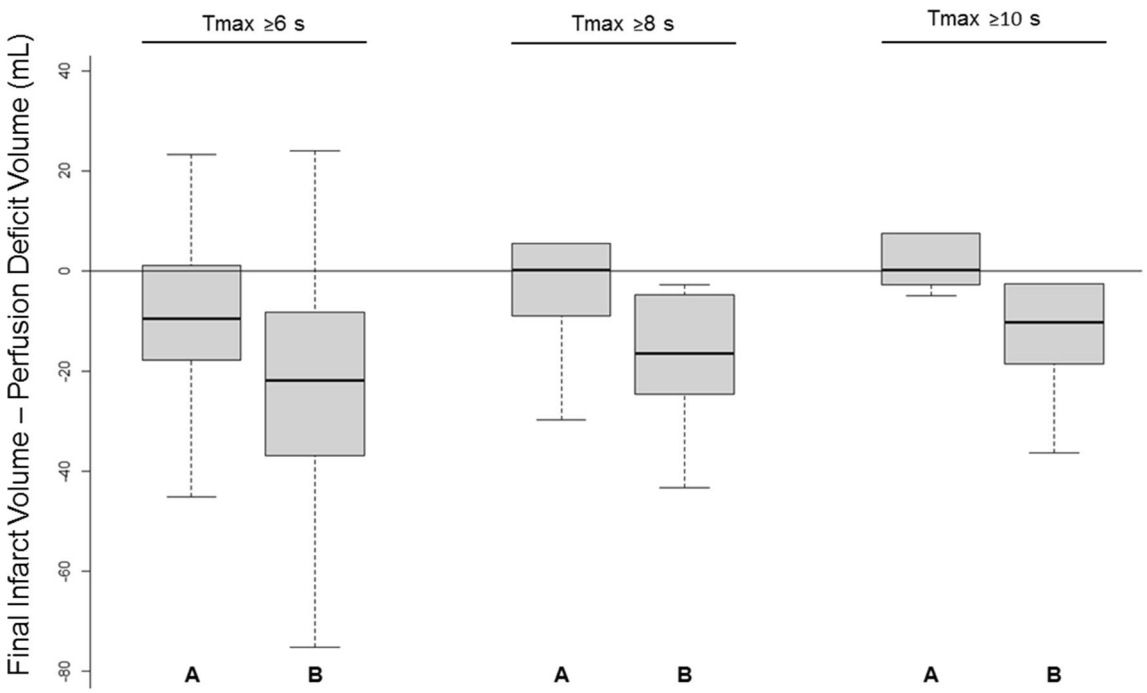

Fig. 2 Boxplots of absolute difference between final infarct volume and perfusion deficit volume according to the Tmax threshold. Boxplots of absolute difference between final infarct volume (FIV) and perfusion deficit volume according to the Time-to-Maximum threshold used for packages A and B. Thick horizontal lines represent median of differences and boxes represent the 25th–75th percentiles. Error bars indicate the range of absolute difference between FIV and presumed penumbra volumes. Horizontal line indicates 0. *A* Package A; *B* Package B, *Tmax* Time-to-Maximum

result from non-standardization of perfusion images post-processing [15].

In agreement with a previous study, we found that PDV obtained using RAPID® were smaller compared to Olea Sphere® despite using the same Tmax threshold [8, 16]. Similarly, a recent study compared RAPID® to another commercially available MRP software package (Carestream®) and reported similar results with smaller PDV with RAPID®

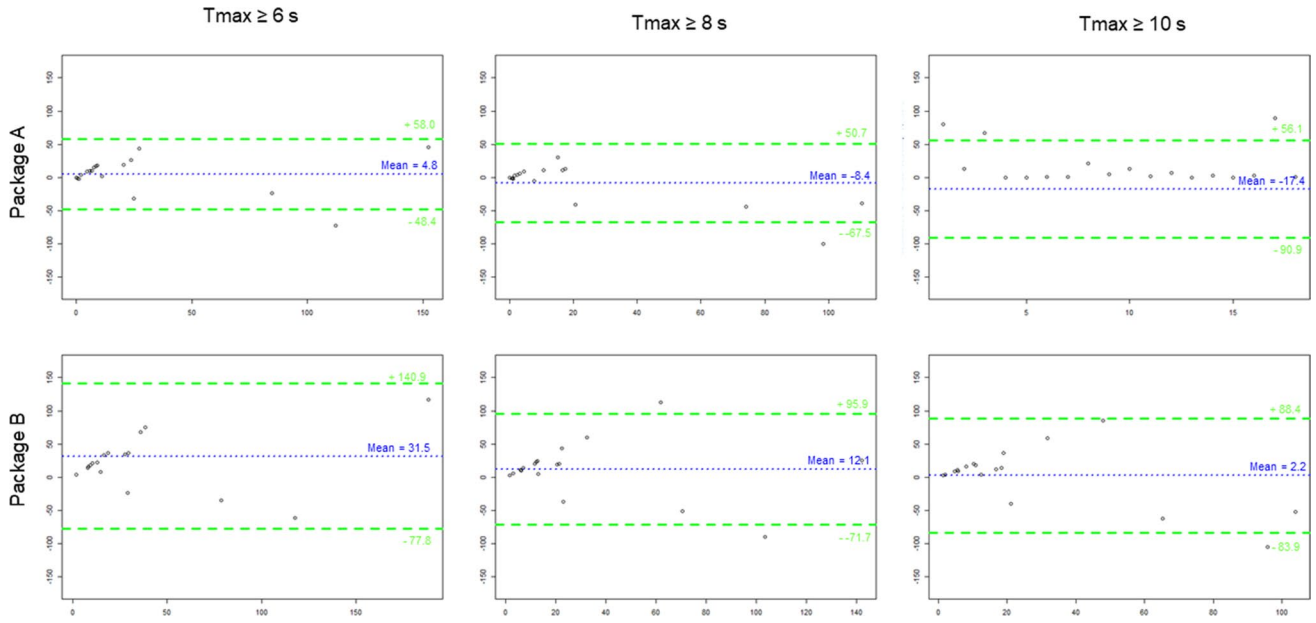

Fig. 3 Bland–Altman plots analyses. Bland–Altman plots comparing measured final infarct volume and expected final infarct volume according to the MR perfusion software package used and the Time-to-Maximum threshold. The plots represent the absolute difference between the measured final infarct volume and the expected final infarct volume (mL) as a function of the mean of the two measurements. The blue dotted horizontal line indicates the mean of the differences and the green dashed lines represent 95% limits of agreement. *Tmax* Time-to-Maximum

Table 3 Spearman's correlation coefficient between final infarct volume and perfusion deficit volume

Package A			Package B		
Tmax ≥ 6 s	Tmax ≥ 8 s	Tmax ≥ 10 s	Tmax ≥ 6 s	Tmax ≥ 8 s	Tmax ≥ 10 s
0.60	0.55	0.49	0.52	0.56	0.55

Tmax Time-to-Maximum

[17]. These studies pointed noticed that these volumetric differences might have dramatic clinical impact, because they may result in different patient selection for MT depending on the MRP software package used [8, 17].

The idea that these two tissues coexist (i.e., the ischemic core and the penumbra) in AIS pathogenesis emerged in the late 70 s when microelectrode studies of the baboon cortex indicated a level of cerebral blood flow that led to cell death when progressive CBF reduction was applied [5, 18]. Since, plethora of techniques have been assessed to map the ischemic penumbra, such as ^{15}O positron emission tomography (PET), single photon-emission computed tomography, Xenon CT scan, perfusion MR, and CT perfusion [19, 20]. Historically, PET with ^{15}O tracers was the first imaging method to assess pathophysiological changes in early AIS [21], and is still the gold-standard for detecting and quantifying penumbra using a widely established CBF threshold < 20 mL/100 g/min [22]. To address the logistical limitations of PET in clinical practice, the MRI-based mismatch concept was developed. While the delineation of the ischemic core using DWI with an Apparent Diffusion Coefficient threshold $\leq 620 \times 10^{-6}$ m^2/s is regarded as robust [23], the delineation of the PDV is the "Achilles' heel" of this concept [24]. Indeed, the quantification of PDV with MRI differs fundamentally from PET-based CBF measurement as it requires an arterial input function that is only an approximation of the true plasma concentration of the contrast agent [24]. As a result, the choice of the best MRP map (i.e., CBF, Time-to-Peak, Mean-Transit-Time, and Tmax) and the best threshold to use have been the object of endless discussions that have not resulted in any consensus [24]. Among these different MRP maps, the Tmax map was used in early multicentric trials' stroke studies evaluating intravenous thrombolysis to delineate PDV using a threshold ≥ 6 s [25, 26]. Using MRI to assess FIV, both an early study and a post hoc analysis of DEFUSE trial have both indicated a Tmax threshold between 4 and 6 s was optimal for early identification of penumbra [27, 28]. Direct PET/MRI comparative studies reported similar thresholds [29]. These studies used different methodologies to define non-reperfusion and study populations were small [27–30]. They mainly used RAPID® and other in-house MRP software packages

to compute Tmax maps [27–30]. Since there is no standardization for MRP images post-processing [15], the results of these studies [27–30] may not be expandable to every MRP software packages. Therefore, the optimal Tmax threshold to define the ischemic penumbra may be variable depending on the MRP software package used. Although most manufacturers recommend the use of a Tmax threshold ≥ 6 s, validation data are lacking in the literature.

The main strength of this study is the inclusion of patients with mTICI score of 0 included in a large observational cohort with prospectively acquired day-6 MRI. This allowed us to assess the difference between PDV and FIV reproducibly thereby fitting best to the mismatch model. In addition, this study is original, because the previous reports were limited to comparing PDV obtained with two MRP software packages without comparison with FIV [8, 17].

However, this study has several limitations. In addition to its single-center nature, the study population was small, because patients with no reperfusion after treatment (mTICI = 0) are very rare. In addition, we performed volumetric comparisons, while similarity comparisons using Dice similarity coefficient would have been more accurate. Nevertheless, this was not technically feasible, because package A does not allow for the export of volume of interest. Finally, some of the included patients may have experienced a delayed recanalization after mechanical thrombectomy, since some had a much smaller final infarct volume than expected [31].

Conclusions

Our pilot study suggests that optimal Tmax threshold delineating the ischemic penumbra varies according to the MRP software package used. Since these results may influence patient selection in clinical practice and trials, future studies are required to validate the optimal Tmax threshold to use for each MRP software package.

Author contributions AB-S and YB conceived and designed the project. YB and OE supervised the project. AB-S, MT, and OE performed the measurements. T-HC, MC, MH, RA, AF, RR, LD, CdB, LM, and OE made substantial contribution in acquisition of data. AB-S, OE, LM, NN, and YB drafted the article and revised it critically. All authors approved the version to be published.

Funding This study was supported by the RHU MARVELOUS (ANR-16-RHUS-0009) of Université de Lyon, within the program "Investissements d'Avenir" operated by the French National Research Agency.

Availability of data and materials Further anonymized data can be made available to qualified investigators on request to the corresponding author.

Code availability Not applicable.

Declarations

Conflict of interest The authors have no financial or proprietary interests in any material discussed in this article.

Ethical approval This study was performed in line with the principles of the Declaration of Helsinki. Approval was granted by the Ethics Committee of Hospices Civils de Lyon (number: 00009118).

Consent to participate All subjects or their relatives signed gave informed consent to participate before taking part.

Consent for publication All subjects or their relatives signed gave informed consent for publication.

References

1. Campbell BCV, Mitchell PJ, Kleinig TJ, Dewey HM, Churilov L, Yassi N, Yan B, Dowling RJ, Parsons MW, Oxley TJ, Wu TY, Brooks M, Simpson MA, Miteff F, Levi CR, Krause M, Harrington TJ, Faulder KC, Steinfort BS, Priglinger M, Ang T, Scroop R, Barber PA, McGuinness B, Wijeratne T, Phan TG, Chong W, Chandra RV, Bladin CF, Badve M, Rice H, de Villiers L, Ma H, Desmond PM, Donnan GA, Davis SM (2015) Endovascular therapy for ischemic stroke with perfusion-imaging selection. N Engl J Med 372:1009–1018
2. Saver JL, Goyal M, Bonafe A, Diener H-C, Levy EI, Pereira VM, Albers GW, Cognard C, Cohen DJ, Hacke W, Jansen O, Jovin TG, Mattle HP, Nogueira RG, Siddiqui AH, Yavagal DR, Baxter BW, Devlin TG, Lopes DK, Reddy VK, de Rochemont RM, Singer OC, Jahan R (2015) Stent-retriever thrombectomy after intravenous t-PA vs. t-PA alone in stroke. N Engl J Med 372:2285–2295
3. Nogueira RG, Jadhav AP, Haussen DC, Bonafe A, Budzik RF, Bhuva P, Yavagal DR, Ribo M, Cognard C, Hanel RA, Sila CA, Hassan AE, Millan M, Levy EI, Mitchell P, Chen M, English JD, Shah QA, Silver FL, Pereira VM, Mehta BP, Baxter BW, Abraham MG, Cardona P, Veznedaroglu E, Hellinger FR, Feng L, Kirmani JF, Lopes DK, Jankowitz BT, Frankel MR, Costalat V, Vora NA, Yoo AJ, Malik AM, Furlan AJ, Rubiera M, Aghaebrahim A, Olivot J-M, Tekle WG, Shields R, Graves T, Lewis RJ, Smith WS, Liebeskind DS, Saver JL, Jovin TG (2018) Thrombectomy 6 to 24 hours after stroke with a mismatch between deficit and infarct. N Engl J Med 378:11–21
4. Albers GW (2018) Use of imaging to select patients for late window endovascular therapy. Stroke 49:2256–2260
5. Astrup J, Symon L, Branston NM, Lassen NA (1977) Cortical evoked potential and extracellular K+ and H+ at critical levels of brain ischemia. Stroke 8:51–57
6. Austein F, Riedel C, Kerby T, Meyne J, Binder A, Lindner T, Huhndorf M, Wodarg F, Jansen O (2016) Comparison of perfusion CT software to predict the final infarct volume after thrombectomy. Stroke 47:2311–2317
7. Koopman MS, Berkhemer OA, Geuskens RREG, Emmer BJ, van Walderveen MAA, Jenniskens SFM, van Zwam WH, van Oostenbrugge RJ, van der Lugt A, Dippel DWJ, Beenen LF, Roos YBWEM, Marquering HA, Majoie CBLM (2019) Comparison of three commonly used CT perfusion software packages in patients with acute ischemic stroke. J NeuroIntervent Surg 11:1249–1256
8. Deutschmann H, Hinteregger N, Wießpeiner U, Kneihsl M, Fandler-Höfler S, Michenthaler M, Enzinger C, Hassler E, Leber S, Reishofer G (2021) Automated MRI perfusion-diffusion mismatch estimation may be significantly different in individual

patients when using different software packages. Eur Radiol 31:658–665
9. Powers WJ, Rabinstein AA, Ackerson T, Adeoye OM, Bambakidis NC, Becker K, Biller J, Brown M, Demaerschalk BM, Hoh B, Jauch EC, Kidwell CS, Leslie-Mazwi TM, Ovbiagele B, Scott PA, Sheth KN, Southerland AM, Summers DV, Tirschwell DL, on behalf of the American Heart Association Stroke Council (2019) Guidelines for the early management of patients with acute ischemic stroke: 2019 update to the 2018 guidelines for the early management of acute ischemic stroke: a guideline for healthcare professionals from the American Heart Association/American Stroke Association. Stroke. https://doi.org/10.1161/STR.0000000000000211
10. Albers GW, Goyal M, Jahan R, Bonafe A, Diener H-C, Levy EI, Pereira VM, Cognard C, Cohen DJ, Hacke W, Jansen O, Jovin TG, Mattle HP, Nogueira RG, Siddiqui AH, Yavagal DR, Baxter BW, Devlin TG, Lopes DK, Reddy VK, de Rochemont RM, Singer OC, Bammer R, Saver JL (2016) Ischemic core and hypoperfusion volumes predict infarct size in SWIFT PRIME. Ann Neurol 79:76–89
11. Wheeler HM, Mlynash M, Inoue M, Tipirneni A, Liggins J, Zaharchuk G, Straka M, Kemp S, Bammer R, Lansberg MG, Albers GW (2013) Early diffusion-weighted imaging and perfusion-weighted imaging lesion volumes forecast final infarct size in DEFUSE 2. Stroke 44:681–685
12. Rao V, Christensen S, Yennu A, Mlynash M, Zaharchuk G, Heit J, Marks MP, Lansberg MG, Albers GW (2019) Ischemic core and hypoperfusion volumes correlate with infarct size 24 hours after randomization in DEFUSE 3. Stroke 50:626–631
13. Ostergaard L, Weisskoff RM, Chesler DA, Gyldensted C, Rosen BR (1996) High resolution measurement of cerebral blood flow using intravascular tracer bolus passages. Part I: mathematical approach and statistical analysis. Magn Reson Med 36:715–725
14. Wu O, Østergaard L, Weisskoff RM, Benner T, Rosen BR, Sorensen AG (2003) Tracer arrival timing-insensitive technique for estimating flow in MR perfusion-weighted imaging using singular value decomposition with a block-circulant deconvolution matrix. Magn Reson Med 50:164–174
15. Demeestere J, Wouters A, Christensen S, Lemmens R, Lansberg MG (2020) Review of perfusion imaging in acute ischemic stroke: from time to tissue. Stroke 51:1017–1024
16. Bani-Sadr A, Cho T-H, Cappucci M, Hermier M, Ameli R, Filip A, Riva R, Derex L, De Bourguignon C, Mechtouff L, Eker OF, Nighoghossian N, Berthezene Y (2022) Assessment of three MR perfusion software packages in predicting final infarct volume after mechanical thrombectomy. J NeuroIntervent Surg Neurintsurg. https://doi.org/10.1136/neurintsurg-2022-018674
17. Pistocchi S, Strambo D, Bartolini B, Maeder P, Meuli R, Michel P, Dunet V (2021) MRI software for diffusion-perfusion mismatch analysis may impact on patients' selection and clinical outcome. Eur Radiol. https://doi.org/10.1007/s00330-021-08211-2
18. Branston NM, Strong AJ, Symon L (1977) Extracellular potassium activity, evoked potential and tissue blood flow: relationships during progressive ischaemia in baboon cerebral cortex. J Neurol Sci 32:305–321
19. Heiss W-D (2000) Ischemic penumbra: evidence from functional imaging in man. J Cereb Blood Flow Metab 20:1276–1293
20. Baron J-C (2001) Perfusion thresholds in human cerebral ischemia: historical perspective and therapeutic implications. Cerebrovasc Dis 11:2–8
21. Baron JC, Bousser MG, Comar D, Soussaline F, Castaigne P (1981) Noninvasive tomographic study of cerebral blood flow and oxygen metabolism in vivo. Potentials, limitations, and clinical applications in cerebral ischemic disorders. Eur Neurol 20:273–284
22. Marchal G, Beaudouin V, Rioux P, de la Sayette V, Le Doze F, Viader F, Derlon JM, Baron JC (1996) Prolonged persistence of substantial volumes of potentially viable brain tissue after stroke: a correlative PET-CT study with voxel-based data analysis. Stroke 27:599–606
23. Purushotham A, Campbell BCV, Straka M, Mlynash M, Olivot J-M, Bammer R, Kemp SM, Albers GW, Lansberg MG (2015) Apparent diffusion coefficient threshold for delineation of ischemic core. Int J Stroke 10:348–353
24. Sobesky J (2012) Refining the mismatch concept in acute stroke: lessons learned from PET and MRI. J Cereb Blood Flow Metab 32:1416–1425
25. Albers GW, Thijs VN, Wechsler L, Kemp S, Schlaug G, Skalabrin E, Bammer R, Kakuda W, Lansberg MG, Shuaib A, Coplin W, Hamilton S, Moseley M, Marks MP (2006) Magnetic resonance imaging profiles predict clinical response to early reperfusion: the diffusion and perfusion imaging evaluation for understanding stroke evolution (DEFUSE) study. Ann Neurol 60:508–517
26. Davis SM, Donnan GA, Parsons MW, Levi C, Butcher KS, Peeters A, Barber PA, Bladin C, De Silva DA, Byrnes G, Chalk JB, Fink JN, Kimber TE, Schultz D, Hand PJ, Frayne J, Hankey G, Muir K, Gerraty R, Tress BM, Desmond PM (2008) Effects of alteplase beyond 3 h after stroke in the Echoplanar Imaging Thrombolytic Evaluation Trial (EPITHET): a placebo-controlled randomised trial. Lancet Neurol 7:299–309
27. Olivot J-M, Mlynash M, Thijs VN, Kemp S, Lansberg MG, Wechsler L, Bammer R, Marks MP, Albers GW (2009) Optimal Tmax threshold for predicting penumbral tissue in acute stroke. Stroke 40:469–475
28. Shih LC, Saver JL, Alger JR, Starkman S, Leary MC, Vinuela F, Duckwiler G, Gobin YP, Jahan R, Villablanca JP, Vespa PM, Kidwell CS (2003) Perfusion-weighted magnetic resonance imaging thresholds identifying core, irreversibly infarcted tissue. Stroke 34:1425–1430
29. Zaro-Weber O, Fleischer H, Reiblich L, Schuster A, Moeller-Hartmann W, Heiss W (2019) Penumbra detection in acute stroke with perfusion magnetic resonance imaging: validation with ^{15}O-positron emission tomography. Ann Neurol 85:875–886
30. Zaro-Weber O, Moeller-Hartmann W, Heiss W-D, Sobesky J (2010) MRI perfusion maps in acute stroke validated with ^{15}O-water positron emission tomography. Stroke 41:443–449
31. Molina CA, Montaner J, Abilleira S, Ibarra B, Romero F, Arenillas JF, Alvarez-Sabín J (2001) Timing of spontaneous recanalization and risk of hemorrhagic transformation in acute cardioembolic stroke. Stroke 32:1079–1084

Étude n°4 : Le brush sign et l'apport collatéral comme marqueurs potentiels de la croissance de la lésion ischémique après une thrombectomie réussie.

Contexte et état de la question.

Le volume final de l'infarctus cérébral est un déterminant majeur du devenir fonctionnel en cas d'infarctus cérébral [103,104]. Malgré une recanalisation réussie (score mTICI 2B-3), les lésions ischémiques continuent à se développer avec une croissance moyenne de 14.8mL [105]. L'identification de facteurs prédictifs de croissance malgré recanalisation est essentielle pour le développement de thérapies neuroprotectrices ciblant les lésions d'ischémie-reperfusion [55,56]. Le statut des collatérales cérébrales est un facteur pronostic reconnu [16,106]. Cependant, les collatérales ne donnent pas d'indication sur la tolérance du tissu cérébral à l'ischémie. Le brush sign, à savoir la visualisation anormale des veines sous-épendymaires et médullaires en IRM T2*, reflète une désoxygénation sévère [107,108]. Bien que sa valeur pronostique négative soit établie dans le cadre de la thrombolyse, l'impact du brush sign est mal connu dans le cadre de la thrombectomie mécanique, en particulier chez les patients bénéficiant d'une reperfusion efficace [107-112]. Ce quatrième travail visait à étudier les relations entre le brush sign et le statut des collatérales cérébrales sur la croissance de l'infarctus après une recanalisation réussie.

Principaux résultats.

Nos résultats indiquent que le brush sign est indépendamment associé à une croissance large (>11.6mL) des lésions ischémiques malgré une recanalisation réussie. A l'inverse, nous n'avons pas identifié d'association entre le statut des collatérales et une croissance large des lésions ischémiques.

European Radiology
https://doi.org/10.1007/s00330-022-09387-x

European Radiology
ESR EUROPEAN SOCIETY OF RADIOLOGY

NEURO

Brush sign and collateral supply as potential markers of large infarct growth after successful thrombectomy

Alexandre Bani-Sadr[1,2] · Dylan Pavie[1] · Laura Mechtouff[3,4] · Matteo Cappucci[1] · Marc Hermier[1] · Roxana Ameli[1] · Laurent Derex[3,5] · Charles De Bourguignon[6] · Tae-Hee Cho[3,4] · Omer Eker[1,2] · Norbert Nighoghossian[3,4] · Yves Berthezene[1,2]

Received: 31 October 2022 / Revised: 13 December 2022 / Accepted: 22 December 2022

Abstract

Objectives To investigate the relationships between brush sign and cerebral collateral status on infarct growth after successful thrombectomy.

Methods HIBISCUS-STROKE cohort includes acute ischemic stroke patients treated with thrombectomy after MRI triage and undergoing a day-6 MRI including FLAIR images to quantify final infarct volume (FIV). Successful reperfusion was defined as a modified thrombolysis in cerebral infarction score ≥ 2B. Infarct growth was calculated by subtracting FIV from baseline ischemic core after co-registration and considered large (LIG) when >11.6 mL. Brush sign was assessed on T2*-weighted-imaging and collaterals were assessed using the hypoperfusion intensity ratio, which is the volume of Time-To-Tmax (Tmax) ≥ 10 s divided by the volume of Tmax ≥ 6 s. Good collaterals were defined by a hypoperfusion intensity ratio < 0.4.

Results One hundred and twenty-nine patients were included, of whom 45 (34.9%) had a brush sign and 63 (48.8%) good collaterals. Brush sign was associated with greater infarct growth ($p = 0.01$) and larger FIV ($p = 0.02$). Good collaterals were associated with a smaller baseline ischemic core ($p < 0.001$), larger penumbra ($p = 0.04$), and smaller FIV ($p < 0.001$). Collateral status was not significantly associated with brush sign ($p = 0.20$) or with infarct growth ($p = 0.67$). Twenty-eight (22.5%) patients experienced LIG. Univariate regressions indicated that brush sign (odds ratio (OR) = 4.8; 95% confidence interval (CI): [1.9;13.3]; $p = 0.004$) and hemorrhagic transformation (OR = 1.7; 95%CI: [1.2;2.6]; $p = 0.04$) were predictive of LIG. In multivariate regression, only the brush sign remained predictive of LIG (OR = 5.2; 95%CI: [1.8–16.6], $p = 0.006$).

Conclusions Brush sign is a predictor of LIG after successful thrombectomy and cerebral collateral status is not.

Key Points

- *Few predictors of ischemic growth are known in ischemic stroke patients achieving successful mechanical thrombectomy.*
- *Our results suggest that the brush sign—a surrogate marker of severe hypoperfusion—is independently associated with large ischemic growth (> 11.6 mL) after successful thrombectomy whereas cerebral collateral status does not.*

Keywords Stroke · Thrombectomy · MR imaging

Alexandre Bani-Sadr and Dylan Pavie contributed equally to this work.

✉ Alexandre Bani-Sadr
apbanisadr@gmail.com; alexandre.bani-sadr@chu-lyon.fr

[1] Department of Neuroradiology, East Group Hospital, Hospices Civils de Lyon. 59 Bd Pinel, 69500 Bron, France

[2] CREATIS Laboratory, CNRS UMR 5220, INSERM U 5220, Claude Bernard Lyon I University. 7 Avenue Jean Capelle O, 69100 Villeurbanne, France

[3] Stroke Department, East Group Hospital, Hospices Civils de Lyon. 59 Bd Pinel, 69500 Bron, France

[4] CarMeN Laboratory, INSERM U1060, Claude Bernard Lyon I University, 59 Bd Pinel, 69500 Bron, France

[5] Research On Healthcare Performance (RESHAPE), INSERM U 1290, Claude Bernard Lyon I University. Domaine Rockfeller, 8 Avenue Rockfeller, 69373 Cedex 08 Lyon, France

[6] Clinical Investigation Center, INSERM 1407. 59 Bd Pinel, 69500 Bron, France

Published online: 12 January 2023

Abbreviations

AIS	Acute ischemic stroke
DSC-MRI	Dynamic-susceptibility-contrast MRI
DWI	Diffusion-weighted imaging
FIV	Final infarct volume
FLAIR	Fluid-attenuated inversion recovery
GRE T2*WI	Gradient recalled echo-T2*-weighted imaging
HIR	Hypoperfusion intensity ratio
ICA	Internal carotid artery
IQR	Interquartile range
LIG	Large infarct growth
MCA	Middle cerebral artery
mTICI	Modified thrombolysis in cerebral infarction
NIHSS	National Institute of Health Stroke Scale
OR	Odds ratio
rCBV	Relative cerebral blood volume
Tmax	Time-to-maximum

Introduction

Final infarct volume (FIV) is a fundamental determinant of functional outcome in acute ischemic stroke (AIS) patients [1, 2]. In AIS patients with large vessel occlusion, mechanical thrombectomy significantly improves functional outcomes in selected patients by restoring cerebral blood flow to the ischemic penumbra, thereby limiting infarct growth. The time from symptoms onset to effective reperfusion and the degree of reperfusion are critical factors [3, 4]. However, it is increasingly recognized that ischemic lesions continue to grow despite the restoration of blood flow [5]. A recent meta-analysis of 10 studies reported a mean infarct growth of 14.8 mL after effective reperfusion [6]. Predicting infarct growth despite effective reperfusion is essential as it may provide valuable information for neuroprotective therapies targeting ischemia–reperfusion injury [7, 8].

Cerebral collateral status is a recognized prognostic factor in AIS that can be assessed using cerebral angiography, multiphasic CT angiography, and perfusion imaging [9, 10]. The hypoperfusion intensity ratio (HIR) is a robust indicator of cerebral collateral status derived from CT or MR perfusion imaging [11, 12]. It is correlated with patient eligibility for mechanical thrombectomy and predicts infarct growth during transfer for mechanical thrombectomy center [12, 13]. However, cerebral collateral status does not provide insight into the tolerance of brain tissue to ischemia.

The brush sign refers to abnormal visualization of subependymal and medullary veins on gradient-weighted echo-T2* imaging (GRE T2*WI) and susceptibility-weighted imaging (SWI). It is thought to reflect severe deoxygenation of ischemic tissue [14, 15]. Many studies have reported its negative prognostic value, but its impact in the setting of mechanical thrombectomy is poorly understood, specifically in patients with effective reperfusion [14–19].

This study aimed to investigate the relationships between brush sign and cerebral collateral status on infarct growth after effective reperfusion.

Methods

Data availability statement

Further anonymized data can be made available to qualified investigators on request to the corresponding author.

Ethic statement

The local ethics committee approved the study, and all subjects or their relatives signed an informed consent form (IRB number: 00009118).

Study population

HIBISCUS-STROKE Cohort (CoHort of Patients to Identify Biological and Imaging markerS of CardiovascUlar Outcomes in Stroke; NCT: 03,149,705) is an ongoing observational study since October 2016 that included all anterior circulation AIS patients with large vessel occlusion (i.e., occlusions of the internal carotid artery, M1 or M2 proximal segments of the middle cerebral artery) treated with mechanical thrombectomy after MRI triage. In accordance with international guidelines, eligible patients were additionally treated with intravenous thrombolysis [20]. A board-certified neurologist collected baseline clinical characteristics including the National Institute of Health Stroke Scale (NIHSS) score and pre-stroke mRS.

The inclusion criteria of patients for this cohort study were as follows: (1) successful reperfusion defined as a modified thrombolysis in infarction score (mTICI) $\geq$ 2B, (2) follow-up MRI at day 6 available, and (3) baseline and follow-up MRI of adequate quality.

MR image acquisition

Brain MRIs were performed with 1.5-Tesla or 3-Tesla *Ingenia* scanners (*Philips Healthcare)*. The admission brain MRI protocol included axial diffusion-weighted-imaging (DWI), axial T2 Fluid-attenuated inversion recovery (FLAIR), GRE T2*WI, 3D Time-Of-Flight, dynamic-susceptibility-contrast MRI (DSC-MRI), and contrast-enhanced MR angiography of the supra-aortic trunks. A CT scan was systematically performed on day 1 to assess hemorrhagic transformation according to the European Cooperative Acute

Stroke Study II classification [21] and a follow-up MRI on day 6 including axial FLAIR was performed to quantify FIV.

Imaging biomarkers analysis

Two neuroradiologists assessed independently the presence of the brush sign on GRE T2*WI blinded to clinical findings and follow-up MRI. As illustrated in Fig. 1, the brush sign was defined as abnormal visualization of subependymal and medullary cerebral veins homolateral to large vessel occlusion. Any discrepancies were resolved by a third experienced neuroradiologist.

Baseline ischemic core and perfusion deficit volumes were measured with a fully automatic MR software package (RAPID®, iSchemaView Inc.) using an apparent diffusion coefficient threshold $\leq 620 \times 10^{-6}$ m^2/s and a time-to-maximum (Tmax) ≥ 6 s, respectively. Relative cerebral blood volume (rCBV) measurements were obtained from masks of DWI lesions and contralateral symmetric areas. Ischemic penumbra was defined as the difference between perfusion deficit volumes and ischemic core volume. Cerebral collateral status was assessed using the hypoperfusion intensity ratio, which is the volume of Tmax ≥ 10 s divided by the volume of Tmax ≥ 6 s. Good collaterals were defined by a hypoperfusion ratio <0.4 [11].

Quantification of FIV

FIV was segmented using day-6 FLAIR images using a semi-automated method (3D Slicer: https://www.slicer.org/) after nonlinear co-registration of day-6 FLAIR images and admission DWI images. Infarct growth was calculated by subtracting FIV to baseline ischemic core volume and considered large (LIG) when ischemic core expansion >11.6 mL. This threshold corresponds to the mean infarct growth of the Diffusion and Perfusion Imaging for Understanding Stroke Evolution cohort and was used in a previous study to define LIG [22, 23].

Statistical analysis

Continuous variables were expressed as means and standard deviations or medians and interquartile ranges (IQR) according to the normality of their distribution and categorical data were summarized as counts and proportions.

Inter-rater agreement for brush sign was assessed using Cohen's kappa coefficient.

The normal or non-normal distributions of each dataset were verified using the Shapiro–Wilk test and appropriate parametric or non-parametric tests were subsequently used to assess factors associated with brush sign and cerebral collateral status.

Uni- and multivariable logistic regression was performed to assess the relationship between LIG and brush sign as well as collateral status. The multivariable logistic model included covariates identified as statistically significant in univariate logistic regression ($p < 0.05$) and others selected a priori independent of their univariate p value hypothesized as causal (baseline ischemic core, good collaterals, time from MRI to reperfusion and mTICI). The multivariable logistic regression was therefore adjusted for brush sign, hemorrhagic transformation,

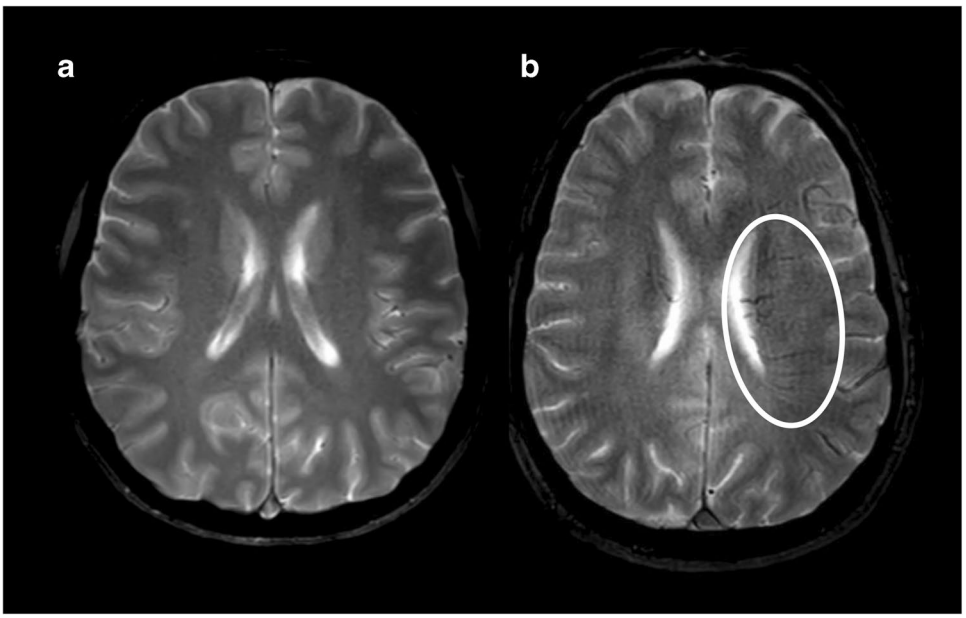

Fig. 1 Example of brush sign. **a**: Gradient recalled echo-T2*-weighted imaging of a normal subject. **b**: Gradient recalled echo-T2*-weighted imaging in a patient with acute ischemic stroke due to left middle cerebral artery occlusion showing hyposignal of medullary veins defining a brush sign

baseline ischemic core, good collaterals, time from MRI to reperfusion, and mTICI score.

Results

Study population

From October 2016 to June 2021, 129 patients fulfilled the inclusion criteria (Fig. 2). Seventy-four (57.4%) patients were males and the median age was 71.0 years (IQR: [60.0; 79.3]). The median time from symptoms onset to MRI was 129.5 min (IQR: [81.0; 248.0]) and the median time from symptoms onset to reperfusion was 235.0 min (IQR: [165.0; 372.2]). MRIs were performed on a 1.5-T magnet in 101 patients (78.3%) and on a 3-T magnet in 28 patients (21.7%).

Univariate analyses of brush sign and cerebral collateral status

Detailed clinical and radiological findings of the study population are presented in Table 1. Of the study population, 45 (34.9%) patients had brush sign and 63 (48.8%) had good collaterals. Inter-observer agreement was very good for brush sign (kappa coefficient: 0.81; 95% confidence interval (95% CI): [0.71; 0.87]; rate of agreements: 91.5%).

Patients with a brush sign were more likely to have hypertension ($p < 0.001$) and had higher rCBV ($p = 0.05$), larger penumbra ($p < 0.001$), larger infarct growth ($p = 0.01$), and larger FIV ($p = 0.02$). There was no significant association between the brush sign and hemorrhagic transformation ($p = 0.09$). Patients with good collaterals were more likely to have lower baseline NIHSS score ($p = 0.03$) and to achieve mTICI score 3 after mechanical thrombectomy ($p < 0.001$). They had lower baseline ischemic core ($p < 0.001$), larger penumbra ($p = 0.04$), and lower FIV ($p < 0.001$). Cerebral collateral status was not significantly associated with the brush sign ($p = 0.20$) or with infarct growth ($p = 0.67$).

The percentage of subjects combining a negative brush sign and good collaterals tended to be higher in patients with an mTICI score 2B (23 (46.9%) subjects with mTICI score 2B, 12 (24.0%) with mTICI score 3, and 10 (33.3%) with mTICI score 2C, $p = 0.06$).

Factors associated with LIG

Of the study population, 28 (21.7%) patients experienced LIG of whom 8 (16.0%) achieved mTICI 3, 8 achieved mTICI 2C (26.7%), and 12 achieved (24.0%) mTICI 2B. Univariable logistic regressions indicated that brush sign was associated with LIG (odds ratio (OR) = 4.8; 95% CI: [1.9; 13.3], $p = 0.004$) in combination with hemorrhagic transformation (OR = 1.7; 95% CI: [1.2; 2.6], $p = 0.04$). There was no significant association between LIG and baseline ischemic core ($p = 0.67$), cerebral collateral status ($p = 0.41$), time from MRI to mechanical thrombectomy ($p = 0.81$), and degree of reperfusion ($p = 0.75$). Multiple variable regressions confirmed that brush sign was independently associated with LIG (OR = 5.2, 95% CI: [1.8–16.6], $p = 0.006$). Table 2 summarizes crude and adjusted OR of factors associated with LIG.

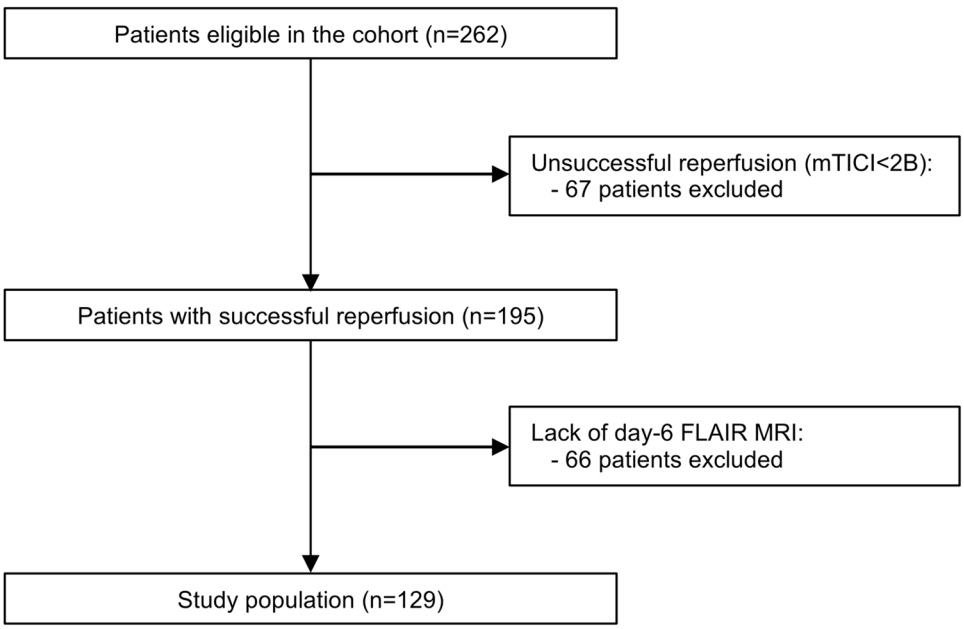

Fig. 2 Flowchart of the study population. Abbreviations: mTICI, modified Thrombolysis in Cerebral Infarction score; FLAIR, fluid-attenuated inversion recovery images

Table 1 Baseline clinical and radiological characteristics of the study population

	Brush Sign			Cerebral collateral status		
	Positive	Negative	*p* value	Good	Poor	*p* value
Patients, *n* (%)	45 (34.9)	84 (65.1)	-	63 (48.8)	66 (51.2)	-
Clinical characteristics						
Age (years), median [IQR]	71.5 [64.5; 77.5]	71.0 [60.0; 79.5]	0.83	71.5 [64.5; 79.0]	70.5 [57.0; 77.3]	0.69
Males, *n* (%)	29 (64.4)	45 (53.6)	0.27	35 (55.6)	39 (59.1)	0.72
Tobacco, *n* (%) (a)	16 (35.6)	33 (39.3)	0.71	29 (46.0)	20 (30.3)	0.07
Current smoking, *n* (%)	12 (26.7)	27 (32.1)	0.55	21 (33.3)	18 (27.3)	0.57
History of smoking, *n* (%)	4 (8.9)	6 (7.1)	0.14	8 (12.7)	2 (2.4)	0.10
Hypertension, *n* (%) (a)	31 (68.9)	30 (35.7)	< 0.001	29 (46.0)	32 (48.5)	0.86
Mellitus diabetes, *n* (%) (a)	10 (22.2)	10 (11.9)	0.13	12 (19.0)	8 (12.1)	0.33
Dyslipidemia, *n* (%) (a)	13 (28.9)	15 (17.9)	0.18	16 (25.4)	12 (18.2)	0.40
Peripheral vascular disease (a)	2 (4.4)	3 (3.6)	0.99	2 (3.2)	3 (4.5)	0.99
Baseline NIHSS, median [IQR] (a)	15.5 [12.0; 18.0]	15.0 [8.0; 18.5]	0.21	14.3 [7.5; 18.0]	15.5 [12.0; 19.0]	0.03
Pre-stroke MRS, median [IQR] (a)	0.0 [0.0; 0.0]	0.0 [0.0; 0.0]	0.99	0.0 [0.0; 0.0]	0.0 [0.0; 0.0]	0.99
Intravenous thrombolysis, *n* (%)	25 (55.6)	43 (51.2)	0.71	36 (57.1)	32 (48.5)	0.38
mTICI score:						
- mTICI 2B, *n* (%)	16 (35.6)	33 (39.3)	0.71	18 (28.6)	31 (47.0)	0.05
- mTICI 2C, *n* (%)	13 (28.8)	17 (20.2)	0.39	12 (19.0)	18 (27.3)	0.30
- mTICI 3, *n* (%)	16 (35.6)	34 (40.5)	0.70	33 (54.0)	17 (24.2)	< 0.001
Time from symptoms onset to MRI (min), median [IQR] (b)	123.0 [84.5; 230.0]	103.5 [75.0; 226.0]	0.21	103.0 [77.0; 236.5]	156.0 [85.0; 252.3]	0.34
Time from MRI to reperfusion (min), median [IQR]	100.5 [77.3; 119.8]	103.5 [81.3; 132.5]	0.41	101.5 [79.5; 126.8]	104.5 [83.5; 127.5]	0.68
Occlusion site						
Extra-cranial ICA, *n* (%)	5 (11.1)	11 (13.1)	0.99	9 (14.3)	7 (10.6)	0.60
Intra-cranial ICA, *n* (%)	9 (20.0)	15 (17.9)	0.81	11 (17.4)	13 (19.7)	0.82
M1 segment of MCA, *n* (%)	28 (62.2)	53 (63.1)	0.99	39 (61.9)	42 (63.4)	0.86
M2 segment of MCA, *n* (%)	3 (6.7)	5 (6.0)	0.99	4 (6.3)	4 (6.1)	0.99
Radiological characteristics						
Ischemic core (mL), median [IQR]	27.7 [12.6; 65.5]	22.2 [4.5; 48.7]	0.70	12.3 [1.0; 28.2]	41.5 [14.7; 69.6]	< 0.001
Perfusion deficit volume (mL), median [IQR]	132.0 [95.1; 171.2]	93.2 [39.7; 129.1]	< 0.001	95.0 [43.5; 123.5]	82.0 [71.5; 123.5]	0.08
Penumbra (mL), median [IQR]	106.0 [67.0; 136.5]	46.0 [22.3; 105.0]	< 0.001	70.3 [43.5; 112.5]	59.2 [22.3; 76.3]	0.04
Relative cerebral blood volume, median [IQR]	1.44 [0.93; 1.72]	0.79 [0.57; 1.42]	0.05	1.31 [0.77; 1.78]	0.87 [0.32; 1.17]	0.01
Good Collaterals, *n* (%)	18 (40.0)	45 (53.6)	0.20	-	-	-
Brush Sign, *n* (%)	-	-	-	18 (28.6)	27 (42.8]	0.20
Hemorrhagic transformation, *n* (%)	15 (33.3)	16 (19.0)	0.09	11 (17.4)	20 (30.3)	0.10
-HI1, *n* (%)	6 (13.3)	7 (8.3)	0.37	7 (11.1)	6 (9.1)	0.78
-HI2, *n* (%)	8 (17.8)	5 (6.0)	0.06	3 (4.8)	10 (15.2)	0.08
-PH1, *n* (%)	0 (0.0)	0 (0.0)	0.99	0 (0.0)	0 (0.0)	0.99
-PH2, *n* (%)	0 (0.0)	0 (0.0)	0.99	0 (0.0)	0 (0.0)	0.99
-SAH, *n* (%)	1 (2.2)	4 (4.8)	0.66	1 (1.6)	4 (6.1)	0.37
Outcome						
Infarct growth (mL), median [IQR]	7.3 [0.5; 19.5]	0.1 [-15.3; 7.1]	0.01	0.3 [-4.9; 4.2]	0.5 [-12.3; 9.7]	0.67
Final infarct volume (mL), median [IQR]	26.4 [13.3; 66.3]	14.2 [4.9; 36.7]	0.02	10.4 [1.9; 23.0]	35.5 [14.9; 71.3]	< 0.001

Categorical variables were compared using Fischer exact test and quantitative variables were compared with the Wilcoxon-Mann–Whitney-U test

(a): 7 missing values, (b): 31 missing values

Abbreviations: *IQR*, interquartile range; *NIHSS*, National Institutes of Health Stoke Scale; *MRS*, Modified Rankin Scale; *mTICI*, modified thrombolysis in cerebral infarction; *ICA*, internal carotid artery; *MCA*, middle cerebral artery; *HI1*, hemorrhagic infarction type 1; *HI2*, hemorrhagic infarction type 2; *PH1*, parenchymal hematoma type 1; *PH2*, parenchymal hematoma type 2; *SAH*, subarachnoid hemorrhage

Table 2 Multivariable analysis of large infarct growth

	Crude OR (95% CI)	*p* value	Adjusted OR (95% CI)	*p* value
Brush Sign	4.8 [1.9; 13.3]	0.004	5.2 [1.8; 16.6]	0.006
Hemorrhagic transformation	1.7 [1.2; 2.6]	0.04	1.5 [0.9; 2.5]	0.08
Baseline ischemic core (a)	1.1 [0.9; 1.1]	0.67	1.0 [0.9; 1.1]	0.69
Good collaterals	0.6 [0.3; 1.5]	0.41	0.9 [0.4; 3.2]	0.92
Time from MRI to reperfusion (b)	1.1 [0.9; 1.1]	0.81	1.1 [0.9; 1.2]	0.31
mTICI score	0.9 [0.6; 1.6]	0.75	0.9 [0.5; 1.8]	0.79

a: per 10 mL increase

b: per 10 min increase

Abbreviations: *OR*, odds ratio; *mTICI*, modified thrombolysis in cerebral infarction

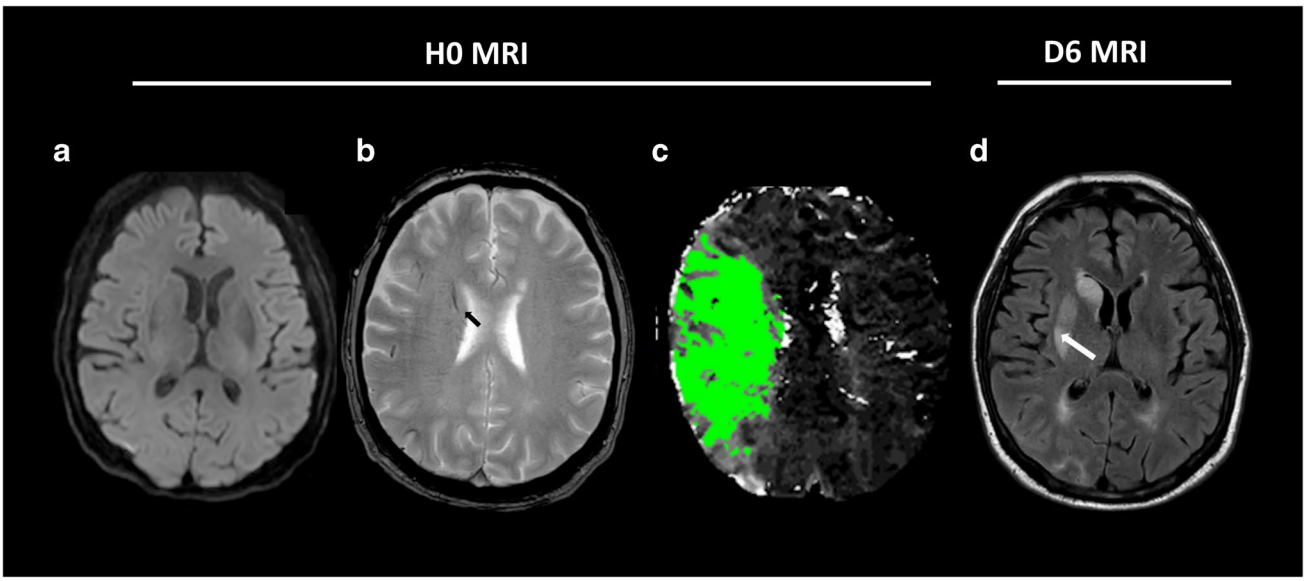

Fig. 3 Example of brush sign. This figure shows an MRI of a patient with diffusion-negative acute ischemic stroke (**a**: diffusion-weighted imaging) (**a**), a brush sign (black arrow, gradient recalled echo-T2*-weighted imaging) and a large ischemic penumbra (**c**: Time-To-Maximum > 6 s map). The patient underwent intravenous thrombolysis and complete reperfusion after mechanical thrombectomy within 90 min. Follow-up MRI on day 6 (**d**: fluid-attenuated inversion recovery-weighted imaging) indicated ischemic growth in deep right Sylvian territory (white arrow)

Figure 3 shows an MRI of a patient with a brush sign and ischemic growth despite complete reperfusion (mTICI 3).

Discussion

The purpose of this study was to investigate the relationships between brush sign and cerebral collateral status and infarct growth after effective reperfusion. Our results indicate that the brush sign is independently associated with LIG after effective reperfusion.

Consistent with previous studies, we found that the brush sign was associated with larger perfusion deficit volumes and increased rCBV [14, 24]. In a recent paper including AIS patients undergoing MRI triage, Guenego et al noted that patients with the brush sign and robust collaterals had a lower baseline ischemic core volume [25]. Conversely, patients with the brush sign and poor collaterals had larger baseline ischemic core [25]. They postulated that the brush sign might reflect a maladaptive response to ischemia [25]. In the present study, we found that the brush was independently associated with LIG. The possible mechanism explaining infarct growth includes ischemic-reperfusion injury [6]. Ischemic reperfusion injury is thought to result from a complex series of events including oxidative stress and brain acidosis [26]. Because the brush sign reflects severe deoxygenation of ischemic tissue [14], our results suggest that it may be a marker of tissue at risk for ischemic-reperfusion injury. In agreement, it has been established that cerebral acidosis and decreased tissue PH induce a decrease in the GRE-T2*WI signal [27, 28].

The status of cerebral collaterals is a major determinant of tissue outcome because robust collaterals can maintain a viable ischemic penumbra pending effective reperfusion [9]. Patients with poorer collateral status have faster ischemic core growth [29]. Consistent with previous studies, we found that robust collaterals were associated with lower baseline NIHSS score, higher rate of complete reperfusion, lower rate of hemorrhagic transformation, and lower FIV [30, 31]. We did not find a significant association between cerebral collateral status and LIG. These results are consistent with two previous studies that assessed cerebral collaterals using DSC-MRI [23] and angiography [32] and did not report a significant association with infarct growth. Conversely, another study reported that patients with poor collaterals had large infarct growth during the transfer from a primary to a comprehensive stroke center [13]. A possible explanation for this discrepancy is the very shorter time between baseline imaging and effective reperfusion in our study. In agreement, patients with poor collaterals have a faster infarct growth rate [29, 33]. In addition, the percentage of patients, although not statistically significant, with positive brush sign was higher in the case of poor collaterals.

Effective reperfusion encompasses mTICI 2B, mTICI 2C, and mTICI 3 scores. However, mTICI 2B reperfusion is associated with the worst outcome compared with mTICI 2C and mTICI 3. Several studies reported reduced infarct growth in patients achieving mTICI2B [6, 34]. In our study, the degree of reperfusion was not associated with LIG on multivariable analysis. Nevertheless, the rate of patients with mTICI 3 reperfusion experiencing LIG was lower compared with patients with mTICI2B and mTICI2C reperfusion. In addition, our results may be biased because the percentage of subjects combining a negative brush sign and good collaterals tended to be higher in patients with an mTICI score 2B.

The main strength of this study is the inclusion of patients from an observational cohort study with prospectively acquired data including a baseline MRI and follow-up MRI on day 6 allowing reproducible assessment of FIV.

Besides the monocentric design and the limited sample size, this study has several limitations. First, the study population was limited and multiple tests comparisons were performed which may have increased the statistical risk. In addition, we assessed the brush sign using GRE T2*WI whereas susceptibility-weighted-imaging is more accurate in assessing subependymal and medullary veins [35]. In addition, we assessed the brush sign using a binary approach. Quantitative susceptibility mapping is a development of susceptibility-weighted-imaging that can quantify cerebral vein oxygen saturation by measuring susceptibility values resulting in a more quantitative assessment of cerebral ischemia [36] Another potential limitation is that we evaluated the brush sign using both 1.5-T and 3-T magnets which may influence the detection of GRE-T2*WI abnormalities.

Conclusion

In conclusion, the brush sign is independently associated with LIG in patients achieving effective reperfusion. This finding should prompt further prospective studies, because the identification of biomarkers of ischemic-reperfusion injury may warrant neuroprotective therapies.

Funding This study was supported by the RHU MARVELOUS (ANR-16-RHUS-0009) of Université de Lyon, within the program "Investissements d'Avenir" operated by the French National Research Agency.

Declarations

Guarantor The scientific guarantor of this publication is Yves Berthezène.

Conflict of interest The authors of this manuscript declare no relationships with any companies whose products or services may be related to the subject matter of the article.

Statistics and biometry Alexandre Bani-Sadr and Omer Faruk Eker provided statistical advice for this manuscript. Two of the authors have significant statistical expertise.

Informed consent Written informed consent was obtained from all patients in this study.

Ethical approval Institutional Review Board approval was obtained.

Methodology

- retrospective
- diagnostic study
- performed at one institution

References

1. Yoo AJ, Chaudhry ZA, Nogueira RG et al (2012) Infarct volume is a pivotal biomarker after intra-arterial stroke therapy. Stroke 43:1323–1330. https://doi.org/10.1161/STROKEAHA.111.639401
2. Zaidi SF, Aghaebrahim A, Urra X et al (2012) Final infarct volume is a stronger predictor of outcome than recanalization in patients with proximal middle cerebral artery occlusion treated with endovascular therapy. Stroke 43:3238–3244. https://doi.org/10.1161/STROKEAHA.112.671594
3. Fransen PSS, Berkhemer OA, Lingsma HF et al (2016) Time to reperfusion and treatment effect for acute ischemic stroke: a randomized clinical trial. JAMA Neurol 73:190. https://doi.org/10.1001/jamaneurol.2015.3886
4. Liebeskind DS, Bracard S, Guillemin F et al (2019) eTICI reperfusion: defining success in endovascular stroke therapy. J Neurointervent Surg 11:433–438. https://doi.org/10.1136/neurintsurg-2018-014127
5. De Meyer SF, Denorme F, Langhauser F et al (2016) Thromboinflammation in stroke brain damage. Stroke 47:1165–1172. https://doi.org/10.1161/STROKEAHA.115.011238
6. Bala F, Ospel J, Mulpur B et al (2021) Infarct growth despite successful endovascular reperfusion in acute ischemic stroke: a meta-analysis. AJNR Am J Neuroradiol 42:1472–1478. https://doi.org/10.3174/ajnr.A7177

7. Chamorro Á, Amaro S, Castellanos M et al (2014) Safety and efficacy of uric acid in patients with acute stroke (URICO-ICTUS): a randomised, double-blind phase 2b/3 trial. Lancet Neurol 13:453–460. https://doi.org/10.1016/S1474-4422(14)70054-7
8. Hill MD, Goyal M, Menon BK et al (2020) Efficacy and safety of nerinetide for the treatment of acute ischaemic stroke (ESCAPE-NA1): a multicentre, double-blind, randomised controlled trial. Lancet 395:878–887. https://doi.org/10.1016/S0140-6736(20)30258-0
9. Bang OY, Goyal M, Liebeskind DS (2015) Collateral circulation in ischemic stroke: assessment tools and therapeutic strategies. Stroke 46:3302–3309. https://doi.org/10.1161/STROKEAHA.115.010508
10. Liu L, Ding J, Leng X et al (2018) Guidelines for evaluation and management of cerebral collateral circulation in ischaemic stroke 2017. Stroke Vasc Neurol 3:117–130. https://doi.org/10.1136/svn-2017-000135
11. Olivot JM, Mlynash M, Inoue M et al (2014) Hypoperfusion intensity ratio predicts infarct progression and functional outcome in the DEFUSE 2 cohort. Stroke 45:1018–1023. https://doi.org/10.1161/STROKEAHA.113.003857
12. Guenego A, Fahed R, Albers GW et al (2020) Hypoperfusion intensity ratio correlates with angiographic collaterals in acute ischaemic stroke with M1 occlusion. Eur J Neurol 27:864–870. https://doi.org/10.1111/ene.14181
13. Guenego A, Mlynash M, Christensen S et al (2018) Hypoperfusion ratio predicts infarct growth during transfer for thrombectomy. Ann Neurol 84:616–620. https://doi.org/10.1002/ana.25320
14. Hermier M, Nighoghossian N, Derex L et al (2003) Hypointense transcerebral veins at T2∗-weighted MRI: a marker of hemorrhagic transformation risk in patients treated with intravenous tissue plasminogen activator. J Cereb Blood Flow Metab 23:1362–1370. https://doi.org/10.1097/01.WCB.0000091764.61714.79
15. Morita N, Harada M, Uno M et al (2008) Ischemic findings of T2*-weighted 3-Tesla MRI in acute stroke patients. Cerebrovasc Dis 26:367–375. https://doi.org/10.1159/000151640
16. Kao H-W, Tsai FY, Hasso AN (2012) Predicting stroke evolution: comparison of susceptibility-weighted MR imaging with MR perfusion. Eur Radiol 22:1397–1403. https://doi.org/10.1007/s00330-012-2387-4
17. Zhang X, Zhang S, Chen Q et al (2017) Ipsilateral prominent thalamostriate vein on susceptibility-weighted imaging predicts poor outcome after intravenous thrombolysis in acute ischemic stroke. AJNR Am J Neuroradiol 38:875–881. https://doi.org/10.3174/ajnr.A5135
18. Luo Y, Gong Z, Zhou Y et al (2017) Increased susceptibility of asymmetrically prominent cortical veins correlates with misery perfusion in patients with occlusion of the middle cerebral artery. Eur Radiol 27:2381–2390. https://doi.org/10.1007/s00330-016-4593-y
19. Wang Y, Shi T, Chen B et al (2018) Prominent hypointense vessel sign on susceptibility-weighted imaging is associated with clinical outcome in acute ischaemic stroke. Eur Neurol 79:231–239. https://doi.org/10.1159/000488587
20. Powers WJ, Rabinstein AA, Ackerson T et al (2019) Guidelines for the early management of patients with acute ischemic stroke: 2019 update to the 2018 Guidelines for the Early Management of Acute Ischemic Stroke: a guideline for healthcare professionals from the American Heart Association/American Stroke Association. Stroke 50(12):e344–e418. https://doi.org/10.1161/STR.0000000000000211
21. Hacke W, Kaste M, Fieschi C et al (1998) Randomised double-blind placebo-controlled trial of thrombolytic therapy with intravenous alteplase in acute ischaemic stroke (ECASS II). Second European-Australasian Acute Stroke Study Investigators. Lancet 352:1245–1251. https://doi.org/10.1016/s0140-6736(98)08020-9
22. Olivot J-M, Mlynash M, Thijs VN et al (2008) Relationships between infarct growth, clinical outcome, and early recanalization in Diffusion and Perfusion Imaging for Understanding Stroke Evolution (DEFUSE). Stroke 39:2257–2263. https://doi.org/10.1161/STROKEAHA.107.511535
23. Haussen DC, Nogueira RG, Elhammady MS et al (2016) Infarct growth despite full reperfusion in endovascular therapy for acute ischemic stroke. J Neurointerv Surg 8:117–121. https://doi.org/10.1136/neurintsurg-2014-011497
24. Park M-G, Yang T-I, Oh S-J et al (2014) Multiple hypointense vessels on susceptibility-weighted imaging in acute ischemic stroke: surrogate marker of oxygen extraction fraction in penumbra? Cerebrovasc Dis 38:254–261. https://doi.org/10.1159/000367709
25. Guenego A, Leipzig M, Fahed R, Sussman ES, Faizy TD, Martin BW, Marcellus DG, Wintermark M, Olivot J-M, Albers GW et al (2021) Effect of oxygen extraction (brush-sign) on baseline core infarct depends on collaterals (HIR). Front Neurol 11:618765. https://doi.org/10.3389/fneur.2020.618765
26. Eltzschig HK, Eckle T (2011) Ischemia and reperfusion—from mechanism to translation. Nat Med 17:1391–1401. https://doi.org/10.1038/nm.2507
27. Rehncrona S, Rosén I, Siesjö BK (1981) Brain lactic acidosis and ischemic cell damage: 1. Biochemistry and Neurophysiology. J Cereb Blood Flow Metab 1:297–311. https://doi.org/10.1038/jcbfm.1981.34
28. Schilling A, Blankenburg F, Bernarding J et al (2002) Intracerebral pH affects the T2 relaxation time of brain tissue. Neuroradiology 44:968–972. https://doi.org/10.1007/s00234-002-0873-0
29. Lin L, Yang J, Chen C et al (2021) Association of collateral status and ischemic core growth in patients with acute ischemic stroke. Neurology 96:e161. https://doi.org/10.1212/WNL.0000000000011258
30. Bang OY, Saver JL, Kim SJ et al (2011) Collateral flow averts hemorrhagic transformation after endovascular therapy for acute ischemic stroke. Stroke 42:2235–2239. https://doi.org/10.1161/STROKEAHA.110.604603
31. Liebeskind DS, Tomsick TA, Foster LD et al (2014) Collaterals at angiography and outcomes in the Interventional Management of Stroke (IMS) III Trial. Stroke 45:759–764. https://doi.org/10.1161/STROKEAHA.113.004072
32. Regenhardt RW, Etherton MR, Das AS et al (2021) Infarct growth despite endovascular thrombectomy recanalization in large vessel occlusive stroke. J Neuroimaging 31:155–164. https://doi.org/10.1111/jon.12796
33. Seo W-K, Liebeskind DS, Yoo B et al (2020) Predictors and functional outcomes of fast, intermediate, and slow progression among patients with acute ischemic stroke. Stroke 51:2553–2557. https://doi.org/10.1161/STROKEAHA.120.030010
34. Chamorro Á, Blasco J, López A et al (2017) Complete reperfusion is required for maximal benefits of mechanical thrombectomy in stroke patients. Sci Rep 7:11636. https://doi.org/10.1038/s41598-017-11946-y
35. Horie N, Morikawa M, Nozaki A et al (2011) "Brush Sign" on susceptibility-weighted MR imaging indicates the severity of moyamoya disease. AJNR Am J Neuroradiol 32:1697–1702. https://doi.org/10.3174/ajnr.A2568
36. Darwish EAF, Abdelhameed-El-Nouby M, Geneidy E (2020) Mapping the ischemic penumbra and predicting stroke progression in acute ischemic stroke: the overlooked role of susceptibility weighted imaging. Insights Imaging 11:6. https://doi.org/10.1186/s13244-019-0810-y

Annexe n°1 : Editorial en préambule de l’étude n°4

European Radiology
https://doi.org/10.1007/s00330-023-09537-9

European Radiology
ESR EUROPEAN SOCIETY OF RADIOLOGY

COMMENTARY

Brush strokes on MRI

Jeffrey P. Guenette[1]

Received: 16 January 2023 / Revised: 16 January 2023 / Accepted: 5 February 2023

Acute ischemic stroke therapy aims to preserve and/or restore neurological function and maximize functional outcomes largely by restoring blood flow to ischemic but not yet infarcted regions of brain and thus limit the extent of infarct. However, inflammatory processes, such as endothelial interactions with regulatory T cells and oxidative stress, can trigger and contribute to secondary infarct growth after reperfusion [1, 2]. If we could predict patients at risk of secondary infarct growth, we could better study drugs that mediate thromboinflammatory and neuroinflammatory responses and thereby, perhaps, mitigate ischemia–reperfusion injury. Given that acute ischemic stroke algorithms in highly resourced regions of the world include rapid imaging with CTA and/or MRI/MRA prior to mechanical intervention, imaging features that serve as proxy for more advanced inflammatory responses could be ideal components of prediction models for secondary infarct growth.

In this issue of *European Radiology*, Bani-Sadr et al show that the "brush sign" — subjectively abnormal visualization of subependymal and medullary veins ipsilateral to the large vessel occlusion on T2*-weighted MRI images — appears to be an independent predictor of secondary large infarct growth (defined as growth > 11.6 mL from baseline ischemic core) following mechanical thrombectomy [3]. It is hypothesized that the brush sign reflects a high degree of venous blood deoxygenation due to a high oxygen extraction fraction in the ischemic tissue [4].

The authors of the current manuscript show that, in their cohort, the brush sign was associated with secondary large infarct growth while cerebral collateralization was not. Cerebral collateralization was instead associated with more rapid initial infarct growth, which corroborates results from prior studies. They explain that robust collaterals allow ongoing partial perfusion of a penumbra whereas brain tissue with poor collaterals is more likely to rapidly infarct. They contrast this pathophysiology with the hypothesized venous deoxygenation of the brush sign, which they intimate reflects that a component of penumbra is highly ischemic and therefore prone to inflammation following reperfusion. Hence, their rationale for the study that the brush sign would be a predictor for downstream reperfusion-related secondary large infarct growth.

Images from a single vendor product GRE T2*-weighted sequence were subjectively analyzed in this study, so it is unclear how generalizable the finding is to other sequences and other platforms. However, images from both 1.5-T and 3-T MRI systems were included. As the authors point out, susceptibility-weighted imaging, which is now commonly used in place of T2*-weighted imaging, is likely to be more sensitive to the brush sign, but it's unclear whether that increased sensitivity would positively or negatively impact the association with secondary large infarct growth. More detailed analysis with quantitative susceptibility mapping could potentially yield more precise results in the future; however, the simplicity of the subjective finding as investigated is more clinically relevant and potentially useful at this time.

While this study is not a prediction modeling study, it aims to inform prediction model building and some of the methods used are similar to those in building prediction models. Unlike in prediction models, where the nature of the relationship between the variable and outcome is frequently irrelevant, the authors of this study nicely frame the biophysical and pathophysiological rationale for studying the brush sign as a predictor. However, as in many prediction models, many factors included in the final multivariate analysis were chosen based on statistical significance in univariate analyses. This methodology leads to bias with potential overestimation of the association.

Overall, Bani-Sadr et al thoughtfully study and distinguish the implications of the brush sign (as a proxy for venous deoxygenation) and cerebral collateralization in the

This comment refers to the article available at https://doi.org/10.1007/s00330-022-09387-x

✉ Jeffrey P. Guenette
jpguenette@bwh.harvard.edu

[1] Division of Neuroradiology, Brigham and Women's Hospital, Harvard Medical School, 75 Francis Street, Boston, MA 02115, USA

Published online: 28 March 2023

prediction of acute ischemic stroke outcomes. They show the potentially important role that diagnostic radiology could have in determining treatment to prevent secondary large infarct growth following mechanical thrombectomy. It would be nice to see validation studies of the brush sign association with large infarct growth across vendor platforms and pulse sequences. This study suggests that the brush sign is a factor that should be included in future clinical prediction models for ischemia–reperfusion injury following large vessel occlusion.

Funding The authors state that this work has not received any funding.

Declarations

Guarantor The scientific guarantor of this publication is Jeffrey P. Guenette MD.

Conflict of interest The author of this manuscript declares relationships with the following companies: Funded in part by the GE Radiology Research Academic Fellowship through the Association of University Radiologists.

Statistics and biometry Not applicable.

Informed consent Not applicable.

Ethical approval Not applicable.

Methodology
- Invited commentary

References

1. De Meyer SF, Denorme F, Langhauser F et al (2016) Thromboinflammation in stroke brain damage. Stroke 47:1165–1172. https://doi.org/10.1161/STROKEAHA.115.011238
2. Kishimoto M, Suenaga J, Takase H et al (2019) Oxidative stress-responsive apoptosis inducing protein (ORAIP) plays a critical role in cerebral ischemia/reperfusion injury. Sci Rep 9:13512. https://doi.org/10.1038/s41598-019-50073-8
3. Bani-Sadr A, Pavie D, Mechtouff L et al (2023) Brush sign and collateral supply as potential markers of large infarct growth after successful thrombectomy. Eur Radiol. https://doi.org/10.1007/s00330-022-09387-x
4. Tamura H, Hatazawa J, Toyoshima H et al (2002) Detection of deoxygenation-related signal change in acute ischemic stroke patients by T2*-weighted magnetic resonance imaging. Stroke 33:967–971. https://doi.org/10.1161/01.str.0000013672.70986.e2

Étude n°5 : Les hypersignaux FLAIR vasculaires sont associés au résultat fonctionnel chez les patients à recanalisation effective après thrombectomie mécanique.

Contexte et état de la question.

Malgré une recanalisation réussie, 25 à 54 % des patients ont un mauvais résultat fonctionnel à trois mois après thrombectomie mécanique [49-52]. Certains auteurs ont qualifié cette situation de recanalisation futile c'est-à-dire un score mRs à 3 mois > 2 chez les patients ayant un score mTICI 2B-3 [69]. Des facteurs comme l'âge avancé, l'hypertension, un noyau ischémique initial important, une microangiopathie, des microbleeds, une atrophie cérébrale et un délai plus long entre l'apparition des symptômes et la recanalisation sont associés à un moindre bénéfice de la thrombectomie mécanique [113-118]. Les hypersignaux FLAIR vasculaires sont considérés comme un marqueur de l'état des collatérales cérébrales [119,120]. Des hypersignaux FLAIR vasculaires étendus sur l'IRM d'admission sont associés à un bon résultat fonctionnel et ont été proposées comme alternative pour la sélection des patients [121]. Néanmoins, la valeur pronostique des hypersignaux FLAIR vasculaires est moins bien connue chez les patients présentant une recanalisation réussie après thrombectomie. L'objectif de ce cinquième travail était d'examiner la valeur pronostique des hypersignaux FLAIR vasculaires chez les patients à recanalisation réussie après thrombectomie mécanique.

Principaux résultats.

Dans cette étude, nous avons constaté que des hypersignaux FLAIR vasculaires peu étendus (grade ≤ 3 c'est-à-dire un défaut d'hypersignaux FLAIR vasculaires dans sulci de la convexité) étaient associés à un moins bon résultat fonctionnel (mRS >2 à 3 mois) malgré une recanalisation réussie.

Diagnostic and Interventional Imaging 000 (2023) 1–6

Original article

Vascular hyperintensities on baseline FLAIR images are associated with functional outcome in stroke patients with successful recanalization after mechanical thrombectomy

Alexandre Bani-Sadr[a,b,*], Raphaël Escande[a], Laura Mechtouff[c,d], Dylan Pavie[a], Marc Hermier[a], Laurent Derex[c,e], Tae-Hee Choc[c,d], Omer F. Eker[a,b], Norbert Nighoghossian[c,d], Yves Berthezène[a,b]

[a] *Department of Neuroradiology, East Group Hospital, Hospices Civils de Lyon, 69500, Bron, France*
[b] *CREATIS Laboratory, CNRS UMR 5220, INSERM U 5220, Claude Bernard Lyon I University, 69100, Villeurbanne, France*
[c] *Stroke Department, East Group Hospital, Hospices Civils de Lyon, 69500, Bron, France*
[d] *CarMeN Laboratory, INSERM U1060, Claude Bernard Lyon I University, 69500, Bron, France*
[e] *Research on Healthcare Performance (RESHAPE), INSERM U 1290, Claude Bernard Lyon I University, 69373, Lyon Cedex 08, France*

ARTICLE INFO

Keywords:
Collateral circulation
Magnetic resonance imaging
Stroke
Thrombectomy
Treatment outcome

ABSTRACT

Purpose: The purpose of this study was to assess the prognostic value of vascular hyperintensities on FLAIR images (VHF) at admission MRI in patients with acute ischemic stroke (AIS) achieving successful recanalization after mechanical thrombectomy.
Materials and methods: Patients with AIS treated by mechanical thrombectomy following admission MRI from the single-center HIBISCUS-STROKE cohort were assessed for eligibility. VHF were categorized using a four-scale classification and were considered poor when grade < 3 (*i.e.*, absence of distal VHF). Recanalization was considered successful when modified thrombolysis in cerebral infarction score was ≥ 2B Functional outcome was considered poor if modified Rankin scale (mRS) at three months was > 2. Univariable and multiple variable logistic regressions were performed to identify factors associated with poor functional outcome despite successful recanalization.
Results: A total of 108 patients were included. There were 65 men and 43 women with a median age of 70.5 years (interquartile range: 55.0, 81.0; age range: 22.0–93.0 years). Among them, 39 subjects (36.1%) had poor functional outcome at three months. Univariable logistic regressions indicated that poorly extended VHF (VHF grade < 3) were associated with a poor functional outcome ($P = 0.008$) as well as age, hypertension and diabetes, baseline National Institute of Health Stroke Scale (NIHSS) score, pre-stroke mRS, lack of intravenous thrombolysis, cerebral microangiopathy and the presence of microbleeds. Multivariable analysis confirmed that poor VHF status was independently associated with a poor functional outcome (odds ratio [OR], 4.26; 95% confidence interval [CI]: 1.55–12.99; $P = 0.007$) in combination with hypertension (OR, 1.25; 95% CI: 0.87–1.85; $P = 0.02$), baseline NIHSS score (OR, 1.09; 95% CI: 1.04–1.20; $P = 0.03$), pre-stroke mRS (OR, 2.05; 95% CI: 1.07–4.61; $P = 0.05$) and lack of intravenous thrombolysis (OR, 0.23; 95% CI: 0.08–0.61; $P = 0.004$).
Conclusion: Poorly extended VHF (grade <3) at admission MRI are associated with a poor functional outcome at three months despite successful recanalization by mechanical thrombectomy.

1. Introduction

Mechanical thrombectomy (MT) has dramatically improved the treatment of acute ischemic stroke (AIS) due to large-vessel occlusion. However, recent studies indicated that 25% to 54% of patients experience a poor functional outcome at 3-months despite a successful angiographic recanalization [1–3]. Some authors have termed this condition futile recanalization, which is defined by a 3-month modified Rankin Scale (mRs) > 2 in patients with a modified

Abbreviations: AIS, Acute ischemic stroke; CI, Confidence interval; DWI, Diffusion-weighted imaging; FLAIR, Fluid-attenuated inversion recovery; IQR, Interquartile range; MT, Mechanical thrombectomy; mRs, modified Rankin scale; mTICI, modified thrombolysis in cerebral infarction; NIHSS, National Institutional of Health Stroke Scale.; OR, Odds ratio; VHF, Vascular hyperintensities on FLAIR images

* Corresponding author.
E-mail address: alexandre.bani-sadr@chu-lyon.fr (A. Bani-Sadr).

https://doi.org/10.1016/j.diii.2023.02.005
2211-5684/

Thrombolysis In Cerebral Infarction (mTICI) score 2B-3. Several factors modifying the efficacy of MT have been identified [1,3–9]. In this regard, older age, hypertension, large baseline ischemic core, microangiopathy, microbleeds, brain atrophy and longer time from symptoms onset to recanalization are associated with less benefit [1,3–9]. Conversely, MT is more beneficial as stroke severity, as assessed by baseline National Institute of Health Stroke Scale (NIHSS) score, increases [10,11].

The degree of collateral circulation is a critical prognostic factor in AIS because it promotes a higher rate of effective recanalization and contributes to the salvage of ischemic penumbra, thereby limiting infarct growth, and basically improving clinical outcome[12,13].

Vascular hyperintensities on fluid-attenuated inversion recovery (FLAIR) images (VHF) are thought to be a surrogate marker of cerebral collateral status [14,15]. Extensive VHF on magnetic resonance imaging (MRI) examination at admission are associated with a good functional outcome and have been proposed as an alternative for patient selection [16]. However, the prognostic value of VHF is less known in patients achieving effective recanalization after MT.

The purpose of this study was to examine the prognostic value of VHF observed on admission MRI in patients with AIS and successful recanalization after MT.

2. Materials and methods

2.1. Study population

The local ethics committee approved the HIBISCUS-STROKE Cohort studyand all subjects or their relatives signed an informed consent form (IRB number: 00009118). Because of the retrospective nature of this sub-analysis, no specific amendment was needed.

HIBISCUS-STROKE Cohort (CoHort of Patients to Identify Biological and Imaging markerS of CardiovascUlar Outcomes in Stroke; NCT: 03149705) is an ongoing observational study since October 2016 that included all patients with anterior circulation AIS with large vessel occlusions (*i.e.*, occlusions of internal carotid artery, M1 or M2 proximal segments of middle cerebral artery) treated with MT after brain MRI. In accordance with international guidelines, eligible patients were additionally treated with intravenous thrombolysis [17]. Board-certified neurologists (L.M. with 13 years of experience; L.D. with 25 years of experience and N.N. with 35 years of experience) collected baseline clinical characteristics including NIHSS and, assessed mRS at three months during a face-to-face follow-up visit. The mTICI score was assessed by post-hoc consensus analysis of post-MT digital-subtraction angiography by two neuroradiologists (O.E. with 15 years of experience and T.H.C. with 16 years of experience).

Inclusion criteria were: (*i*), Adequate quality for FLAIR images (no or minor motion artifacts); (*ii*), Available mRS at three months; and (*iii*), Successful recanalization (mTICI 2B-3). Patients were excluded when: (*i*), baseline FLAIR images were not interpretable due to major artifacts; (*ii*), no mRS at three months was available; or (*iii*), mTICI score was < 2.Functional outcome was considered poor if 3-month mRS was > 2.

2.2. Neuroimaging

Brain MRIs were performed with 1.5- or 3-Tesla MRI scanners (Ingenia, Philips Healthcare). MRI examinations at admission included axial T2-weighted FLAIR, axial T2-weighted gradient echo, axial diffusion-weighted imaging (DWI), 3D time-of-flight MR angiography, dynamic-susceptibility-contrast MRI and contrast-enhanced MR angiography. Table 1 summarizes the acquisition parameter of the FLAIR sequences [18,19]. For patients with available dynamic-susceptibility-contrast MRI, DWI and penumbra volumes were measured using a fully automatic MR software package (RAPID®, iSchemaView Inc). Computed tomography examination was systematically performed at day-1 to rule out any hemorrhagic transformation according to the European Cooperative Acute Stroke Study II classification [20].

Table 1
Acquisition parameters of T2-fluid-attenuated inversion recovery sequences.

Variable	1.5T MRI	3T MRI
Receiver coil	16-channel brain and neck combination coil	16-channel brain and neck combination coil
Time of repetition (ms)	9000	8000
Time of emission (ms)	120	111
Inversion time (ms)	2400	2500
Flip angle (°)	120	120
Acquisition plane	Axial	Axial
Field of view (mm)	230 × 230	230 × 230
Bandwidth (Hz/pixel)	373.8	264.1
Section thickness (after interpolation)	5	4.5
Acquired voxel size (mm^2)	0.98 × 0.98	0.99 × 0.99
Number of sections	22	24
Acquisition times (s)	108	100

T indicates tesla; MRI indicates magnetic resonance imaging.

2.3. FLAIR images analysis

Two neuroradiologists (A. B.-S. with four years of experience and R.E. with one year of experience) independently reviewed FLAIR images to grade the extent of VHF using a previously described classification, blinded to clinical and follow-up data [21]. VHF were defined as linear or serpentine high signal intensities relative to gray matter along the cortical sulci or brain surface in the cerebral hemisphere on at least two consecutive FLAIR images [14,15]. Grade 0 indicated absence of VHF; Grade 1 indicated VHF limited in the Sylvian fissure; Grade 2 indicated VHF limited to the Sylvian fissure and temporo-occipital junction, Grade 3 indicated VHF extended to the cerebral sulci of fronto-parietal lobe besides the location of the Grade 1 or Grade 2 VHF. Poor VHF were defined by grade < 3. They also reported the presence of microbleeds ($n \geq 5$) and cerebral microangiopathy as defined by an age-related white matter changes scale score ≥ 2 [22]. In case of discordant opinions, a third senior neuroradiologist (Y. B. with 25 years of experience) evaluated FLAIR images. Fig. 1 illustrates the VHF classification used.

2.4. Statistical analysis

The normality of the distribution of quantitative variables was tested using the Shapiro-Wilk test. Continuous variables were expressed as means and standard deviations or medians and interquartile ranges (IQR; Q1, Q3)) according to the normality of their distribution and, categorical variables were expressed as raw numbers and percentages [23]. Interobserver agreement was evaluated using Fleiss' kappa coefficient for the four-classification and Cohen's kappa coefficient was used for the binary classification (*i.e.*, VHF grades < 3 or = 3). Kappa values were reported along with their 95% confidence intervals (CI). Descriptive analyses were conducted according to the grade of VHF using parametric or non-parametric tests as appropriate.

Univariable and multiple variable logistic regressions were performed to search for independent variables associated with a poor functional outcome in patient achieving successful recanalization after MT. The multiple variable logistic model included covariates identified as associated with a poor outcome at univariable logistic regression using a *P*-value threshold of 0.025. The multiple variable logistic model was therefore adjusted for VHF grade < 3, hypertension, baseline NIHSS score, pre-stroke mRS and intravenous thrombolysis status.

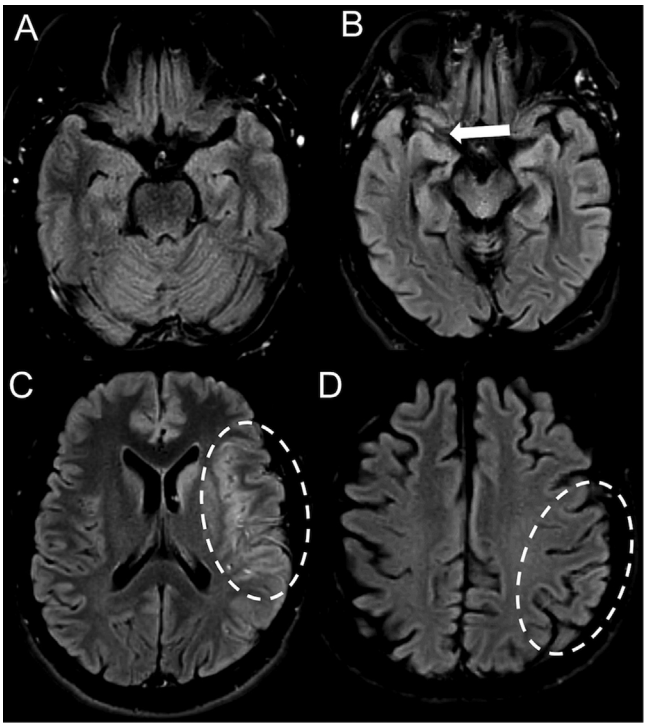

Fig. 1. Classification of vascular hyperintensities on fluid-attenuated inversion recovery images (VHF). VHF are defined as linear or serpentine hyperintensities and graded as follows: Grade 0: No VHF (A); Grade 1: VHF limited to the Sylvian fissure (arrow) (B); Grade 2: VHF extended to the Sylvian fissure and temporoparietal junction (C) and Grade 3: Grade 2 associated with distal VHF in parietal and/or frontal sulci (D).

All tests were two-sided and a *P*-value < 0.05 was considered to indicate statistically significant difference. All statistical analyses were performed with R software, version 4.2.2 (R foundation for Statistical Computing).

3. Results

3.1. Clinical characteristics of study population

During the study period, among the 191 patients included in the HIBISCUS-STROKE cohort 83 patients were excluded and 108 were ultimately included. There were 65 men (60.2%) and 43 women (39.8%) with a median age of 70.5 years (IQR: 55.0, 81.0; age range: 22.0–93.0 years). Fig. 2 shows the study flow-chart. The baseline NIHSS was 15.0 (IQR: 10.0, 19.0) and median time from symptoms onset to MRI was 109 min (IQR: 78.0, 237.0). Baseline MRIs were performed with at 1.5 T in 82 patients (75.9%) and at 3 T in 26 patients (24.1%). Sixty-three (58.3%) patients were additionally treated with intravenous thrombolysis and 39 (36.1%) had a poor functional outcome at three months.

3.2. VHF in the whole study population

Inter-observer agreement in the assessment of VHF was good using both a four-level scale classification (weighted kappa coefficient, 0.82; 95% CI: 0.75–0.91, and a binary classification (kappa coefficient, 0.88; 95% CI: 0.83–0.92). There were eight occurrences of discordant readings in VHF classification between the two readers.

Table 2 presents clinical and, radiological characteristics of the whole study population according to the grade of VHF. Using a four-scale classification, patients with poor VHF had a smaller ischemic penumbra, greater mRS at three months, and were more likely to have of a poor functional outcome at three months.

When using a binary classification of VHF (grade < 3 indicating poor VHF *vs.* grade = 3), patients with VHF grade < 3 had smaller median ischemic penumbra (55.0 mL; IQR: 24.8, 99.5) compared to those with VHF grade 3 (105.0 mL; IQR: 44.0, 115.0) (*P* = 0.04). No differences in median ischemic core volume was found between patients with VHF grade < 3 (25.5 mL; IQR: 8.3, 60.5) and those with VHF grade 3 (23.0 mL; IQR: 0.0, 49.0) (*P* = 0.67).

3.3. Factors associated with a poor functional outcome in subjects achieving successful recanalization

In patients with successful recanalization (*n* = 108), univariable analyses indicated that poorly extended VHF (*i.e.*, VHF grade < 3) was associated with a poor functional outcome despite successful recanalization (odds ratio [OR], 3.10; 95% CI: 1.38–7.31; *P* = 0.008) as well as with age (*P* = 0.008), hypertension (*P* < 0.001), diabetes (*P* = 0.04), baseline NIHSS score (*P* = 0.02), pre-stroke mRS (*P* < 0.001), lack of intravenous thrombolysis (*P* < 0.001), cerebral microangiopathy and the presence of microbleeds (*P* = 0.049). There was not association between baseline ischemic core volume (*P* = 0.97) and time from symptoms onset to MRI (*P* = 0.12).

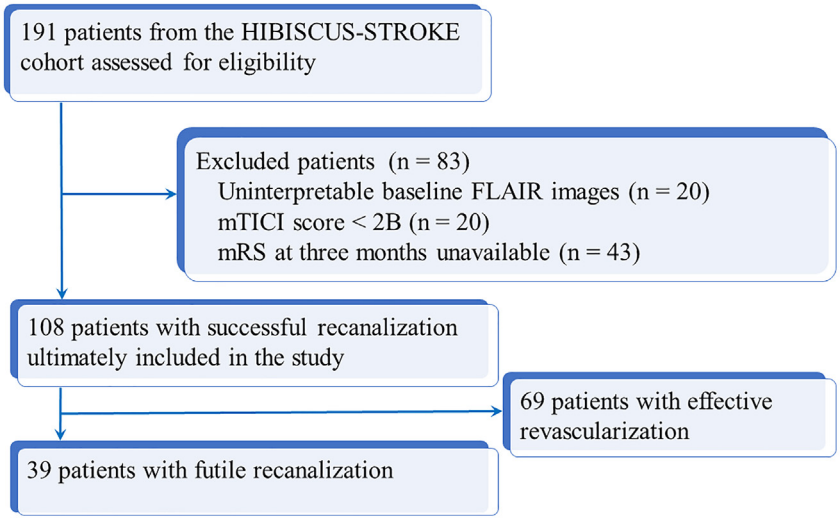

Fig. 2. Study flow-chart.
FLAIR indicates fluid-attenuated inversion recovery; mTICI indicates modified thrombolysis in cerebral infarction; mRS indicates modified Rankin scale.

Table 2
Clinical and imaging characteristics and outcomes of study population according to the extent of vascular hyperintensities on FLAIR images.

Variable	Grade 1	Grade 2	Grade 3	*P* value
Number of subjects	14 (13.0)	42 (38.9)	52 (48.1)	–
Clinical characteristics				
Male sex	8 (57.1)	25 (59.5)	32 (62.7)	0.95
Age	72.0 [54.3, 85.6]	73.0 [59.5, 80.5]	69.0 [55.0, 79.0]	0.55
Smoking	3 (21.4)	15 (35.7)	24 (46.2)	0.21
Hypertension	7 (50.0)	20 (47.6)	24 (46.2)	0.97
Diabetes	1 (7.1)	8 (19.0)	8 (15.4)	0.57
Dyslipidemia	2 (14.3)	13 (31.0)	14 (26.9)	0.48
Obesity	0 (0.0)	5 (11.9)	2 (3.8)	0.17
Atrial fibrillation*	2 (14.3)	11 (26.2)	15 (28.8)	0.50
Pre-stroke mRS	0.0 [0.0, 0.0]	0.0 [0.0, 0.0]	0.0 [0.0, 0.0]	0.97
Time from symptoms onset to MRI (min) †	235.0 [129.0, 407.0]	113.5 [79.0; 197.8]	101.0 [71.3, 175.0]	0.11
Baseline NIHSS score	15.0 [10.5, 17.0]	14.5 [10.3, 18.8]	16.0 [9.8, 19.0]	0.90
Intravenous thrombolysis	7 (50.0)	29 (69.2)	27 (51.9)	0.20
Radiological characteristics				
1.5T MRI magnet	9 (90.0%)	33 (78.6%)	40 (76.9)	0.54
Ischemic core volume (mL)	23.0 [4.0, 58.0]	26.5 [0.0, 49.0]	25.5 [8.3, 60.5]	0.90
Ischemic penumbra volume (mL) ‡	45.0 [8.0, 71.5]	63.0 [33.3, 129.0]	105.0 [44.0, 115.0]	0.05
Microangiopathy	11 (78.6)	31 (73.8)	34 (65.4)	0.52
Microbleeds	2 (14.3)	5 (11.9)	12 (23.1)	0.39
Occlusion locations				
Tandem occlusions	4 (28.6)	15 (35.7)	9 (17.4)	0.13
Intra-cranial internal carotid artery	1 (7.1)	5 (11.9)	4 (7.7)	0.75
M1 segment of middle cerebral artery	11 (78.6)	27 (64.4)	44 (84.6)	0.07
M2 segment of middle cerebral artery	2 (14.3)	10 (23.8)	4 (7.7)	0.09
Outcomes				
Hemorrhagic transformation	4 (28.6)	14 (33.3)	15 (28.8)	0.88
Parenchymal hematoma	0 (0.0)	2 (2.4)	1 (1.9)	0.56
Subarachnoid hemorrhage	0 0.0)	1 (4.8)	0 (0.0)	0.46
3-month mRS	3.0 [2.0, 4.0]	2.0 [1.0, 3.0]	2.0 [1.0, 2.0]	<0.001
3-month mRS > 2	8 (57.1)	18 (42.9)	12 (23.1)	0.03

Continuous variables are expressed as medians followed by interquartile ranges in brackets [IQR; Q1, Q3]. Categorical variables are expressed as raw numbers followed by percentages in parentheses.
mRS indicates modified rankin scale; IQR indicates interquartile range (Q1, Q3); NIHSS indicates National Institute of Health Stroke Scale.
* 12 missing values.
† 25 missing values.
‡ 43 missing values.

Multivariable analysis confirmed that VHF Grade < 3 was independently associated with a poor functional outcome (OR, 4.26; 95% CI: 1.55–12.99, $P = 0.007$) as well as with hypertension ($P = 0.02$), baseline NIHSS score ($P = 0.03$), pre-stroke mRS ($P = 0.05$) and lack of intravenous thrombolysis ($P = 0.004$). Table 3 summarizes crude and adjusted odds ratio of univariable and multivariable logistic regression models.

4. Discussion

In the present study, we found that poorly extended VHF at admission MRI examination are associated with poor functional outcome (mRS >2 at three months) despite successful recanalization in patients with AIS treated with MT.

VHF are thought to be a surrogate marker of cerebral collateral status [14,15]. Direct comparisons between FLAIR images and brain digital subtraction arteriography revealed a strong correlation between the extent of VHF and collateral status [15,21,24]. In our study, two patients with M2 segment occlusions had grade 1 VHF, which is upstream of the arterial occlusion site and may reflect a diminished blood flow rather than a leptomeningeal collateral flow. Similarly, a recent study indicated that proximal VHF were observed in 100% of AIS patients caused by internal carotid artery occlusion, 90.6% caused by M1 occlusion and 92.9% caused by M2 occlusion [25]. We assume that the pathophysiological significance of VHF may be polyvocal depending on its location. In agreement, Legrand et al. compared the value of the extent of VHF *versus* VHF-DWI mismatch (*i.e.*, VHF beyond the ischemic core) using the hypoperfusion intensity ratio as a surrogate marker of collateral status in patients referred for a MT [26]. These researchers concluded that VHF-DWI mismatch outperformed the extent of VHF in predicting the collateral status [26].

Notwithstanding, there is accumulating evidences that extensive VHF are associated with better outcome [14,16,27,28]. We evaluated the prognostic value of VHF on functional outcome at three months according to recanalization success. Our results reinforce the prognostic value of VHF specifically in patients with successful recanalization. In this population, the beneficial effect of extensive collaterals might consist in sustaining tissue viability pending for effective recanalization and, preventing early arterial reocclusions after recanalization [29]. Few studies have compared the degree of collaterals and functional outcome in this population. Weiss et al. reported an association between mRS at three months and the extent of collaterals, whereas Van Horn et al. reported the opposite [3,30]. We assume that these conflicting findings may be related to the use of single-phase computed-tomography angiography for collaterality assessment instead of multiphasic computed tomography angiography which is more reproducible [31].

Previous studies also reported that extensive VHF was associated with smaller baseline ischemic core and a larger ischemic penumbra [14,32–34]. We found that patients with poor VHF (grade <3) had smaller penumbra. However, we did not find a significant difference in ischemic core volume and none of the included patients had grade 0 VHF, which may be related to our sample size.

In agreement with previous studies, we found that older age, hypertension, diabetes, pre-stroke mRS, lack of intravenous

Table 3
Results of uni- and multivariable logistic regression analysis of markers of futile recanalization.

Variable	Crude OR (95% CI)	*P* value	Adjusted OR (95% CI)	*P* value
VHF Grade <3	3.10 (1.38–7.32)	0.008	4.26 (1.55–12.99)	0.007
Age*	1.11 (1.05–1.17)	<0.001	1.25 (0.87–1.85)	0.23
Hypertension	4.22 (1.85–10.07)	<0.001	3.56 (1.27–10.75)	0.02
Diabetes	3.05 (1.07–9.19)	0.04	–	–
Baseline NIHSS score†	1.08 (1.02–1.16)	0.02	1.09 (1.0–1.20)	0.03
Pre-stroke mRS (b)	1.20 (1.09–1.33)	<0.001	2.05 (1.07–4.61)	0.05
Intravenous thrombolysis	0.25 (0.10–0.55)	<0.001	0.23 (0.08–0.61)	0.004
Vascular Microangiopathy	2.59 (1.04–7.17)	0.05	–	–
Microbleeds	2.99 (1.09–8.53)	0.03	–	–
Time from symptoms onset to recanalization‡	1.03 (0.99–1.06)	0.07	–	–
mTICI score	0.94 (0.85–1.05)	0.26	–	–

VHF indicates vessel hyperintensities on fluid-attenuated inversion recovery images; NIHSS indicates National Institute of Health Stroke Scale; mRS indicates modified Rankin scale; mTICI indicates modified thrombolysis in cerebral infarction score; OR indicates Odds ratio; CI indicates confidence interval.
* per 10-year increase–.
† per 1-unit increase–.
‡ per 1-hour increase.

thrombolysis, microangiopathy and microbleeds were associated with poor functional outcome despite successful recanalization [3,4,6,7,10,11].

This study has some limitations including a single-center cohort and a small sample size. The number of patients with a poor functional outcome despite successful recanalization (n = 39) was low compared with the number of predictors included in the multiple variable model, which may have underpowered the principal analysis. This also prevented us from adjusting the multivariable model for essential factors including time from symptom onset to recanalization, occlusion site and mTICI score. Effective recanalization encompasses the mTICI 2B, mTICI2C and mTICI3 scores. However, the mTICI 2B score is associated with poorer outcome compared to the mTICI 2C and 3 scores [2]. Finally, 20 patients were excluded because of uninterpretable FLAIR images due to major motion artifacts. These motion artifacts are common in clinical practice and may limit the evaluation of VHF.

In conclusion, the results of our study reveal that poorly extended VHF (grade < 3) at admission MRI is associated with a poor functional outcome at three months despite successful recanalization with mechanical thrombectomy.

Disclosure of interest

All authors declare no actual or potential conflict of interest related to the submitted study

Credit author statement

ABS, and YB conceived and designed the project.
YB and NN supervised the project.
ABS, RR, LM, DP, MH, LD, THC and OE performed the measurements.
All authors have made substantial contribution in acquisition of data.
ABS, LM, LD, NN and YB drafted the article and revised it critically.
All authors approved the version to be published.

Human rights

The authors declare that the work described has been performed in accordance with the Declaration of Helsinki of the World Medical Association revised in 2013 for experiments involving humans.

Informed consent and patient details

The authors declare that this report does not contain any personal information that could lead to the identification.

Funding

This study was supported by the RHU MARVELOUS (Recherche Hospitalo-Universitaire MR Imaging to Prevent Cerebral and Myocardial Injury, ANR-16-RHUS-0009; recipient, Norbert Nighoghossian) of Claude Bernard University, Lyon I within the program “Investissements d’Avenir” operated by French National Research Agency (ANR).

Author contributions

All authors attest that they meet the current International Committee of Medical Journal Editors (ICMJE) criteria for Authorship.

References

[1] Goyal M, Menon BK, van Zwam WH, Dippel DWJ, Mitchell PJ, Demchuk AM, et al. Endovascular thrombectomy after large-vessel ischaemic stroke: a meta-analysis of individual patient data from five randomised trials. Lancet 2016;387:1723–31.
[2] Kaesmacher J, Dobrocky T, Heldner MR, Bellwald S, Mosimann PJ, Mordasini P, et al. Systematic review and meta-analysis on outcome differences among patients with TICI2b *versus* TICI3 reperfusions: success revisited. J Neurol Neurosurg Psychiatry 2018;89:910–7.
[3] van Horn N, Kniep H, Leischner H, McDonough R, Deb-Chatterji M, Broocks G, et al. Predictors of poor clinical outcome despite complete reperfusion in acute ischemic stroke patients. J NeuroIntervent Surg 2021;13:14–8.
[4] Malhotra A, Wu X, Payabvash S, Matouk CC, Forman HP, Gandhi D, et al. Comparative effectiveness of endovascular thrombectomy in elderly stroke patients. Stroke 2019;50:963–9.
[5] Molina CA. Futile recanalization in mechanical embolectomy trials: a call to improve selection of patients for revascularization. Stroke 2010;41:842–3.
[6] Gilberti N, Gamba M, Premi E, Costa A, Vergani V, Delrio I, et al. Leukoaraiosis is a predictor of futile recanalization in acute ischemic stroke. J Neurol 2017;264:448–52.
[7] Choi KH, Kim JH, Kang KW, Kim JT, Choi SM, Lee SH, et al. Impact of microbleeds on outcome following recanalization in patients with acute ischemic stroke. Stroke 2019;50:127–34.
[8] Pedraza MI, de Lera M, Bos D, Calleja AI, Cortijo E, Gómez-Vicente B, et al. Brain Atrophy and the risk of futile endovascular reperfusion in acute ischemic stroke. Stroke 2020;51:1514–21.
[9] Jahan R, Saver JL, Schwamm LH, Fonarow GC, Liang L, Matsouaka RA, et al. Association between time to treatment with endovascular reperfusion therapy and outcomes in patients with acute ischemic stroke treated in clinical practice. JAMA 2019;322:252.
[10] Hussein HM, Saleem MA, Qureshi AI. Rates and predictors of futile recanalization in patients undergoing endovascular treatment in a multicenter clinical trial. Neuroradiology 2018;60:557–63.
[11] Lee SH, Kim BJ, Han MK, Park TH, Lee KB, Lee BC, et al. Futile reperfusion and predicted therapeutic benefits after successful endovascular treatment according to initial stroke severity. BMC Neurol 2019;19:11.
[12] Liebeskind DS, Tomsick TA, Foster LD, Yeatts SD, Carrozzella J, Demchuk AM, et al. Collaterals at angiography and outcomes in the interventional management of stroke (IMS) III Trial. Stroke 2014;45:759–64.

[13] Vagal A, Aviv R, Sucharew H, Reddy M, Hou Q, Michel P, et al. Collateral clock is more important than time clock for tissue fate: a natural history study of acute ischemic Strokes. Stroke 2018;49:2102–7.
[14] Lee KY, Latour LL, Luby M, Hsia AW, Merino JG. Distal hyperintense vessels on FLAIR: an MRI marker for collateral circulation in acute stroke? Neurology 2009;72:1134–9.
[15] Sanossian N, Saver JL, Alger JR, Kim D, Duckwiler GR, Jahan R, et al. Angiography reveals that fluid-attenuated inversion recovery vascular hyperintensities are due to slow flow, not thrombus. AJNR Am J Neuroradiol 2009;30:564–8.
[16] on behalf of the THRACE Investigators, Legrand L, Turc G, Edjlali M, Beaumont M, Gautheron V, et al. Benefit from revascularization after thrombectomy according to FLAIR vascular hyperintensities: DWI mismatch. Eur Radiol 2019;29:5567–76.
[17] Powers WJ, Rabinstein AA, Ackerson T, Adeoye OM, Bambakidis NC, Becker K, et al. Guidelines for the early management of patients with acute ischemic stroke: 2019 update to the 2018 guidelines for the early management of acute ischemic stroke: a guideline for healthcare professionals from the American Heart Association/American Stroke Association. Stroke 2019;50:e344–418.
[18] Eliezer M, Vaussy A, Toupin S, Barbe R, Kannengiesser S, Stemmer A, et al. Iterative denoising accelerated 3D SPACE FLAIR sequence for brain MR imaging at 3T. Diagn Interv Imaging 2022;103:13–20.
[19] Osman S, Hautefort C, Attyé A, Vaussy A, Houdart E, Eliezer M. Increased signal intensity with delayed post contrast 3D-FLAIR MRI sequence using constant flip angle and long repetition time for inner ear evaluation. Diagn Interv Imaging 2022;103:225–9.
[20] Hacke W, Kaste M, Fieschi C, von Kummer R, Davalos A, Meier D, et al. Randomised double-blind placebo-controlled trial of thrombolytic therapy with intravenous alteplase in acute ischaemic stroke (ECASS II). Second European-Australasian Acute Stroke Study Investigators. Lancet 1998;352:1245–51.
[21] Liu W, Xu G, Yue X, Wang X, Ma M, Zhang R, et al. Hyperintense vessels on FLAIR: a useful non-invasive method for assessing intracerebral collaterals. Eur J Radiol 2011;80:786–91.
[22] Wahlund LO, Barkhof F, Fazekas F, Bronge L, Augustin M, Sjögren M, et al. A new rating scale for age-related white matter changes applicable to MRI and CT. Stroke 2001;32:1318–22.
[23] Barat M, Jannot AS, Dohan A, Soyer P. How to report and compare quantitative variables in a radiology article. Diagn Interv Imaging 2022;103:571–3.
[24] Huang X, Liu W, Zhu W, Ni G, Sun W, Ma M, et al. Distal hyperintense vessels on FLAIR: a prognostic indicator of acute ischemic stroke. Eur Neurol 2012;68:214–20.
[25] Shin DH, Han SK, Lee JH, Choi PC, Park SO, Lee YH, et al. Proximal hyperintense vessel sign on initial FLAIR MRI in hyper-acute middle cerebral artery ischemic stroke: a retrospective observational study. Acta Radiol 2021;62:922–31.
[26] Legrand L, Le Berre A, Seners P, Benzakoun J, Ben Hassen W, Lion S, et al. FLAIR vascular hyperintensities as a surrogate of collaterals in acute stroke: DWI matters. AJNR Am J Neuroradiol 2023;44:26–32.
[27] Liu D, Scalzo F, Rao NM, Hinman JD, Kim D, Ali LK, et al. Fluid-attenuated inversion recovery vascular hyperintensity topography, novel imaging marker for revascularization in middle cerebral artery occlusion. Stroke 2016;47:2763–9.
[28] Nave AH, Kufner A, Bücke P, Siebert E, Kliesch S, Grittner U, et al. Hyperintense vessels, collateralization, and functional outcome in patients with stroke receiving endovascular treatment. Stroke 2018;49:675–81.
[29] Nie X, Pu Y, Zhang Z, Liu X, Duan W, Liu L. Futile recanalization after endovascular therapy in acute ischemic stroke. BioMed Res Int 2018;2018:1–5.
[30] Weiss D, Kraus B, Rubbert C, Kaschner M, Jander S, Gliem M, et al. Systematic evaluation of computed tomography angiography collateral scores for estimation of long-term outcome after mechanical thrombectomy in acute ischaemic stroke. Neuroradiol J 2019;32:277–86.
[31] Wang Z, Xie J, Tang T-Y, Zeng C-H, Zhang Y, Zhao Z, et al. Collateral status at single-phase and multiphase CT angiography *versus* CT perfusion for outcome prediction in anterior circulation acute ischemic stroke. Radiology 2020;296:393–400.
[32] Legrand L, Tisserand M, Turc G, Naggara O, Edjlali M, Mellerio C, et al. Do FLAIR vascular hyperintensities beyond the DWI lesion represent the ischemic penumbra? AJNR Am J Neuroradiol 2015;36:269–74.
[33] Mahdjoub E, Turc G, Legrand L, Benzakoun J, Edjlali M, Seners P, et al. Do fluid-attenuated inversion recovery vascular hyperintensities represent good collaterals before reperfusion therapy? AJNR Am J Neuroradiol 2018;39:77–83.
[34] Zhou Z, Malavera A, Yoshimura S, Delcourt C, Mair G, Al-Shahi Salman R, et al. Clinical prognosis of FLAIR hyperintense arteries in ischemic stroke patients: a systematic review and meta-analysis. J Neurol Neurosurg Psychiatry 2020;91:475–82.

Étude n°6 : Perméabilité de la BHE et cinétique des marqueurs inflammatoires chez les patients traités par thrombectomie mécanique pour un infarctus cérébral

Contexte et état de la question.

Au décours de l'infarctus cérébral, la rupture de la BHE obéit à un processus physiopathologique complexe. Au cours de la dernière décennie, les MMP ont été largement étudiées pour leur rôle dans la dégradation de la matrice extracellulaire [122,123]. Il a été démontré que la MMP-9 était associée à une rupture de la BHE sur les IRM de suivi précoce [124,125]. Néanmoins, la relation entre la perméabilité de la BHE sur l'IRM d'admission et les marqueurs de la réponse neuroinflammatoire reste peu explorée. Une meilleure compréhension apporterait des informations précieuses sur la pathogenèse des lésions l'ischémie-reperfusion [17,29]. L'objectif de cette sixième étude était d'étudier la relation entre la perméabilité de la BHE évaluée sur l'IRM d'admission et un panel de marqueurs inflammatoires circulants.

Principaux résultats.

Sur la population totale, nous avons observé qu'une perméabilité accrue de la BHE était associée à un noyau ischémique plus étendue. Dans une analyse en sous-groupe sur les patients dont les symptômes étaient apparus il y a moins de 6h, nous avons objectivé qu'une perméabilité accrue de la BHE était indépendamment associée à des taux sanguins de MMP9 plus élevés à l'admission et à un noyau ischémique plus étendu.

Gmail **Alexandre Pedram BANI SADR <apbanisadr@gmail.com>**

TR: NEUROLOGY MS ID#: NEUROLOGY/2022/188500 - Final Acceptance l Embargo Policy

alexandre.bani-sadr@chu-lyon.fr <alexandre.bani-sadr@chu-lyon.fr> 26 mai 2023 à 19:25
À : apbanisadr@gmail.com

De : journal@neurology.org <journal@neurology.org>
Envoyé : jeudi 13 avril 2023 21:58
À : BANI-SADR, Alexandre
Cc : MECHTOUFF, Laura; DE-BOURGUIGNON, Charles; aela.mauffrey@orange.fr; timothe.boutelier@olea-medical.com; CHO, Tae-Hee; m.cappucci86@gmail.com; AMELI, Roxana; HERMIER, Marc; DEREX, Laurent; NIGHOGHOSSIAN, Norbert; BERTHEZENE, Yves
Objet : NEUROLOGY MS ID#: NEUROLOGY/2022/188500 - Final Acceptance l Embargo Policy

13 April 2023

NEUROLOGY MS ID#: NEUROLOGY/2022/188500
MS TITLE: Brain-Blood Barrier Permeability and Kinetics of Inflammatory Markers in Acute Stroke Patients Treated by Thrombectomy
Alexandre Bani-Sadr, Laura MECHTOUFF, Charles de Bourguignon, Aela Mauffrey, Timothe Boutelier, Tae-Hee Cho, Matteo Cappucci, Roxana AMELI, Marc Hermier, Laurent Derex, Norbert Nighoghossian, and Yves Berthezene

Dear Dr. Bani-Sadr:

We are pleased to accept your paper for publication in NEUROLOGY.

Your paper is now in production. To facilitate production, the corresponding author may receive communication from the Neurology Editorial Office and Editage during this time, requesting additional action or materials.

If your paper is eligible for online-first publication, you can expect the accepted manuscript to be posted online in approximately 3 to 9 weeks. Not all papers publish online-first ahead of the assigned journal issue. You should be aware that the embargo will be lifted when the accepted manuscript is posted online. ***IMPORTANT:*** *If your article is designated for open access, you must pay the article publication charge when prompted---the corresponding author should receive an email within 24 hours from publicationservices@copyright.com with the subject line "Please Submit Your Open Access Article Publication Charge(s)." Open access articles will publish behind a paywall until the article publication charge payment is received or an invoice is raised.*

Please refer to our embargo policy, press release information, production timelines, and other important information at the end of this letter.

Sincerely,

José G. Merino, MD, MPhil, FAAN
Editor-in-Chief, NEUROLOGY

Embargo Policy

Your paper and its findings are embargoed. Prior to publication, authors may not reveal that the paper is under consideration

when presenting at scientific meetings, or release information to the press. News media and institutional public relations departments must not publicize the paper or its findings until 4:00PM Eastern the day of first online publication. *Consequences for an embargo break are serious*: Neurology.org/research-policies-and-guidelines.

Embargo policy
Andrea Rahkola (arahkola@neurology.org)

Embargo lift date inquiries—*only upon receipt of the "Welcome to Production" email*
PE-AAN@wolterskluwer.com

Please Note: If you or a coauthor are contacted by representatives from the AAN's *Neurology Today* or *Brain & Life,* you may communicate with them for coverage of your paper. However, please do not directly engage with any other news source prior to embargo lift.

Press Release

If your institution has plans to issue a press release at the time the embargo is lifted, ≤8 weeks from the date of this letter, please encourage your institutional PR team to contact AAN PR staff (information below). Direct all reporters to contact AAN PR staff for an embargoed copy of the research article. Embargoed articles should not be distributed by anyone other than the AAN. Please also send a separate email to Production Editor Andrea Rahkola (arahkola@neurology.org) expressing the intention to publish an institutional press release.

Press release policy/inquiries
Renee Tessman (rtessman@aan.com)

Please Note: The AAN will notify you if it plans to issue a press release on the study.

Production Timeline

In 2 to 8 weeks: A "**Welcome to Production**" email will be sent from our publisher (Wolters Kluwer) after the paper is transmitted by the journal. **To ensure the corresponding author receives important communications from our publisher**, the corresponding author should add **editorialmanager.com** and **wolterskluwer.com** to their safe senders list.

In 3 to 10 weeks: Online-first publication of a water-marked manuscript version, prior to copyediting and proof review, will occur 1 to 2 weeks after receipt of the "**Welcome to Production**" email.

Online-first publication date inquiries—*only upon receipt of the "Welcome to Production" email*
PE-AAN@wolterskluwer.com

In 5 to 11 weeks: The corresponding author will receive proofs approximately 3 weeks after the "**Welcome to Production**" email is received. The proof will come via email from **editorialmanager.com**. The subject line will read **Please Pick Up Your Proofs for Your Article in Neurology**.

Proof inquiries—*only after receipt of the "Welcome to Production" email*
PE-AAN@wolterskluwer.com

The corresponding author must be available to review proofs within a 48 hours (2 business days) period. If necessary, please arrange to have proofs sent to a coauthor for review and notify PE-AAN@wolterskluwer.com. We are not able to modify the production schedule to accommodate author absences.

Final publication of a composed article version, after copyediting and proof review, will occur on the assigned journal issue's publication date.

Reader Comments
Readers may comment on your published article via *Disputes & Debates: Rapid online correspondence* (the letters-to-the-editor section of NEUROLOGY). The corresponding author of your paper will be notified via email 1 day prior to online posting of reader comments. Authors are expected to respond promptly to comments (within 10 business days). Comments of great interest will be chosen for print (*Disputes & Debates: Editors' Choice)* and indexed in PubMed.

Corresponding Author from UKB institution in the Netherlands

If the corresponding author is from a UKB institution in the Netherlands, please contact your library (http://www.openaccess.nl/en/references/contacts) for information on their open access requirements.

Many thanks for your contribution to NEUROLOGY. As a valued author, we are pleased to offer you a 20% discount on any LWW book. Please go to http://journals.lww.com/dm/Pages/BookDiscountMedical.aspx for details.

American Board of Psychiatry and Neurology (ABPN) diplomates

NEUROLOGY is a peer-reviewed journal indexed in the MEDLINE database. Therefore, ABPN diplomates who have published an article in NEUROLOGY may self-report the non-CME self-assessment activity to waive 8 self-assessment CME credits. Contact the ABPN directly for details: mquestions@abpn.com or tel: (847) 229-6500.

Neurology®
201 Chicago Ave
Minneapolis, MN 55415
tel. (612) 928-6400
fax (612) 454-2748

TITLE OF THE MANUSCRIPT

Brain-Blood Barrier Permeability and Kinetics of Inflammatory Markers in Acute Stroke Patients Treated by Thrombectomy

Authors:

Alexandre BANI-SADR[1,2] *, MD; Laura MECHTOUFF[3,4] *, MD-PhD; Charles de BOURGUIGNON[5], Eng; Aela MAUFFREY[6], PhD; Timothe BOUTELIER[6], PhD Tae-Hee CHO[3,4], MD-PhD; Matteo CAPPUCCI[1], MD Roxana AMELI[1], MD; Marc HERMIER[1], MD-PhD; Laurent DEREX[3], MD-PhD; Norbert NIGHOGHOSSIAN[3,4], MD-PhD; Yves BERTHEZENE[1,2], MD-PhD.

*: Both authors contributed equally to this work

ABSTRACT.

Background and Objectives:

To investigate the relationship between baseline blood-brain barrier (BBB) permeability and the kinetics of circulating inflammatory markers in a cohort of acute ischemic stroke (AIS) patients treated with mechanical thrombectomy.

Methods:

The HIBISCUS-STROKE cohort includes AIS patients treated with mechanical thrombectomy following admission MRI, and undergoing a sequential assessment of circulating inflammatory markers. Baseline dynamic-susceptibility perfusion MRI was post-processed with arrival time correction to provide K2 maps reflecting BBB permeability. After co-registration of apparent-diffusion-coefficient and K2 maps, 90th percentile of K2 value was extracted within baseline ischemic core and expressed as a percentage change compared to contralateral normal appearing white matter. Population was dichotomized according to median K2 value. Uni- and multiple variable logistic regressions analyses were performed to investigate factors associated with increased pretreatment BBB permeability in the whole population and in patients with symptoms onset <6h.

Results:

In the whole population (n=105 patients, median K2=1.59), patients with increased BBB permeability had higher serum levels of MMP-9 at H48 (p=0.02), higher CRP serum level at H48 (p=0.01), poorer collateral status (p=0.01), and larger baseline ischemic core (p<0.001). They were more likely to have hemorrhagic transformation (p=0.008), larger final lesion volume (p=0.02), and worst neurologic outcome at 3-months (p=0.04). The multiple variable logistic regression indicated that increased BBB

permeability was only associated with ischemic core volume (Odds Ratio (OR)= 1.04; 95% Confidence Interval (CI): [1.01; 1.06], p<0.0001).

Restricting analysis to patients with symptoms onset < 6h (n=72, median K2=1.27), subjects with increased BBB permeability had higher serum levels of MMP-9 at both H0 (p=0.005), H6 (p=0.004), H24 (p=0.02) and H48 (p=0.01), higher CRP levels at H48 (p=0.02) and larger baseline ischemic core (p<0.0001). The multiple variable logistic analysis showed that increased BBB permeability was independently associated with higher H0 MMP-9 levels (OR=1.33; 95% CI: [1.12; 1.65]; p=0.01) and larger ischemic core (OR=1.27; 95% CI: [1.08; 1.59]; p=0.04).

Discussion:

In AIS patients, increased BBB permeability is associated with larger ischemic core. In the subgroup of patients with symptoms onset <6h, increased BBB permeability is independently associated with higher H0-MMP-9 levels and larger ischemic core.

Introduction.

Blood brain barrier (BBB) breakdown following acute ischemic stroke (AIS), is a dynamic process triggered by a series of pathophysiological events where the inflammatory response plays a major role[1,2]. Over the last decade, the matrix metalloproteinases (MMPs) have been widely investigated for their role in disruption of BBB, particularly the extracellular matrix[3,4]. Proteolytic degradation of the BBB increases its permeability within hours of ischemia resulting in vasogenic edema, leukocyte infiltration, and hemorrhagic transformation (HT)[5–9]. Specifically, several studies indicated that MMP-9 was associated with BBB disruption at early follow-up MRI[10,11].

MR perfusion techniques can quantify BBB permeability by modelling the efflux rate of the contrast agent from the plasma within the tissue. Dynamic susceptibility contrast (DSC) MRI has been investigated to predict HT using K2 as a surrogate marker of BBB permeability[12].

However, the relationship between BBB permeability at admission MRI and biological markers of neuroinflammation remains poorly explored, particularly in the clinical setting of acute ischemic stroke (AIS) due to large vessel occlusion treated by mechanical thrombectomy. The coupled assessment of BBB permeability and the kinetics of systemic markers reflecting central neuroinflammatory response may provide additional insight in the pathogenesis of ischemic/reperfusion injury[2,13,14].

In this study, we aimed to assess the relationship between BBB permeability assessed at admission MRI and a panel of circulating inflammatory markers in a cohort of AIS patients treated with mechanical thrombectomy.

Material and methods.

Data Availability Statement

Further anonymized data can be made available to qualified investigators on request to the corresponding author**.**

Ethic Statement

This study was approved by the local ethics committee (IRB number: 00009118).

All subjects or their relative signed an informed consent form.

Study design and cohort.

The HIBISCUS-STROKE Cohort (CoHort of Patients to Identify Biological and Imaging markerS of CardiovascUlar Outcomes in Stroke; NCT: 03149705) is an observational single-center study that prospectively includes AIS patients with large vessel occlusion of the anterior circulation treated with MT after MRI triage. Eligible patients were additionally treated with intravenous thrombolysis after admission MRI[15].

Peripheral blood samples were collected for each patient: at admission (H0), 6h (H6), 24h (H24) and 48h (H48). A brain CT scan at Day-1 was systematically performed to assess hemorrhagic transformation according to the European Cooperative Acute Stroke Study II classification[16]

Successful reperfusion was defined as achieving a modified thrombolysis in cerebral infarction (mTICI) score ≥ 2B.

Baseline data on demographic characteristics and National Institute of Health Stroke Scale (NIHSS) score were collected at admission, and modified Rankin Score (mRS) was assessed at 3-months by a board-certified neurologist. Revascularization was considered futile when revascularization was successful and 3-months mRS ≥ 3[17]

Inclusion criteria in this study were: (1) Availability of DSC-MRI and (2) availability of admission biological assays.

Neuroimaging and post-processing.

Admission MRIs were performed with 1.5 – Tesla or 3 – Tesla *Ingenia* scanners (*Philips Healthcare, Best, The Netherlands)*. They included axial diffusion-weighted imaging (DWI), axial T2-gradient echo, axial T2-Fluid attenuated inversion recovery (FLAIR), 3D-time-of-flight, contrast-enhanced MR angiography, and DSC-MRI. For DSC-MRI, a bolus of contrast medium (*Dotarem; Guerbet, Aulnay-sous-Bois, France*) was injected at a standard dose of 0.1mmol/kg at 4mL/s, followed by 20mL of saline solution.

The ischemic core was segmented from the baseline DWI with a semi-automated method (3D Slicer: https:// www.slicer.org/) by using both a validated ADC threshold (ADC <620 × 10−6 mm2/s) and visual assessment of b1000 images.

On DSC-MRI, the administration of a contrast medium induces a decrease in signal intensity (T2* effect) during the first pass of gadolinium followed by a gradual return to baseline. In case of increased BBB permeability, the extravasation of contrast medium induces an increase in signal (T1 effect) and a more rapid return to baseline. This extravasation during the first pass can be quantified by means of K2[18]. In case of diminished blood flow, an arrival time correction methods is required before calculating permeability maps as previously proposed [12,19,20]. Corrected K2 maps were generated from DSC-MRI using a pre-commercial version of OleaSphere (Oleasphere ®, La Ciotat, France). After co-registration of K2 and ADC maps, 90th percentiles of K2 values within the ischemic core (ADC <620 × 10−6 mm2/s) were extracted and expressed as a percentage change compared to normal appearing white matter in the contralateral centrum semi-ovale as previously proposed[21,22]. Cerebral collateral status was assessed using the hypoperfusion intensity ratio (HIR), which is the volume of Tmax ≥ 10s divided by the volume of Tmax ≥ 6s[23].

Follow-up MRI was performed at day 6 with an axial T2-FLAIR sequence. Final lesion volume was segmented using a semi-automated method (3D Slicer: https://www.slicer.org/) after co-registration of day-6 T2-FLAIR images and initial DWI images.

Blood Sampling Protocol

Sera were obtained and stored at -80°C within 3 hours of collection at the NeuroBioTec biobank (CRB-HCL: BB-0033-00046, France). All samples were thawed only once for study measurements. C-reactive protein (CRP), interleukin (IL)-6, IL-8, IL-10 were measured using enzyme linked immunosorbent assay (ELISA) kits from e-Bioscience (Affymetrix). Monocyte Chemoattractant Protein-1 (MCP-1), soluble tumor necrosis factor receptor 1 (TNFR1), soluble form of Suppression of Tumorigenicity 2 (sST2), P-selectin, matrix metalloproteinase-9 (MMP-9), soluble P-selectin (sP-selectin) and Vascular Cellular Adhesion Molecule-1 (VCAM-1) were measured using ELISA kits from R&D (Duoset). If serum concentrations of blood biomarkers were below the detection limit, values were replaced by a fixed value of 0.

Statistical analysis

Continuous variables are expressed as means (standard deviation) or medians (interquartile range [IQR]) depending on their distributions, and categorical variables as percentages. Medians were compared using the Mann-Whitney test and percentages were compared with Chi-square test.

Because the assumptions of the linear models were not satisfied, the K2 values were dichotomized into low and high levels based on their median values.

For the whole study population, uni- and multiple variable logistic regressions were performed to assess factors associated with an increased BBB permeability. The multiple variable model included covariates with a $p<0.1$ at univariable analyses and

others selected a priori independent of their univariate p value, assumed to be causal (baseline ischemic core volume, baseline NIHSS score[19]). It was adjusted for baseline NIHSS score, H0-MMP9 level, baseline ischemic core volume and HIR.

Because some authors have reported a nonlinear and biphasic evolution of BBB permeability and MMP-9 expression with a peak at 6 h after ischemic injury onset, a subgroup analysis was conducted in patients with symptoms onset <6h[1,24]. Similarly, uni- and multiple variable logistic regression analyses were performed to assess factors associated with an increased BBB permeability. The multiple variable model included covariates with a $p<0.1$ at univariable analyses and others selected a priori independent of their univariate p value hypothesized as causal (baseline ischemic core volume, baseline NIHSS score[19]). To prevent expected collinearity between H0 MMP-9 and H6 MMP-9 levels, only H0 MMP-9 level was entered in the multiple variable models. Therefore, it was adjusted for baseline NIHSS score, H0-MMP9 level, baseline ischemic core volume and HIR.

All statistical analyses were performed using R software, version 4.2.2 (*R foundation for Statistical Computing, Vienna, Austria*). Statistical significance was set by a two-tailed p-value <0.05.

Results:

Study population.

From October 2016 to April 2019, 105 patients were included in the study among the 225 patients in the cohort. Flow-chart is shown in **Figure 1**.

Excluded patients did not differ in age (68.7 $\pm$ 14.7 years vs 67.9 $\pm$ 15.1 years), sex (56.6% male vs 57.1%), baseline NIHSS score (median: 14.0, interquartile range (IQR): [6.5; 19.0] vs 15.0, IQR: [10.0; 19.0]), baseline ischemic core volume (median:

14.1 mL, IQR: [5.8; 53.5] vs 21.5 mL, IQR: [8.6; 39.8]) nor time from symptoms onset to MRI (median: 96.0 min, IQR: [76.5; 139.5] versus 96.0 min, [73.5; 125.5]).

Factors associated with increased BBB permeability in the whole study population.

In the whole study population, median K2 was 1.59 (IQR: [0.27; 5.90]). Patients with a high K2 had higher serum levels of MMP-9 at H48 (p=0.02), higher CRP serum level at H48 (p=0.01), higher HIR indicating poorer collateral status (p=0.01), and larger baseline ischemic core (p<0.001). They were more likely to have hemorrhagic transformation (p=0.008), larger final lesion volume (p=0.02) and worst neurologic outcome at 3-months (p=0.04). **Table 1** presents clinical, biological, radiological characteristics and outcomes of patients according to K2 status in the whole study population. **Figure 2** presents the kinetics of MMP-9 levels as a function of K2 status. The K2 value did not differ significantly according to the thrombolysis status (p=0.44) nor did the serum MMP-9 levels at H0, H6, H24 and H48 (all p ≥0.09). **eTable 1** presents MMP-9 levels at H0, H6, H24 and H48 according to the thrombolysis status. **eFigure 1** presents violin plots of circulating inflammatory markers studied according to K2 status.

The multiple variable analysis indicated that only ischemic core volume was significantly associated with an increased BBB permeability (Odds Ratio (OR)= 1.04; 95% Confidence Interval (CI): [1.01; 1.06]; p<0.0001). There was a statistical trend for H0-MMP9 level but no significant association (OR=1.01; 95% CI: [0.99; 1.02]; p=0.06). **Table 2** presented crude and adjusted odds ratio.

Factors associated with increased BBB permeability in patients with symptoms onset <6h.

In patients with symptoms onset < 6h (n=72), median K2 was 1.27 (IQR: [0.27; 5.90]. In this subgroup, patients with a high K2 had higher serum levels of MMP-9 at both H0 (p=0.005), H6 (p=0.04), H24 (p=0.02) and H48 (p=0.01), higher CRP levels at H48 (p=0.02) and larger baseline ischemic core (p<0.0001). They were more likely to have hemorrhagic transformation (p=0.01) and had larger final lesion volume (p=0.04). **eTable 2** details clinical, biological, radiological characteristics and outcomes in this subgroup.

The multiple variable regression analysis indicated that increased BBB permeability was independently associated with higher H0 MMP-9 serum levels (OR=1.33; 95% CI: [1.12; 1.65]; p=0.01) and larger baseline ischemic core (OR=1.27; 95% CI: [1.08; 1.59]; p=0.04). **Table 3** presents crude and adjusted odds ratio.

Figure 3 presents the admission MRIs of a patient with increased BBB permeability

Discussion.

The purpose of this study was to evaluate the relationships between BBB permeability and the kinetics of circulating markers reflecting central neuroinflammatory response in AIS patients treated with mechanical thrombectomy. In the whole study population, we observed that increased BBB permeability was associated with larger ischemic core while in a subgroup analysis of patients with symptoms onset < 6h, it was independently associated with larger ischemic core and higher H0-MMP9 levels.

The pathophysiological mechanisms involved in BBB breakdown following arterial occlusion are highly complex. In addition to reactive oxygen species, metalloproteinases are considered as a major contributor to BBB breakdown as they directly degrade tight junction proteins and extracellular matrix[1,4]. Numerous studies have documented that an increase in MMP-9 levels was associated with BBB breakdown[25–27]. In early studies, authors identified BBB disruption as a late

enhancement of cerebrospinal fluid space on follow-up T2-FLAIR that was termed hyperacute reperfusion marker (HARM)[14,28]. They reported that this phenomenon was associated with HT, worsened functional outcomes and higher MMP-9 levels[10,11,14,28]. In agreement, we found that H0 MMP-9 levels were associated with increased BBB permeability in patients with symptoms onset < 6h. Compared with HARM, K2 maps have the advantage of allowing assessment of BBB permeability during admission MRI and do not require additional MRI acquisition. However, increased BBB permeability was only associated with baseline ischemic core volume in the whole study population. This implies that BBB permeability may be mainly correlated with ischemic core volume rather than H0-MMP9 levels.

In the whole population including patients with <6h, >6h and unknown symptoms onset, only H48 MMP-9 levels were significantly higher in patients with high baseline K2 values. This subsequent rise in levels of MMP-9 might be related to the dynamic nature of the BBB disruption. Indeed, some authors reported a biphasic evolution of BBB permeability, a first peak occurring at the hyperacute phase[29,30] and the second during the following 72/96h [31,32].

The release of proinflammatory cytokines, especially IL-1β, IL-6, IL-17, IL-18, and TNF-α are believed to initiate a local immune response which is associated with BBB dysfunction after stroke[33]. Higher IL-6 levels have been reported to be associated with early neurologic deterioration, futile recanalization and worsened functional outcome[34–36]. In this study, we did not observe significant associations between high baseline K2 values and other circulating inflammatory markers. We assume that this is related to a later systemic release of these proteins. For example, the neuronal expression of IL-6 starts 3.5 h after ischemia, peaks after 24 h of reperfusion, and, remains for 7 days[36]. Thus, our data support that MMP-9 expression is one of the

earliest events involved in the neuroinflammatory process affecting BBB permeability. In addition, we found that patients with increased BBB permeability were more likely to have HT and poorer neurologic outcome in agreement with previous studies [19,37,38].

The main strength of this study lies in the coupled analysis of BBB permeability and a sequential analysis of a panel of circulating inflammatory markers. To our knowledge, no study has directly correlated the markers of the neuroinflammatory response and baseline BBB permeability imaging specifically in patients treated by mechanical thrombectomy.

Nevertheless, this study has some limitations including its limited sample size and the fact that only 3 (2.9%) patients had PH type hemorrhagic transformation. However, this rate is in the low range of rates reported in clinical trials (2-7%)[39]. We assessed BBB permeability binary while a continuous assessment would have been more precise. Nevertheless, the assumptions of linear models were not satisfied, which precluded their use. In addition, we used DSC-MRI whereas dynamic contrast enhanced MRI by means of Ktrans is considered to be more accurate[40]. However, this technique is more time consuming in the setting of acute stroke imaging. We applied an arrival time correction to improve the robustness of K2 measurements as previously reported in stroke patients[12]. MMP-9 was the only metalloproteinase included in the panel of inflammatory markers. While most studies have focused on gelatinases (MMP-2 and MMP-9), some reports indicate that MMP-3 and MMP-12 are also implicated in neuroinflammation-mediated BBB damage after stroke[3]. Finally, increased serum levels of MMP-9 may reflect an increased BBB permeability rather than the dynamics of MMP-9 expression and activity within the ischemic core.

In conclusion, increased BBB permeability is independently associated with increased H0 MMP-9 levels and larger ischemic core in AIS patients with symptoms onset <6h.

Previous studies have reported biphasic roles of MMP-9 in stroke pathophysiology. It first mediates injury during the acute phase and then contributing to neurovascular remodeling in the penumbra during the recovery phase[24,42]. Preclinical data suggest that the use of selective MMP inhibitors may have significant therapeutic potential in AIS patients[43,44]. Although a clinical translation is still expected, our results encourage a new evaluation of this strategy in the early stage of AIS treated with mechanical thrombectomy as it may limit BBB damages related to ischemia – reperfusion injury [44,45].

REFERENCES.

1. Bernardo-Castro S, Sousa JA, Brás A, Cecília C, Rodrigues B, Almendra L, Machado C, Santo G, Silva F, Ferreira L, et al. Pathophysiology of Blood–Brain Barrier Permeability Throughout the Different Stages of Ischemic Stroke and Its Implication on Hemorrhagic Transformation and Recovery. *Front. Neurol.* 2020;11:594672.
2. Jiang X, Andjelkovic AV, Zhu L, Yang T, Bennett MVL, Chen J, Keep RF, Shi Y. Blood-brain barrier dysfunction and recovery after ischemic stroke. *Prog Neurobiol*, 2019;163-164:144-171.
3. Lakhan SE. Matrix metalloproteinases and blood-brain barrier disruption in acute ischemic stroke. *Front. Neurol.* 2013;4:32.
4. Yang C, Hawkins KE, Doré S, Candelario-Jalil E. Neuroinflammatory mechanisms of blood-brain barrier damage in ischemic stroke. *American Journal of Physiology-Cell Physiology*. 2019;316:C135–C153.
5. Montaner J, Alvarez-Sabín J, Molina C, Anglés A, Abilleira S, Arenillas J, González MA, Monasterio J. Matrix Metalloproteinase Expression After Human Cardioembolic Stroke: Temporal Profile and Relation to Neurological Impairment. *Stroke*. 2001;32:1759–1766.
6. Montaner J, Alvarez-Sabín J, Molina CA, Anglés A, Abilleira S, Arenillas J, Monasterio J. Matrix Metalloproteinase Expression Is Related to Hemorrhagic Transformation After Cardioembolic Stroke. *Stroke*. 2001;32:2762–2767.
7. Montaner J, Fernández-Cadenas I, Molina CA, Monasterio J, Arenillas JF, Ribó M, Quintana M, Chacón P, Andreu AL, Alvarez-Sabín J. Safety Profile of Tissue Plasminogen Activator Treatment Among Stroke Patients Carrying a Common Polymorphism (C-1562T) in the Promoter Region of the Matrix Metalloproteinase-9 Gene. *Stroke*. 2003;34:2851–2855.
8. Chang D-I, Hosomi N, Lucero J, Heo J-H, Abumiya T, Mazar AP. Activation Systems for Latent Matrix Metalloproteinase-2 are Upregulated Immediately after Focal Cerebral Ischemia. *J Cereb Blood Flow Metab*. 2003;23:12.
9. Castellanos M, Sobrino T, Millán M, García M, Arenillas J, Nombela F, Brea D, Perez de la Ossa N, Serena J, Vivancos J, et al. Serum Cellular Fibronectin and Matrix Metalloproteinase-9 as Screening Biomarkers for the Prediction of

Parenchymal Hematoma After Thrombolytic Therapy in Acute Ischemic Stroke: A Multicenter Confirmatory Study. *Stroke*. 2007;38:1855–1859.
10. Batra A, Latour LL, Ruetzler CA, Hallenbeck JM, Spatz M, Warach S, Henning EC. Increased Plasma and Tissue MMP Levels are Associated with BCSFB and BBB Disruption Evident on Post-Contrast FLAIR after Experimental Stroke. *J Cereb Blood Flow Metab*. 2010;30:1188–1199.
11. Barr TL, Latour LL, Lee K-Y, Schaewe TJ, Luby M, Chang GS, El-Zammar Z, Alam S, Hallenbeck JM, Kidwell CS, et al. Blood–Brain Barrier Disruption in Humans Is Independently Associated With Increased Matrix Metalloproteinase-9. *Stroke.* 2010;41:e123-e128
12. Leigh R, Jen SS, Varma DD, Hillis AE, Barker PB. Arrival Time Correction for Dynamic Susceptibility Contrast MR Permeability Imaging in Stroke Patients. *PLOS ONE*. 2012;7:5.
13. Khatri R, McKinney AM, Swenson B, Janardhan V. Blood-brain barrier, reperfusion injury, and hemorrhagic transformation in acute ischemic stroke. *Neurology*. 2012;79:S52–S57.
14. Warach S, Latour LL. Evidence of Reperfusion Injury, Exacerbated by Thrombolytic Therapy, in Human Focal Brain Ischemia Using a Novel Imaging Marker of Early Blood–Brain Barrier Disruption. *Stroke*. 2004;35:2659–2661.
15. Berge E, Whiteley W, Audebert H, De Marchis G, Fonseca AC, Padiglioni C, Pérez de la Ossa N, Strbian D, Tsivgoulis G, Turc G. European Stroke Organisation (ESO) guidelines on intravenous thrombolysis for acute ischaemic stroke. *European Stroke Journal*. 2021;6:I–LXII.
16. Hacke W, Kaste M, Fieschi C, von Kummer R, Davalos A, Meier D, Larrue V, Bluhmki E, Davis S, Donnan G, et al. Randomised double-blind placebo-controlled trial of thrombolytic therapy with intravenous alteplase in acute ischaemic stroke (ECASS II). Second European-Australasian Acute Stroke Study Investigators. *Lancet*. 1998;352:1245–1251.
17. Hussein HM, Saleem MA, Qureshi AI. Rates and predictors of futile recanalization in patients undergoing endovascular treatment in a multicenter clinical trial. *Neuroradiology*. 2018;60:557–563.
18. Boxerman JL, Schmainda KM, Weisskoff RM. Relative cerebral blood volume maps corrected for contrast agent extravasation significantly correlate with glioma tumor grade, whereas uncorrected maps do not. *AJNR Am J Neuroradiol*. 2006;27:859–867.
19. Leigh R, Jen SS, Hillis AE, Krakauer JW, Barker PB. Pretreatment Blood–Brain Barrier Damage and Post-Treatment Intracranial Hemorrhage in Patients Receiving Intravenous Tissue-Type Plasminogen Activator. *Stroke*, 2014:2030-2035
20. Leigh R, Christensen S, Campbell BCV, Marks MP, Albers GW, Lansberg MG, For the DEFUSE 2 Investigators. Pretreatment blood–brain barrier disruption and post-endovascular intracranial hemorrhage. *Neurology*. 2016;87:263–269.
21. Simpkins AN, Dias C, Leigh R. Identification of Reversible Disruption of the Human Blood–Brain Barrier Following Acute Ischemia. *Stroke*, 2016:2405-2408.
22. Nael K, Knitter JR, Jahan R, Gornbein J, Ajani Z, Feng L, Meyer BC, Schwamm LH, Yoo AJ, Marshall RS, et al. Multiparametric Magnetic Resonance Imaging for Prediction of Parenchymal Hemorrhage in Acute Ischemic Stroke After Reperfusion Therapy. *Stroke*. 2017;48:664–670.
23. Olivot JM, Mlynash M, Inoue M, Marks MP, Wheeler HM, Kemp S, Straka M, Zaharchuk G, Bammer R, Lansberg MG, et al. Hypoperfusion Intensity Ratio Predicts

Infarct Progression and Functional Outcome in the DEFUSE 2 Cohort. *Stroke*. 2014;45:1018–1023.
24. Maier CM, Hsieh L, Yu F, Bracci P, Chan PH. Matrix Metalloproteinase-9 and Myeloperoxidase Expression: Quantitative Analysis by Antigen Immunohistochemistry in a Model of Transient Focal Cerebral Ischemia. *Stroke*. 2004;35:1169–1174.
25. Pfefferkorn T, Rosenberg GA. Closure of the blood-brain barrier by matrix metalloproteinase inhibition reduces rtPA-mediated mortality in cerebral ischemia with delayed reperfusion. *Stroke*. 2003;34:2025–2030.
26. Rosenberg GA, Yang Y. Vasogenic edema due to tight junction disruption by matrix metalloproteinases in cerebral ischemia. *Neurosurg Focus*. 2007;22:E4.
27. Turner RJ. Implications of MMP9 for Blood Brain Barrier Disruption and Hemorrhagic Transformation Following Ischemic Stroke. *Frontiers in Cellular Neuroscience*. 2016;10:13.
28. Latour LL, Kang D-W, Ezzeddine MA, Chalela JA, Warach S. Early blood-brain barrier disruption in human focal brain ischemia. *Ann Neurol*. 2004;56:468–477.
29. Merali Z, Huang K, Mikulis D, Silver F, Kassner A. Evolution of blood-brain-barrier permeability after acute ischemic stroke. *PLOS ONE*. 2017;11.
30. Abdullahi W, Tripathi D, Ronaldson PT. Blood-brain barrier dysfunction in ischemic stroke: targeting tight junctions and transporters for vascular protection. *American Journal of Physiology-Cell Physiology*. 2018;315:C343–C356.
31. Lin C-Y, Chang C, Cheung W-M, Lin M-H, Chen J-J, Hsu CY, Chen J-H, Lin T-N. Dynamic Changes in Vascular Permeability, Cerebral Blood Volume, Vascular Density, and Size after Transient Focal Cerebral Ischemia in Rats: Evaluation with Contrast-Enhanced Magnetic Resonance Imaging. *J Cereb Blood Flow Metab*. 2008;28:1491–1501.
32. Pillai DR, Dittmar MS, Baldaranov D, Heidemann RM, Henning EC, Schuierer G, Bogdahn U, Schlachetzki F. Cerebral Ischemia–Reperfusion Injury in Rats—A 3 T MRI Study on Biphasic Blood–Brain Barrier Opening and the Dynamics of Edema Formation. *J Cereb Blood Flow Metab*. 2009;29:1846–1855.
33. Gülke E, Gelderblom M, Magnus T. Danger signals in stroke and their role on microglia activation after ischemia. *Ther Adv Neurol Disord,* 2018:14;1756286418774254.
34. Stoll G, Nieswandt B. Thrombo-inflammation in acute ischaemic stroke - implications for treatment. *Nat Rev Neurol*. 2019;15:473–481.
35. De Meyer SF, Denorme F, Langhauser F, Geuss E, Fluri F, Kleinschnitz C. Thromboinflammation in Stroke Brain Damage. *Stroke*. 2016;47:1165–1172.
36. Mechtouff L, Bochaton T, Paccalet A, Da Silva CC, Buisson M, Amaz C, Derex L, Ong E, Berthezene Y, Eker OF, et al. Association of Interleukin-6 Levels and Futile Reperfusion After Mechanical Thrombectomy. *Neurology*. 2021;96:e752–e757.
37. Bivard A, Kleinig T, Churilov L, Levi C, Lin L, Cheng X, Chen C, Aviv R, Choi PMC, Spratt NJ, et al. Permeability Measures Predict Hemorrhagic Transformation after Ischemic Stroke. *Ann Neurol*. 2020;88:466–476.
38. Rost NS, Cougo P, Lorenzano S, Li H, Cloonan L, Bouts MJ, Lauer A, Etherton MR, Karadeli HH, Musolino PL, et al. Diffuse microvascular dysfunction and loss of white matter integrity predict poor outcomes in patients with acute ischemic stroke. *J Cereb Blood Flow Metab*. 2018;38:75–86.
39. Maïer B, Desilles JP, Mazighi M. Intracranial Hemorrhage After Reperfusion Therapies in Acute Ischemic Stroke Patients. *Front. Neurol.* 2020;11:599908.

40. Skinner JT, Moots PL, Ayers GD, Quarles CC. On the Use of DSC-MRI for Measuring Vascular Permeability. *AJNR Am J Neuroradiol*. 2016;37:80–87.
41. Guenego A, Fahed R, Albers GW, Kuraitis G, Sussman ES, Martin BW, Marcellus DG, Olivot J-M, Marks MP, Lansberg MG, et al. Hypoperfusion intensity ratio correlates with angiographic collaterals in acute ischaemic stroke with M1 occlusion. *Eur J Neurol*. 2020;27:864–870.
42. Dong X, Song Y-N, Liu W-G, Guo X-L. MMP-9, a Potential Target for Cerebral Ischemic Treatment. *Curr Neuropharmacol*. 2009;7:269–275.
43. Gu Z. A Highly Specific Inhibitor of Matrix Metalloproteinase-9 Rescues Laminin from Proteolysis and Neurons from Apoptosis in Transient Focal Cerebral Ischemia. *Journal of Neuroscience*. 2005;25:6401–6408.
44. Chaturvedi M, Kaczmarek L. MMP-9 Inhibition: a Therapeutic Strategy in Ischemic Stroke. *Mol Neurobiol*. 2014;49:563–573.
45. Dejonckheere E, Vandenbroucke RE, Libert C. Matrix metalloproteinases as drug targets in ischemia/reperfusion injury. *Drug Discov Today*. 2011;16:762–778.

FIGURES.

Figure 1. Flow-Chart:

Abbreviation: DSC-MRI: dynamic susceptibility-contrast MRI

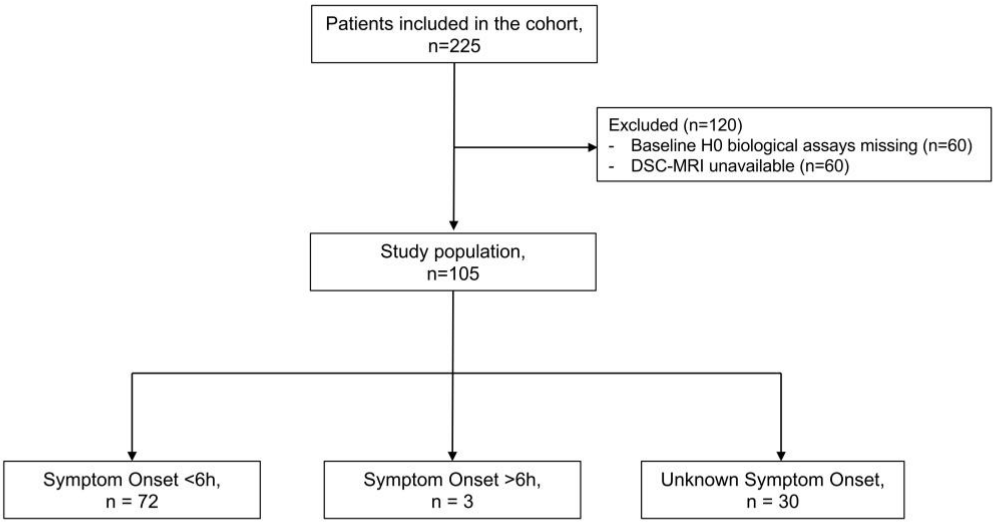

Figure 2. Kinetics of matrix metalloproteinase-9 according to K2 status:

Figure 2 presents the kinetics of matrix metalloproteinase-9 levels (medians) at H0, H6, H24 and H48 according to K2 status.

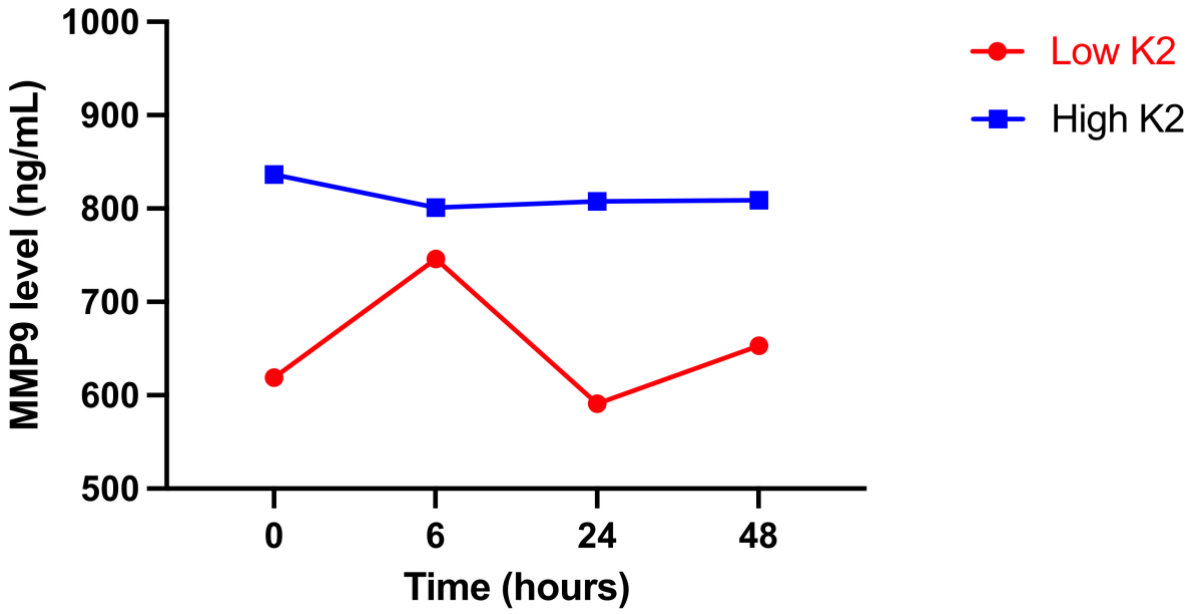

Figure 3. Admission MRI of a stroke patient with increased blood-brain-barrier permeability.

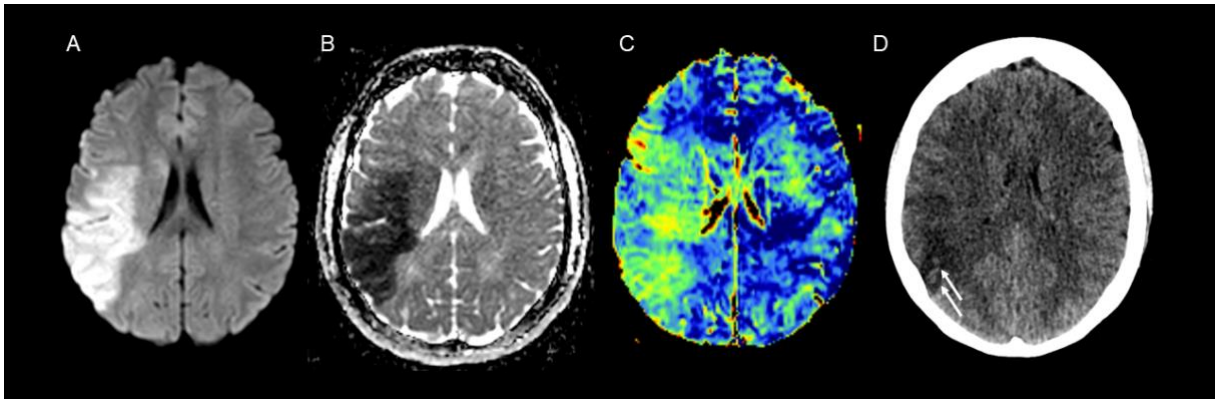

In this patient with acute right sylvian ischemic stroke (A: B1000 diffusion-weighted images; B Apparent-Diffusion-Coefficient map) and symptoms onset <6h, K2 maps (C) indicate increased blood-brain-barrier permeability. She was treated with thrombolysis and mechanical thrombectomy, resulting in a modified Thrombolysis in Cerebral Infarction Score of 3. The 24-hour follow-up non-contrast CT scan (D) revealed confluent hemorrhagic petechiae (white arrows) within the infarct indicating HI-1 hemorrhagic transformation.

TABLES.

Table 1. Characteristics of study population according to K2 status

	Whole Population (n=105)	High K2 (n=52)	Low K2 (n=53)	P-Value
Clinical characteristics				
Age, median [IQR] (years)	69.0 [56.0; 83.0]	68.0 [56.0; 76.0]	71.0 [56.0; 85.3]	0.16
Male sex, n (%)	60 (57.1)	32 (61.5)	28 (52.8)	0.37
Hypertension, n (%)	49 (46.7)	25 (48.1)	24 (45.3)	0.92
Diabetes, n (%)	15 (14.3)	8 (15.4)	7 (13.2)	0.75
Smoking, n (%)				
Current Smoking, n (%)	23 (21.9)	9 (17.3)	14 (26.4)	0.26
Former Smoking, n (%)	18 (17.1)	12 (23.1)	6 (11.3)	0.11
Time from symptoms onset (min), median [IQR]	96.0 [73.5; 125.5]	95.0 [77.0; 126.0]	100.5 [69.3; 123.8]	0.59
Baseline NIHSS score, median [IQR]	15.0 [10.0; 19.0]	15.0 [11.0; 20.0]	14.0 [9.0; 18.0]	0.07
Biological characteristics				
CRP (mg/L), median [IQR]				
H0	11.7 [5.4; 20.7]	12.3 [6.0; 20.2]	8.9 [4.9; 21.1]	0.42
H6	14.7 [5.7; 29.8]	15.3 [6.8; 26.3]	14.2 [5.6; 30.2]	0.92
H24	22.0 [14.3; 35.7]	25.9 [16.5; 39.0]	19.8 [11.6; 29.7]	0.04
H48	29.7 [17.6]	43.0 [21.5; 63.0]	24.7 [16.2; 38.6]	0.01
MMP-9 (ng/mL), median [IQR]				
H0	680.8 [436.1; 1106.6]	836.3 [500.2; 1259.3]	631.9 [370.6; 952.0]	0.06
H6	780.8 [514.6; 1220.5]	801.0 [508.3; 1303.2]	750.7 [532.6; 1071.2]	0.35
H24	674.2 [489.9; 1012.0]	814.1 [571.4; 1036.3]	582.3 [434.9; 939.8]	0.11
H48	745.4 [490.8; 998.7]	809.0 [572.7; 1000.3]	673.9 [383.3; 922.0]	0.02
IL-6 (pg/mL), median [IQR]				
H0	1.6 [0.6; 3.6]	1.8 [0.4; 4.8]	1.5 [0.8; 3.4]	0.73
H6	2.9 [1.5; 5.3]	2.9 [1.3; 4.8]	2.8 [1.5; 6.0]	0.69
H24	3.4 [2.0; 6.3]	3.5 [2.0; 6.3]	3.3 [2.1; 6.3]	0.99
H48	3.3 [1.6; 7.2]	3.5 [2.1; 6.3]	3.2 [1.6; 7.1]	0.77
IL-8 (pg/mL), median [IQR]				
H0	2.2 [1.1; 4.1]	2.2 [1.1; 4.3]	2.4 [1.1; 3.9]	0.91
H6	1.2 [0.5; 2.5]	1.2 [0.4; 2.3]	1.3 [0.7; 2.7]	0.47
H24	1.3 [0.3; 3.2]	1.2 [0.1; 3.2]	17 [0.6; 3.2]	0.43
H48	1.2 [0.4; 3.2]	1.2 [0.5; 3.8]	1.1 [0.3; 2.7]	0.50
IL-10 (pg/mL), median [IQR]				
H0	2.7 [1.4; 5.3]	3.5 [1.4; 6.5]	2.3 [1.3; 3.5]	0.09
H6	2.3 [1.3; 4.3]	2.3 [1.4; 4.6]	2.4 [1.3; 3.7]	0.81
H24	3.1 [1.6; 5.4]	3.3 [1.9; 5.4]	2.9 [1.4; 4.8]	0.67
H48	3.0 [1.6; 4.9]	3.0 [1.9; 5.7]	2.7 [1.5; 4.7]	0.42
MCP-1 (pg/mL), median [IQR]				
H0	64.1 [42.3; 103.1]	64.0 [40.4; 100.6]	65.6 [43.0; 103.8]	0.69
H6	46.2 [29.9; 76.4]	45.3 [28.1; 76.4]	46.8 [33.6; 74.3]	0.52
H24	42.3 [26.4; 65.1]	39.8 [26.2; 65.1]	43.6 [29.2; 60.4]	0.55
H48	39.1 [22.5; 60.0]	37.8 [22.5; 59.9]	39.4 [23.7; 60.9]	0.92
sP-selectin (ng/mL), median [IQR]				
H0	80.4 [61.9; 110.2]	80.4 [59.4; 117.0]	80.6 [68.0; 104.2]	0.71
H6	55.0 [43.6; 75.9]	60.9 [43.6; 75.9]	53.1 [44.2; 75.5]	0.60
H24	56.2 [42.2; 72.4]	58.3 [42.2; 80.0]	53.6 [42.5; 70.8]	0.70
H48	55.5 [40.9; 78.3]	56.8 [41.7; 77.0]	51.8 [39.3; 79.1]	0.65

sST2 (ng/mL), median [IQR]				
H0	12.2 [7.1; 17.1]	10.8 [6.3; 16.8]	13.4 [7.9; 17.3]	0.22
H6	17.3 [11.3; 26.4]	15.9 [11.3; 23.0]	19.3 [11.9; 27.6]	0.26
H24	16.6 [10.4; 28.5]	13.0 [10.3; 23.8]	19.3 [11.3; 29.6]	0.10
H48	13.2 [7.3; 24.3]	11.0 [10.3; 23.8]	15.1 [8.5; 26.6]	0.18
TNFR1 (pg/mL), median [IQR]				
H0	619.7 [433.4; 895.1]	599.3 [438.8; 895.1]	651.4 [428.6; 895.9]	0.95
H6	558.5 [435.7; 836.7]	547.2 [413.7; 717.5]	654.9 [443.9; 897.4]	0.33
H24	595.3 [445.8; 851.7]	561.3 [456.4; 792.2]	703.8 [435.3; 1002.4]	0.34
H48	585.6 [435.5; 903.3]	557.8 [475.3; 724.0]	681.9 [415.2; 971.0]	0.59
VCAM-1 (ng/mL), median [IQR]				
H0	504.0 [384.7; 637.6]	487.6 [372.5; 637.6]	519.4 [407.5; 625.6]	0.28
H6	458.6 [355.4; 623.3]	424.4 [345.3; 623.3]	464.6 [389.8; 623.2]	0.26
H24	458.3 [362.5; 614.7]	432.7 [355.6; 572.9]	485.6 [370.2; 621.0]	0.16
H48	495.3 [395.0; 612.3]	442.5 [362.2; 585.9]	522.4 [410.2; 618.4]	0.21
Neuroimaging characteristics				
Occlusion site				
ICA termination	33 (31.4)	20 (38.4)	13 (24.5)	0.15
M1 segment	55 (52.4)	25 (48.1)	30 (56.6)	0.44
M2 segment	17 (16.2)	7 (13.5)	10 (18.9)	0.60
Baseline ischemic core volume (mL), median [IQR]	21.5 [8.6;39.8]	32.9 [17.0; 65.1]	13.2 [5.7; 29.1]	<0.001
Hypoperfusion Intensity Ratio, median [IQR]	0.58 [0.46; 0.68]	0.64 [0.56; 0.73]	0.54 [0.44; 0.64]	0.01
AWRMC ≥ 2, n (%)	80 (76.2)	37 (71.2)	43 (81.1)	0.23
Microbleeds, n (%)	17 (16.2)	8 (15.4)	9 (17.0)	0.82
Outcome				
Intravenous thrombolysis, n (%)	53 (50.5)	30 (57.7)	23 (43.4)	0.14
Successful revascularization	83 (79.0)	40 (76.9)	43 (81.1)	0.60
Hemorrhagic Transformation, n (%)	30 (28.6)	21 (40.4)	9 (17.0)	0.008
HI-1	10 (9.5)	7 (13.5)	3 (5.7)	
HI-2	13 (12.4)	11 (21.2)	2 (3.8)	
PH-1	3 (2.9)	2 (3.8)	1 (1.9)	
PH-2	0 (0)	0 (0.0)	0 (0.0)	
SAH	4 (3.8)	1 (1.9)	3 (5.7)	
Final lesion volume (mL), median [IQR]	26.1 [9.2; 59.7]	39.5 [14.6; 73.0]	17.6 [8.5; 30.0]	0.02
3-months mRS	2.0 [1.0; 3.0]	2.0 [2.0; 3.0]	2.0 [1.0; 3.0]	0.04
Futile recanalization, n (%)	25 (23.8)	15 (37.5)	10 (23.3)	0.16

Table Legend:

The population was dichotomized according to the median K2 value (1.59)

Abbreviations:

IQR: interquartile range; NIHSS: National Health Institute Stroke Scale; CRP: C-Reactive Protein; MMP-9: Matrix Metalloproteinase-9; IL-6: Interleukin-6; IL-8: Interleukin-8; IL-10: Interleukin-10; MCP-1: Monocyte Chemoattractant-1; sP-selectin: soluble P-selectin; ST2: soluble form Suppression of Tumorigenicity-2; TNFR-1:

Tumor Necrosis Factor Receptor-1; VCAM-1: Vascular Cell Adhesion Molecule-1; ICA: Internal Carotid Artery; M1: M1 segment of middle cerebral artery; M2: M2 segment of middle cerebral artery; ARWMC: Age-Related White Matter Changes; mRS: modified Rankin score

Table 2. Multiple variable logistic regression model of factors associated with a high K2 in whole study population.

	Crude OR [95% CI]	P-Value	Adjusted OR [95% CI]	P-Value
Baseline NIHSS score (a)	1.07 [1.00; 1.15]	0.053	1.04 [0.96; 1.13]	0.38
H0-MMP-9 level (b)	1.00 [1.00; 1.00]	0.053	1.01 [0.99; 1.02]	0.06
Baseline ischemic core volume (c)	1.04 [1.04; 1.07]	< 0.001	1.04 [1.01; 1.06]	< 0.001
Hypoperfusion Intensity Ratio (d)	9.74 [1.00; 112.94]	0.06	3.22 [0.25; 45.01]	0.93

(a): per 1-point increase
(b): per 1-ng/mL increase
(c): per 1-mL increase
(d): per 1-% increase
Abbreviations: OR: Odds Ratio; NIHSS: National Health Institute Stroke Scale; MMP-9: Matrix Metalloproteinase-9

Table 3. Multiple variable logistic regression model of factors associated with a high K2 in patients with symptoms onset <6h.

	Crude OR [95% CI]	P-Value	Adjusted OR [95% CI]	P-Value
Baseline NIHSS score (a)	1.06 [0.84; 1.34]	0.64	1.04 [0.84; 1.28]	0.72
H0-MMP-9 level (b)	1.40 [1.13; 1.75]	0.004	1.33 [1.12; 1.65]	0.01
H6-MMP-9 level (b)	1.25 [0.99; 1.56]	0.06	-	-
Baseline ischemic core (c)	1.39 [1.12; 1.75]	0.004	1.27 [1.08; 1.59]	0.04
Hypoperfusion Intensity Ratio (d)	1.32 [1.05; 1.65]	0.02	1.21 [0.84; 1.28]	0.10

(a): per 1-point increase
(b): per 1-ng/mL increase
(c): per 1-mL increase
(d): per 1-% increase
Abbreviations: OR: Odds Ratio; NIHSS: National Health Institute Stroke Scale; MMP-9: Matrix Metalloproteinase-9

SUPPLEMENTARY MATERIAL.

eTable 1. Serum MMP-9 levels according to the thrombolysis status

MMP-9 (ng/mL), median [IQR]	Thrombolysis (n=53)	No Thrombolysis (n=52)	P-Value
H0	805.2 [467.0; 1173.6]	601.3 [380.2; 1001.5]	0.09
H6	810.0 [540.4; 1303.2]	768.0 [476.3; 1106.9]	0.39
H24	614.9 [398.9; 1059.7]	770.3 [565.4; 996.2]	0.32
H48	708.6 [501.5; 1000.3]	760.4 [501.5; 1000.3]	0.87

Abbreviations:

MMP-9: Matrix Metalloproteinase-9; IQR: interquartile range

eTable 2. Characteristics of patients with symptoms onset < 6h according to K2 status.

	High K2 (n=36)	Low K2 (n=36)	P-Value
Clinical characteristics			
Age, median [IQR] (years)	67.5 [56.8; 76.0]	75.0 [55.0; 86.3]	0.08
Male sex, n (%)	25 (69.4)	17 (47.2)	0.06
Hypertension, n (%)	17 (47.2)	16 (44.4)	0.81
Diabetes, n (%)	2 (13.9)	4 (11.1)	0.39
Smoking, n (%)			
Current Smoking, n (%)	5 (13.9)	12 (33.3)	0.06
Former Smoking, n (%)	8 (22.2)	3 (8.3)	0.10
Time from symptoms onset (min), median [IQR]	92.0 [74.5; 112.3]	100.5 [69.8; 121.3]	0.97
Baseline NIHSS score, median [IQR]	15.0 [11.0; 20.0]	15.0 [9.0; 19.0]	0.39
Biological characteristics			
CRP (mg/L), median [IQR]			
H0	13.4 [5.3; 30.7]	10.7 [5.6; 21.1]	0.51
H6	15.7 [6.3; 34.7]	17.4 [6.7; 30.5]	0.88
H24	28.3 [20.2; 48.8]	20.8 [13.6; 29.7]	0.02
H48	46.4 [22.2; 91.4]	23.1 [15.5; 38.6]	0.02
MMP-9 (ng/mL), median [IQR]			
H0	949.9 [509.4; 1412.1]	592.8 [351.8; 826.6]	0.005
H6	1009.9 [648.3; 1384.1]	719.2 [451.1; 989.0]	0.04
H24	825.0 [604.0; 1187.9]	548.1 [396.9; 806.4]	0.02
H48	808.9 [571.8; 999.1]	609.6 [383.2; 781.0]	0.01
IL-6 (pg/mL), median [IQR]			
H0	1.7 [0.6; 4.7]	1.7 [0.8; 3.4]	0.73
H6	1.5 [1.3; 4.9]	2.8 [1.5; 6.3]	0.59
H24	3.3 [2.0; 5.8]	3.1 [2.1; 5.1]	0.84
H48	3.1 [1.6; 7.4]	2.8 [1.5; 6.1]	0.53
IL-8 (pg/mL), median [IQR]			
H0	2.6 [1.3; 5.2]	2.1 [0.9; 3.6]	0.34
H6	1.3 [0.4; 3.0]	1.2 [0.5; 2.5]	0.69
H24	1.0 [0.2; 3.4]	1.5 [0.2; 3.0]	0.97
H48	1.5 [0.5; 3.8]	0.7 [0.2; 2.0]	0.16
IL-10 (pg/mL), median [IQR]			

H0	3.3 [1.4; 6.0]	2.4 [1.4; 3.2]	0.17
H6	2.2 [1.2; 3.9]	2.1 [1.1; 3.7]	0.97
H24	3.2 [1.5; 4.8]	2.7 [1.4; 4.2]	0.65
H48	2.8 [1.3; 5.0]	2.4 [1.5; 3.7]	0.47
MCP-1 (pg/mL), median [IQR]			
H0	75.7 [50.8; 99.8]	70.0 [43.5; 113.4]	0.92
H6	47.9 [29.7; 76.6]	51.4 [37.5; 68.9]	0.80
H24	43.4 [30.2; 73.8]	46.9 [34.7; 72.9]	0.56
H48	45.8 [24.7; 67.6]	46.2 [25.7; 65.6]	0.99
sP-selectin (ng/mL), median [IQR]			
H0	82.1 [61.5; 125.6]	81.5 [67.2; 101.9]	0.66
H6	61.7 [43.0; 74.5]	51.1 [45.5; 63.4]	0.44
H24	60.7 [41.3; 83.5]	53.1 [43.3; 67.3]	0.66
H48	61.3 [41.6; 88.9]	51.8 [39.5; 68.5]	0.21
sST2 (ng/mL), median [IQR]			
H0	10.3 [6.2; 17.4]	14.0 [10.1; 17.4]	0.18
H6	14.5 [11.5; 23.4]	21.8 [12.6; 28.1]	0.14
H24	13.4 [10.7; 20.6]	21.6 [12.3; 32.3]	0.09
H48	10.8 [7.3; 18.2]	16.5 [10.0; 27.3]	0.09
TNFR1 (pg/mL), median [IQR]			
H0	596.7 [462.0; 840.6]	666.3 [454.4; 895.9]	0.55
H6	543.5 [412.5; 689.3]	654.9 [456.9; 877.5]	0.11
H24	561.0 [453.7; 674.9]	716.1 [485.3; 1002.4]	0.14
H48	563.0 [429.0; 687.8]	681.9 [428.2; 968.9]	0.35
VCAM-1 (ng/mL), median [IQR]			
H0	494.1 [382.0; 571.2]	534.7 [394.7; 630.3]	0.26
H6	429.5 [352.0; 541.3]	464.6 [389.8; 659.2]	0.14
H24	429.8 [354.5; 510.2]	497.7 [368.8; 659.4]	0.08
H48	444.3 [369.3; 577.1]	508.6 [404.2; 624.2]	0.39
Neuroimaging characteristics			
Occlusion site			
ICA termination	12 (33.3)	6 (16.7)	0.17
M1 segment	19 (52.8)	21 (58.3)	0.81
M2 segment	5 (13.9)	9 (25.0)	0.37
Baseline ischemic core volume (mL), median [IQR]	28.4 [15.7; 74.0]	8.5 [5.4; 29.5]	<0.0001
Hypoperfusion Intensity Ratio, median [IQR]	0.64 [0.46; 0.74]	0.55 [0.43; 0.64]	0.08
AWRMC ≥ 2, n (%)	29 (80.6)	29 (80.6)	0.99
Microbleeds, n (%)	6 (16.7)	6 (16.7)	0.99
Outcome			
Intravenous thrombolysis, n (%)	23 (63.9)	18 (50.0)	0.23

Successful revascularization	32 (88.9)	30 (83.3)	0.50
Hemorrhagic Transformation, n (%)	13 (36.1)	4 (11.1)	0.01
HI-1	5 (13.9)	2 (5.6)	
HI-2	7 (19.4)	0 (0.0)	
PH-1	1 (2.8)	0 (0.0)	
PH-2	0 (0.0)	0 (0.0)	
SAH	0 (0.0)	2 (5.6)	
Final lesion volume (mL), median [IQR]	38.0 [10.2; 73.3]	12.4 [7.0; 26.9]	0.04
3-months mRS	2.0 [1.8; 3.0]	2.0 [1.0; 3.0]	0.25
Futile recanalization, n (%)	9 (28.1)	8 (22.2)	0.89

Table Legend:

The population was dichotomized according to the median K2 value (1.27)

Abbreviations:

IQR: interquartile range; NIHSS: National Health Institute Stroke Scale; CRP: C-Reactive Protein; MMP-9: Matrix Metalloproteinase-9; IL-6: Interleukin-6; IL-8: Interleukin-8; IL-10: Interleukin-10; MCP-1: Monocyte Chemoattractant-1; ; sP-selectin: soluble P-selectin; ST2: soluble form suppression of tumorigenicity-2; TNFR-1: Tumor Necrosis Factor Receptor-1; VCAM-1: Vascular Cell Adhesion Protein-1; ICA: Internal Carotid Artery; M1: M1 segment of middle cerebral artery; M2: M2 segment of middle cerebral artery; ARWMC: Age-Related White Matter Changes; mRS: modified Rankin score

eFIGURE 1. Violin plots of circulating inflammatory markers according to K2 status in the whole study population.

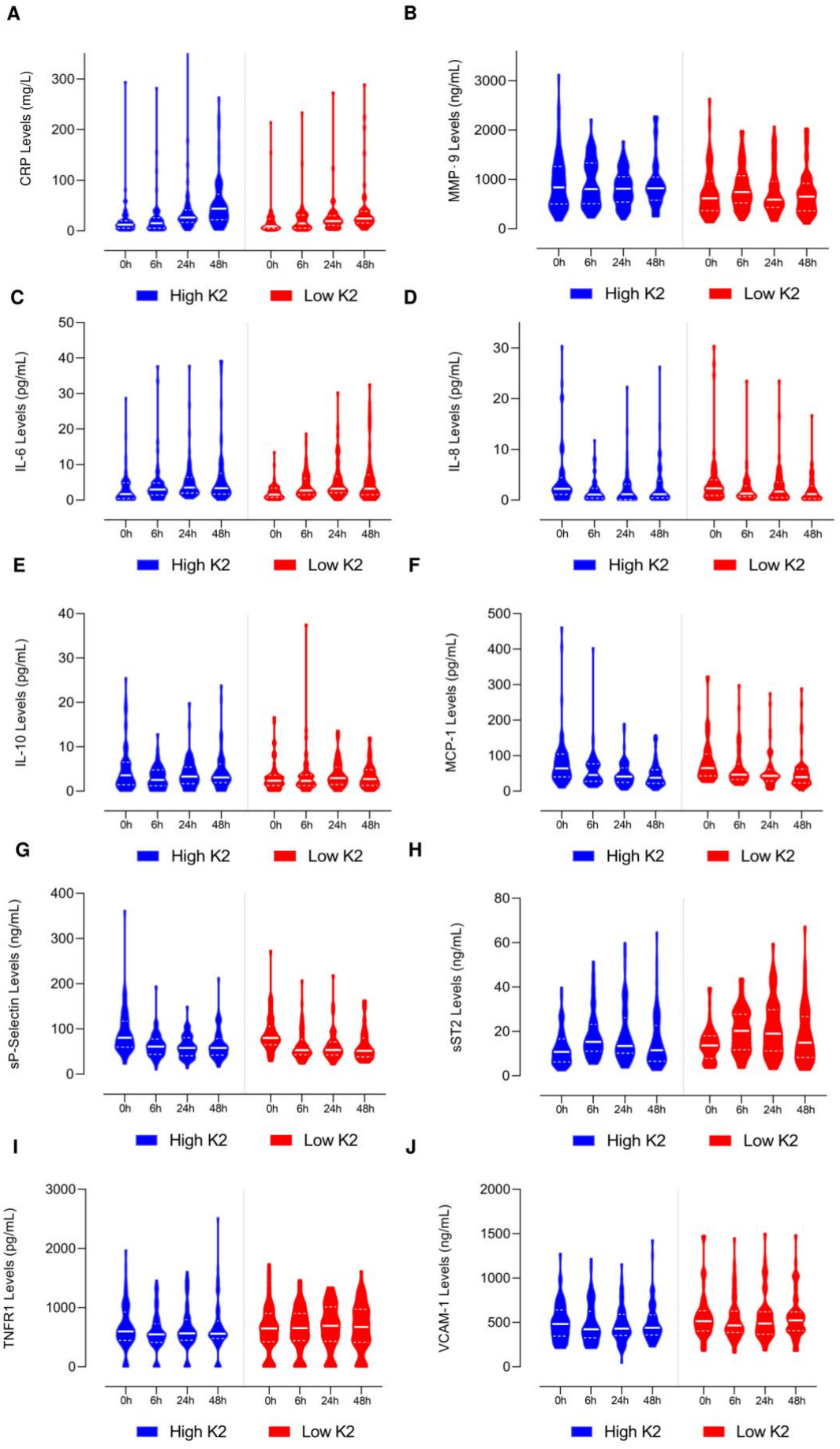

This figure presents the violin plots of serum levels at H0, H0, H24 and H48 for A: C-Reactive Protein (CRP); B: Matrix Metalloproteinase-9 (MMP-9); C: Interleukin-6 (IL-6); D: Interleukin-8 (IL-8); E: Interleukin-10 (IL-10); F: Monocyte Chemoattractant-1 (MCP-1:); G: soluble P-selectin G (sP-selectin); H: soluble form Suppression of Tumorigenicity-2 (sST2); I: Tumor Necrosis Factor Receptor-1 (TNFR-1); J: Vascular Cell Adhesion Protein-1 (VCAM-1).
The solid white lines indicate the medians and the dotted white lines the quartiles.

DISCUSSION :

Étude n°1 : Comparaison des techniques d'angio-IRM et de l'artériographie cérébrale dans le cadre de la thrombectomie mécanique : une étude de non-infériorité.

Nos résultats confirment que l'ARM-CE et l'ARM-TOF sont inférieures à l'artériographie cérébrale dans la localisation de l'occlusion artérielle en cas d'infarctus cérébral malgré la prise en compte du caractère migratoire du thrombus, ce qui est conforme aux études antérieures [89,90]. Les deux techniques d'angio-IRM avaient une précision altérée en cas d'occlusion en tandem soit 20.5% de notre population d'étude. En tant que technique basée sur le flux sanguin, l'ARM-TOF ne permet pas une évaluation précise de la vascularisation intracrânienne en cas d'occlusion et/ou de sténose sévère du bulbe carotidien. De même, l'opacification vasculaire peut être entravée en aval d'une sténose ou d'une obstruction de la portion extra-crânienne de l'artère carotide interne [126,127]. Enfin, un caillot intracrânien peut entraîner une pseudo-occlusion de l'artère carotide interne cervicale d'amont par ralentissement sévère du flux sanguin [128,129].

Cette étude présente plusieurs limites notamment son caractère rétrospectif monocentrique. Aucun des patients inclus ne présentait de sténose artérielle sévère, ce qui explique probablement l'absence de faux positifs pour la TOF-MRA. En pratique clinique, il est difficile de distinguer une sténose intracrânienne sévère d'une occlusion artérielle avec le TOF-MRA [130,131].

Étude n°2 : Comparaison des logiciels de perfusion IRM dans la prédiction du volume final de l'infarctus cérébral après thrombectomie mécanique.

Nous avons publié la première étude ayant évalué la précision de trois logiciels de perfusion IRM dans la prédiction du volume final de la lésion ischémique. Cette étude confirme la pertinence clinique du seuil d'ADC ≤620 × 10^{-6} m^2/s pour estimer le volume du noyau ischémique pour les trois logiciels. Néanmoins, elle démontre une variabilité substantielle dans l'estimation du volume du trouble de perfusion selon le logiciel utilisé. En supposant que la population étudiée comprenait des infarctus cérébraux de présentation tardive et en appliquant les critères de l'essai DEFUSE 3, ces différences volumétriques auraient conduit à une sélection différente selon logiciel utilisé. Ces conclusions sont concordantes avec les travaux de Deutschmann et al. [102]. Après correction manuelle des volumes générés automatiquement, nous avons constaté une amélioration de la reproductibilité des volumes du trouble de perfusion et de la qualité de prédiction du volume final de la lésion ischémique finale. Nos résultats impliquent qu'une vérification soigneuse des segmentations automatiques des cartes de perfusion et une éventuelle correction sont nécessaires avant de décider d'un traitement de reperfusion.

Cette étude présente plusieurs limites dont l'inclusion d'un faible échantillon en échec de thrombectomie (n=26). Ceci a pu limiter la puissance statistique, en particulier pour la comparaison des volumes des troubles de perfusion obtenus avec RAPID® et Philips®. Cela nous a également empêché de réaliser d'autres analyses prenant en compte des facteurs critiques tels que le degré de recanalisation (c'est-à-dire le score mTICI 0 vs 1 et 2A) et le temps écoulé entre l'IRM d'admission et la recanalisation. Enfin, les corrections ont été réalisées par un expert ce qui en limite la valeur en pratique clinique car cette approche peut être chronophage en particulier dans les centres non experts.

Étude n°3 : Le seuil optimal de Tmax identifiant les volumes du trouble de perfusion est-il variable selon les logiciels de perfusion par IRM ? Une étude pilote.

Nous avons publié la première étude suggérant que le seuil de Tmax optimal pour définir le volume du trouble de perfusion variait selon le logiciel de post-traitement utilisé. En IRM-DSC, la quantification du volume du trouble de perfusion est un challenge technique car elle nécessite une fonction d'entrée artérielle qui n'est qu'une approximation de la concentration plasmatique de l'agent de contraste [132]. Le choix de la meilleure carte paramétrique (c'est-à-dire CBF, Time-to-Peak, Mean-Transit-Time et Tmax) et du meilleur seuil à utiliser pour définir le volume du trouble de perfusion a été l'objet d'importants débats dans la littérature [132]. Parmi ces différentes cartes, les cartes de Tmax ont été utilisées dans les premières études multicentriques ayant évalué la thrombolyse intraveineuse pour délimiter le volume du trouble de perfusion en utilisant un seuil ≥ 6s [133,134]. Pour l'IRM, deux études ont indiqué qu'un seuil de Tmax entre 4 et 6s était optimal pour l'identification précoce de la pénombre [135,136]. Des études comparatives directes TEP/IRM ont fait état de seuils similaires [137,138]. Néanmoins, ces études ont utilisé des méthodologies différentes pour définir la non-reperfusion et les populations d'étude étaient de petite taille [135-138]. En outre, elles ont principalement utilisé RAPID® et d'autres logiciels « maisons ». En l'absence de standardisation du post-traitement et tel que nos résultats le suggèrent, un seuil de Tmax ≥ 6s s pourrait ne pas être optimal pour tous les logiciels de post-traitement IRM.

Les principales forces de l'étude sont l'inclusion de patients en échec de thrombectomie avec un score mTICI = 0 permettant d'approcher au mieux le modèle du mismatch diffusion-perfusion et une évaluation reproductible du volume finale de la lésion ischémique par IRM à J6. Toutefois, elle présente des limites. Outre son caractère monocentrique, la population étudiée est restreinte, car les patients sans reperfusion après traitement (mTICI = 0) sont rares. De plus, nous avons effectué des comparaisons volumétriques, alors que des comparaisons de similarité utilisant le coefficient de similarité de Dice auraient été plus efficaces. Néanmoins, cela n'a pas été techniquement possible, car le logiciel RAPID® ne permet pas l'export de volumes d'intérêt. Enfin, certains des patients inclus ont pu connaître une recanalisation tardive après la thrombectomie mécanique, puisque certains sujets avaient un volume final d'infarctus beaucoup plus petit qu'attendu.

Étude n°4 : Le brush sign et l'apport collatéral comme marqueurs potentiels de la croissance de la lésion ischémique après une thrombectomie réussie.

Notre étude a montré que le brush sign était indépendamment associé à une croissance large de la lésion ischémique. Les mécanismes explicatifs possibles comprennent les lésions d'ischémie-reperfusion qui résultent d'une série complexe d'événements physiopathologiques incluant le stress oxydatif et l'acidose cérébrale [139]. En tant que reflet d'une désoxygénation tissulaire sévère du tissu ischémique, nos résultats suggèrent que le brush sign pourrait être un marqueur de tissu à risque d'ischémie-reperfusion. A cet égard, il a été établi que l'acidose cérébrale et la diminution du pH tissulaire induisent une diminution du signal T2* [140].

Cette étude présente plusieurs limites. Nous avons évalué le brush sign en IRM T2* alors l'IRM de susceptibilité magnétique est plus précise pour évaluer le signal des veines sous-épendymaires et trans-médullaires [141]. De plus, l'IRM de susceptibilité magnétique permet une évaluation quantitative de la saturation en oxygène des veines cérébrales, ce qui permet une évaluation plus quantitative de l'ischémie cérébrale [142].

Étude n°5 : Les hypersignaux FLAIR vasculaires sont associés au résultat fonctionnel chez les patients à recanalisation effective après thrombectomie mécanique.

Dans cette étude, nous avons constaté que des hypersignaux FLAIR vasculaires peu étendus sur l'IRM d'admission étaient associés à un résultat fonctionnel moins bon (mRS >2 à 3 mois) malgré une recanalisation réussie. Nos résultats corroborent ceux des études antérieures qui ont établi la valeur pronostique positive des hypersignaux FLAIR vasculaires étendus [119,121,143,144]. L'originalité de notre travail repose sur l'analyse spécifique de patients avec une recanalisation réussie. Dans cette population, l'effet bénéfique de collatérales étendues pourrait consister à maintenir la viabilité des tissus en attendant une recanalisation efficace et à prévenir les réocclusions artérielles précoces après la recanalisation [145].

Cette étude présente certaines limites notamment un échantillon de petite taille. Le nombre de patients ayant un score de mRS > 2 à 3 mois était faible par rapport au nombre de prédicteurs inclus dans le modèle multivarié ce qui a pu affaiblir la puissance statistique de l'analyse principale.

Étude n°6 : Perméabilité de la BHE et cinétique des marqueurs inflammatoires chez les patients traités par thrombectomie mécanique pour un infarctus cérébral

Dans cette étude, nous avons montré que l'augmentation de perméabilité de la BHE sur l'IRM d'admission était associée à un noyau ischémique plus étendu. En analyse en sous-groupe sur les patients dont les symptômes étaient apparus avant 6h, nous avons observé qu'une perméabilité accrue de la BHE était associée à un noyau ischémique plus étendu et des taux sériques plus élevés de MMP-9 à l'admission.

Nos résultats sont concordants avec les études antérieures ayant démontré l'association entre le HARM (hyperacute reperfusion marker) et le taux de MMP9 [124,125]. Par rapport au HARM, les cartes K2 ont l'avantage de fournir une évaluation plus précoce de la perméabilité de la BHE dès l'IRM d'admission et sans acquisition supplémentaire [146]. Dans l'ensemble de la population, seuls les taux de MMP-9 à 48h étaient significativement plus élevés en cas de perméabilité augmentée de la BHE. Cette augmentation ultérieure des niveaux de MMP-9 pourrait être liée au caractère dynamique de la perméabilité de la BHE. A cet égard, certains auteurs ont rapporté une évolution biphasique avec un premier pic à 6h et un second entre 72 et 96h [28,31,36,147]. En accord avec les études antérieures, nous avons constaté que les patients présentant une perméabilité accrue de la BHE étaient plus susceptibles d'avoir une transformation hémorragique et un résultat fonctionnel moins bon à 3 mois [24,25].

La principale force de cette étude réside dans l'analyse couplée de la perméabilité de la BHE et l'analyse séquentielle d'un large panel de marqueurs inflammatoires circulants. Néanmoins, notre étude est limitée par une évaluation binaire du K2 alors qu'une évaluation continue aurait été plus précises. Toutefois, les prérequis d'application des modèles de régression linéaire n'étaient pas réunis sur nos données. Enfin, l'augmentation des taux sériques de MMP-9 pourrait refléter une perméabilité accrue de la BHE plutôt qu'une expression accrue des MMP-9 au sein noyau ischémique.

CONCLUSION ET PERSPETIVES :

Notre travail sur la cohorte HIBISCUS-STROKE a permis de préciser les limites des techniques d'IRM dans la sélection des patients éligibles à un traitement de reperfusion, d'identifier des biomarqueurs radiologiques de recanalisation futile et de croissance de lésion ischémique malgré une recanalisation réussie et de déterminer les facteurs associés à une augmentation de perméabilité la BHE sur l'IRM d'admission.

Cette approche laisse entrevoir une meilleure compréhension des mécanismes d'ischémie-reperfusion. Dans l'immédiat, nous allons poursuivre nos travaux sur la cohorte HIBISCUS-STROKE afin d'étudier les relations entre la collatéralité et la perméabilité de la BHE car certains auteurs ont suggéré que l'œdème vasogénique pourrait être un facteur explicatif de l'épuisement de la collatéralité [9].

REFERENCES

[1] Feigin VL, Stark BA, Johnson CO, Roth GA, Bisignano C, Abady GG, et al. Global, regional, and national burden of stroke and its risk factors, 1990–2019: a systematic analysis for the Global Burden of Disease Study 2019. Lancet Neurol 2021;20:795–820.

[2] Sacco RL, Kasner SE, Broderick JP, Caplan LR, Connors JJ (Buddy), Culebras A, et al. An Updated Definition of Stroke for the 21st Century: A Statement for Healthcare Professionals From the American Heart Association/American Stroke Association. Stroke 2013;44:2064-89

[3] Astrup J, Symon L, Branston NM, Lassen NA. Cortical evoked potential and extracellular K+ and H+ at critical levels of brain ischemia. Stroke 1977;8:51–7.

[4] Branston NM, Strong AJ, Symon L. Extracellular potassium activity, evoked potential and tissue blood flow. J Neurol Sci 1977;32:305–21.

[5] Baron JC, Bousser MG, Rey A, Guillard A, Comar D, Castaigne P. Reversal of focal “misery-perfusion syndrome” by extra-intracranial arterial bypass in hemodynamic cerebral ischemia. A case study with 15O positron emission tomography. Stroke 1981;12:6.

[6] Ackerman RH, Correia JA, Alpert NM, Baron JC, Gouliamos A, Grotta JC, et al. Positron imaging in ischemic stroke disease using compounds labeled with oxygen 15. Initial results of clinicophysiologic correlations. Arch Neurol 1981;38:537–43.

[7] Baron JC. Perfusion thresholds in human cerebral ischemia: historical perspective and therapeutic implications. Cerebrovasc Dis 2001;11 Suppl 1:2–8.

[8] Wheeler HM, Mlynash M, Inoue M, Tipirnini A, Liggins J, Bammer R, et al. The Growth Rate of Early DWI Lesions is Highly Variable and Associated with Penumbral Salvage and Clinical Outcomes following Endovascular Reperfusion. Int J Stroke 2015;10:723–9.

[9] Rocha M, Jovin TG. Fast Versus Slow Progressors of Infarct Growth in Large Vessel Occlusion Stroke: Clinical and Research Implications. Stroke 2017;48:2621–7.

[10] Marchal G, Beaudouin V, Rioux P, de la Sayette V, Le Doze F, Viader F, et al. Prolonged persistence of substantial volumes of potentially viable brain tissue after stroke: a correlative PET-CT study with voxel-based data analysis. Stroke 1996;27:599–606.

[11] Darby DG, Barber PA, Gerraty RP, Desmond PM, Yang Q, Parsons M, et al. Pathophysiological Topography of Acute Ischemia by Combined Diffusion-Weighted and Perfusion MRI. Stroke 1999;30:2043–52.

[12] Liebeskind DS. Collateral Circulation. Stroke 2003;34:2279–84.

[13] Vagal A, Aviv R, Sucharew H, Reddy M, Hou Q, Michel P, et al. Collateral Clock Is More Important Than Time Clock for Tissue Fate: A Natural History Study of Acute Ischemic Strokes. Stroke 2018;49:2102–7.

[14] Wiegers EJA, Mulder MJHL, Jansen IGH, Venema E, Compagne KCJ, Berkhemer OA, et al. Clinical and Imaging Determinants of Collateral Status in Patients With Acute Ischemic Stroke in MR CLEAN Trial and Registry. Stroke 2020;51:1493–502.

[15] Shuaib A, Butcher K, Mohammad AA, Saqqur M, Liebeskind DS. Collateral blood vessels in acute ischaemic stroke: a potential therapeutic target. Lancet Neurol 2011;10:909–21.

[16] Bang OY, Goyal M, Liebeskind DS. Collateral Circulation in Ischemic Stroke: Assessment Tools and Therapeutic Strategies. Stroke 2015;46:3302–9.

[17] Jiang X, Andjelkovic AV, Zhu L, Yang T, Bennett MVL, Chen J, et al. Blood-brain barrier dysfunction and recovery after ischemic stroke. Prog Neurobiol 2018;163–164:144–71.

[18] Nian K, Harding IC, Herman IM, Ebong EE. Blood-Brain Barrier Damage in Ischemic Stroke and Its Regulation by Endothelial Mechanotransduction. Front Physiol 2020;11:605398.

[19] von Kummer R, Dzialowski I. Imaging of cerebral ischemic edema and neuronal death. Neuroradiology 2017;59:545–53.

[20] Le Bihan D, Breton E, Lallemand D, Grenier P, Cabanis E, Laval-Jeantet M. MR imaging of intravoxel incoherent motions: application to diffusion and perfusion in neurologic disorders. Radiology 1986;161:401–7.

[21] Bernardo-Castro S, Sousa JA, Brás A, Cecília C, Rodrigues B, Almendra L, et al. Pathophysiology of Blood–Brain Barrier Permeability Throughout the Different Stages of Ischemic Stroke and Its Implication on Hemorrhagic Transformation and Recovery. Front Neurol 2020;11:594672.

[22] Balkaya M, Kim I, Shakil F, Cho S. CD36 deficiency reduces chronic BBB dysfunction and scar formation and improves activity, hedonic and memory deficits in ischemic stroke. J Cereb Blood Flow Metab 2021;41:486–501.

[23] Khatri R, McKinney AM, Swenson B, Janardhan V. Blood-brain barrier, reperfusion injury, and hemorrhagic transformation in acute ischemic stroke. Neurology 2012;79:S52–7.

[24] Leigh R, Jen SS, Hillis AE, Krakauer JW, Barker PB. Pretreatment Blood–Brain Barrier Damage and Post-Treatment Intracranial Hemorrhage in Patients Receiving Intravenous Tissue-Type Plasminogen Activator. Stroke 2014;45:2030-5

[25] Leigh R, Christensen S, Campbell BCV, Marks MP, Albers GW, Lansberg MG, et al. Pretreatment blood–brain barrier disruption and post-endovascular intracranial hemorrhage. Neurology 2016;87:263–9.

[26] Nael K, Knitter JR, Jahan R, Gornbein J, Ajani Z, Feng L, et al. Multiparametric Magnetic Resonance Imaging for Prediction of Parenchymal Hemorrhage in Acute Ischemic Stroke After Reperfusion Therapy. Stroke 2017;48:664–70.

[27] Ng FC, Churilov L, Yassi N, Kleinig TJ, Thijs V, Wu TY, et al. Microvascular Dysfunction in Blood-Brain Barrier Disruption and Hypoperfusion Within the Infarct Posttreatment Are Associated With Cerebral Edema. Stroke 2022;53:1597-1605

[28] Pillai DR, Dittmar MS, Baldaranov D, Heidemann RM, Henning EC, Schuierer G, et al. Cerebral Ischemia–Reperfusion Injury in Rats—A 3 T MRI Study on Biphasic Blood–Brain Barrier Opening and the Dynamics of Edema Formation. J Cereb Blood Flow Metab 2009;29:1846–55.

[29] Warach S, Latour LL. Evidence of Reperfusion Injury, Exacerbated by Thrombolytic Therapy, in Human Focal Brain Ischemia Using a Novel Imaging Marker of Early Blood–Brain Barrier Disruption. Stroke 2004;35:2659–61.

[30] Crain MR, Yuh WT, Greene GM, Loes DJ, Ryals TJ, Sato Y, et al. Cerebral ischemia: evaluation with contrast-enhanced MR imaging. AJNR Am J Neuroradiol 1991;12:631–9.

[31] Lin C-Y, Chang C, Cheung W-M, Lin M-H, Chen J-J, Hsu CY, et al. Dynamic Changes in Vascular Permeability, Cerebral Blood Volume, Vascular Density, and Size after Transient Focal Cerebral Ischemia in Rats: Evaluation with Contrast-Enhanced Magnetic Resonance Imaging. J Cereb Blood Flow Metab 2008;28:1491–501.

[32] Strbian D, Durukan A, Pitkonen M, Marinkovic I, Tatlisumak E, Pedrono E, et al. The blood-brain barrier is continuously open for several weeks following transient focal cerebral ischemia. Neuroscience 2008;153:175–81.

[33] Durukan A, Marinkovic I, Strbian D, Pitkonen M, Pedrono E, Soinne L, et al. Post-ischemic blood-brain barrier leakage in rats: one-week follow-up by MRI. Brain Res 2009;1280:158–65.

[34] Liu P, Zhang R, Liu D, Wang J, Yuan C, Zhao X, et al. Time-course investigation of blood–brain barrier permeability and tight junction protein changes in a rat model of permanent focal ischemia. J Physiol Sci 2018;68:121–7.

[35] Aviv RI, d'Esterre CD, Murphy BD, Hopyan JJ, Buck B, Mallia G, et al. Hemorrhagic transformation of ischemic stroke: prediction with CT perfusion. Radiology 2009;250:867–77.

[36] Merali Z, Huang K, Mikulis D, Silver F, Kassner A. Evolution of blood-brain-barrier permeability after acute ischemic stroke. PLOS ONE 2017;12:e0171558.

[37] Kim T, Koo J, Kim S-H, Song I-U, Chung S-W, Lee K-S. Blood-brain barrier permeability assessed by perfusion computed tomography predicts hemorrhagic transformation in acute reperfusion therapy. Neurol Sci 2018;39:1579–84.

[38] Carmichael ST. The 3 Rs of Stroke Biology: Radial, Relayed, and Regenerative. Neurotherapeutics 2016;13:348–59.

[39] Candelario-Jalil E, Dijkhuizen RM, Magnus T. Neuroinflammation, Stroke, Blood-Brain Barrier Dysfunction, and Imaging Modalities. Stroke 2022;53:1473-1486

[40] The National Institute of Neurological Disorders and Stroke rt-PA Stroke Study Group. Tissue Plasminogen Activator for Acute Ischemic Stroke. N Engl J Med 1995;333:1581-1588

[41] Hacke W, Kaste M, Bluhmki E, Brozman M, Dávalos A, Guidetti D, et al. Thrombolysis with Alteplase 3 to 4.5 Hours after Acute Ischemic Stroke. N Engl J Med 2008;359:1317–29.

[42] Thomalla G, Simonsen CZ, Boutitie F, Andersen G, Berthezene Y, Cheng B, et al. MRI-Guided Thrombolysis for Stroke with Unknown Time of Onset. N Engl J Med 2018;379:611–22.

[43] Ma H, Campbell BCV, Parsons MW, Churilov L, Levi CR, Hsu C, et al. Thrombolysis Guided by Perfusion Imaging up to 9 Hours after Onset of Stroke. N Engl J Med 2019;380:1795–803.

[44] Ahmed N, Wahlgren N, Grond M, Hennerici M, Lees KR, Mikulik R, et al. Implementation and outcome of thrombolysis with alteplase 3-4.5 h after an acute stroke: an updated analysis from SITS-ISTR. Lancet Neurol 2010;9:866–74.

[45] Saqqur M, Uchino K, Demchuk AM, Molina CA, Garami Z, Calleja S, et al. Site of Arterial Occlusion Identified by Transcranial Doppler Predicts the Response to Intravenous Thrombolysis for Stroke. Stroke 2007;38:948–54.

[46] Berkhemer OA, Fransen PSS, Beumer D, van den Berg LA, Lingsma HF, Yoo AJ, et al. A Randomized Trial of Intraarterial Treatment for Acute Ischemic Stroke. N Engl J Med 2015;372:11–20.

[47] Jovin TG, Chamorro A, Cobo E, de Miquel MA, Molina CA, Rovira A, et al. Thrombectomy within 8 Hours after Symptom Onset in Ischemic Stroke. N Engl J Med 2015;372:2296–306.

[48] Saver JL, Goyal M, Bonafe A, Diener H-C, Levy EI, Pereira VM, et al. Stent-Retriever Thrombectomy after Intravenous t-PA vs. t-PA Alone in Stroke. N Engl J Med 2015;372:2285–95.

[49] Goyal M, Menon BK, van Zwam WH, Dippel DWJ, Mitchell PJ, Demchuk AM, et al. Endovascular thrombectomy after large-vessel ischaemic stroke: a meta-analysis of individual patient data from five randomised trials. Lancet 2016;387:1723–31.

[50] Albers GW, Marks MP, Kemp S, Christensen S, Tsai JP, Ortega-Gutierrez S, et al. Thrombectomy for Stroke at 6 to 16 Hours with Selection by Perfusion Imaging. N Engl J Med 2018;378:708–18.

[51] Nogueira RG, Jadhav AP, Haussen DC, Bonafe A, Budzik RF, Bhuva P, et al. Thrombectomy 6 to 24 Hours after Stroke with a Mismatch between Deficit and Infarct. N Engl J Med 2018;378:11–21.

[52] Maïer B, Desilles JP, Mazighi M. Intracranial Hemorrhage After Reperfusion Therapies in Acute Ischemic Stroke Patients. Front Neurol 2020;11:599908.

[53] Kaesmacher J, Dobrocky T, Heldner MR, Bellwald S, Mosimann PJ, Mordasini P, et al. Systematic review and meta-analysis on outcome differences among patients with TICI2b versus TICI3 reperfusions: success revisited. J Neurol Neurosurg Psychiatry 2018;89:910–7.

[54] van Horn N, Kniep H, Leischner H, McDonough R, Deb-Chatterji M, Broocks G, et al. Predictors of poor clinical outcome despite complete reperfusion in acute ischemic stroke patients. J NeuroIntervent Surg 2021;13:14–8.

[55] Chamorro Á, Amaro S, Castellanos M, Segura T, Arenillas J, Martí-Fábregas J, et al. Safety and efficacy of uric acid in patients with acute stroke (URICO-ICTUS): a randomised, double-blind phase 2b/3 trial. Lancet Neurol 2014;13:453–60.

[56] Hill MD, Goyal M, Menon BK, Nogueira RG, McTaggart RA, Demchuk AM, et al. Efficacy and safety of nerinetide for the treatment of acute ischaemic stroke (ESCAPE-NA1): a multicentre, double-blind, randomised controlled trial. Lancet 2020;395:878–87.

[57] Kidwell CS, Chalela JA, Saver JL, Starkman S, Hill MD, Demchuk AM, et al. Comparison of MRI and CT for detection of acute intracerebral hemorrhage. JAMA 2004;292:1823–30.

[58] Chalela JA, Kidwell CS, Nentwich LM, Luby M, Butman JA, Demchuk M, et al. Magnetic resonance imaging and computed tomography in emergency assessment of patients with suspected acute stroke: a prospective comparison. Lancet 2007;369:293-8.

[59] Donnan GA, Baron J-C, Ma H, Davis SM. Penumbral selection of patients for trials of acute stroke therapy. Lancet Neurol 2009;8:261–9.

[60] Kane I, Carpenter T, Chappell F, Rivers C, Armitage P, Sandercock P, et al. Comparison of 10 Different Magnetic Resonance Perfusion Imaging Processing Methods in Acute Ischemic Stroke: Effect on Lesion Size, Proportion of Patients With Diffusion/Perfusion Mismatch, Clinical Scores, and Radiologic Outcomes. Stroke 2007;38:3158–64.

[61] Liu X, Almast J, Ekholm S. Lesions masquerading as acute stroke. J Magn Reson Imaging 2013;37:15–34.

[62] Powers WJ, Rabinstein AA, Ackerson T, Adeoye OM, Bambakidis NC, Becker K, et al. Guidelines for the Early Management of Patients With Acute Ischemic Stroke: 2019 Update to the 2018 Guidelines for the Early Management of Acute Ischemic Stroke: A Guideline for Healthcare Professionals From the American Heart Association/American Stroke Association. Stroke 2019;50:e344-e418.

[63] Demeestere J, Wouters A, Christensen S, Lemmens R, Lansberg MG. Review of Perfusion Imaging in Acute Ischemic Stroke: From Time to Tissue. Stroke 2020;51:1017–24.

[64] Nguyen TN, Abdalkader M, Nagel S, Qureshi MM, Ribo M, Caparros F, et al. Noncontrast Computed Tomography vs Computed Tomography Perfusion or Magnetic Resonance Imaging Selection in Late Presentation of Stroke With Large-Vessel Occlusion. JAMA Neurol 2022;79:22.

[65] Kim J-T, Cho B-H, Choi K-H, Park M-S, Kim BJ, Park J-M, et al. Magnetic Resonance Imaging Versus Computed Tomography Angiography Based Selection for Endovascular Therapy in Patients With Acute Ischemic Stroke. Stroke 2019;50:365–72.

[66] Provost C, Soudant M, Legrand L, Hassen WB, Xie Y, Soize S, et al. Magnetic Resonance Imaging or Computed Tomography Before Treatment in Acute Ischemic Stroke. Stroke 2019;50(3):659-664

[67] Meinel TR, Kaesmacher J, Mosimann PJ, Seiffge D, Jung S, Mordasini P, et al. Association of initial imaging modality and futile recanalization after thrombectomy. Neurology 2020;95:e2331–42.

[68] Chen M. Why futile recanalization matters. J NeuroIntervent Surg 2020;12:925–6.

[69] Hussein HM, Saleem MA, Qureshi AI. Rates and predictors of futile recanalization in patients undergoing endovascular treatment in a multicenter clinical trial. Neuroradiology 2018;60:557–63.

[70] Meinel TR, Lerch C, Fischer U, Beyeler M, Mujanovic A, Kurmann C, et al. Multivariable Prediction Model for Futile Recanalization Therapies in Patients With Acute Ischemic Stroke. Neurology 2022;99:e1009–18.

[71] Elschot EP, Backes WH, Postma AA, van Oostenbrugge RJ, Staals J, Rouhl RPW, et al. A Comprehensive View on MRI Techniques for Imaging Blood-Brain Barrier Integrity. Invest Radiol 2021;56:10–9.

[72] Quarles CC, Bell LC, Stokes AM. Imaging vascular and hemodynamic features of the brain using dynamic susceptibility contrast and dynamic contrast enhanced MRI. NeuroImage 2019;187:32–55.

[73] Tofts PS, Brix G, Buckley DL, Evelhoch JL, Henderson E, Knopp MV, et al. Estimating kinetic parameters from dynamic contrast-enhanced T(1)-weighted MRI of a diffusable tracer: standardized quantities and symbols. J Magn Reson Imaging 1999;10:223–32.

[74] Kety SS. The theory and applications of the exchange of inert gas at the lungs and tissues. Pharmacol Rev 1951;3:1–41.

[75] Yan Y, Sun X, Shen B. Contrast agents in dynamic contrast-enhanced magnetic resonance imaging. Oncotarget 2017;8:43491–505.

[76] Meier P, Zierler KL. On the theory of the indicator-dilution method for measurement of blood flow and volume. J Appl Physiol 1954;6:731–44.

[77] Axel L. Cerebral blood flow determination by rapid-sequence computed tomography: theoretical analysis. Radiology 1980;137:679–86.

[78] Rempp KA, Brix G, Wenz F, Becker CR, Gückel F, Lorenz WJ. Quantification of regional cerebral blood flow and volume with dynamic susceptibility contrast-enhanced MR imaging. Radiology 1994;193:637–41.

[79] Quarles CC, Gochberg DF, Gore JC, Yankeelov TE. A theoretical framework to model DSC-MRI data acquired in the presence of contrast agent extravasation. Phys Med Biol 2009;54:5749–66.

[80] Boxerman JL, Schmainda KM, Weisskoff RM. Relative cerebral blood volume maps corrected for contrast agent extravasation significantly correlate with glioma tumor grade, whereas uncorrected maps do not. AJNR Am J Neuroradiol 2006;27:859–67.

[81] Paulson ES, Schmainda KM. Comparison of Dynamic Susceptibility-weighted Contrast-enhanced MR Methods: Recommendations for Measuring Relative Cerebral Blood Volume in Brain Tumors. Radiology 2008;249:601–13.

[82] Marstrand JR, Rostrup E, Rosenbaum S, Garde E, Larsson HB. Cerebral hemodynamic changes measured by gradient-echo or spin-echo bolus tracking and its correlation to changes in ICA blood flow measured by phase-mapping MRI. J Magn Reson Imaging 2001;14:391–400.

[83] Blockley NP, Jiang L, Gardener AG, Ludman CN, Francis ST, Gowland PA. Field strength dependence of R1 and R2* relaxivities of human whole blood to ProHance, Vasovist, and deoxyhemoglobin. Magn Reson Med 2008;60:1313–20.

[84] Provenzale JM, Wang GR, Brenner T, Petrella JR, Sorensen AG. Comparison of Permeability in High-Grade and Low-Grade Brain Tumors Using Dynamic Susceptibility Contrast MR Imaging. American Journal of Roentgenology 2002;178:711–6.

[85] Thornhill RE, Chen S, Rammo W, Mikulis DJ, Kassner A. Contrast-Enhanced MR Imaging in Acute Ischemic Stroke: T2* Measures of Blood-Brain Barrier Permeability and Their Relationship to T1 Estimates and Hemorrhagic Transformation. AJNR Am J Neuroradiol 2010;31:1015–22.

[86] Skinner JT, Moots PL, Ayers GD, Quarles CC. On the Use of DSC-MRI for Measuring Vascular Permeability. AJNR Am J Neuroradiol 2016;37:80–7.

[87] Cuenod C-A, Balvay D. Imagerie de la perfusion tissulaire et de la perméabilité. Journal de Radiologie Diagnostique et Interventionnelle 2013;94:1184–202.

[88] Leigh R, Jen SS, Varma DD, Hillis AE, Barker PB. Arrival Time Correction for Dynamic Susceptibility Contrast MR Permeability Imaging in Stroke Patients. PLOS ONE 2012;7:5.

[89] Boujan XT, Neuberger XU, Pfaff XJ, Nagel XS, Herweh XC, Bendszus XM, et al. Value of Contrast-Enhanced MRA versus Time-of-Flight MRA in Acute Ischemic Stroke MRI. AJNR Am J Neuroradiol 2018;39:1710-1716

[90] Dhundass S, Savatovsky J, Duron L, Fahed R, Escalard S, Obadia M, et al. Improved detection and characterization of arterial occlusion in acute ischemic stroke using contrast enhanced MRA. J Neuroradiol 2020;47:278–83.

[91] Alves HC, Treurniet KM, Jansen IGH, Yoo AJ, Dutra BG, Zhang G, et al. Thrombus Migration Paradox in Patients With Acute Ischemic Stroke. Stroke 2019;50:3156–63.

[92] Lee S-J, Lee T-K, Kim B-T, Shin D-S. Clinical Implications of Preinterventional Thrombus Migration in Patients with Emergent Large Vessel Occlusion. World Neurosurg 2020;146:e1012-e1020

[93] Lim JC, Churilov L, Bivard A, Ma H, Dowling RJ, Campbell BCV, et al. Does Intravenous Thrombolysis Within 4.5 to 9 Hours Increase Clot Migration Leading to Endovascular Inaccessibility? Stroke 2021;52:1083–6.

[94] Campbell BC, Parsons MW. Imaging selection for acute stroke intervention. Int J Stroke 2018;13:554–67.

[95] Bivard A, Parsons M. Tissue is more important than time: insights into acute ischemic stroke from modern brain imaging. Curr Opin Neurol 2018;31:23–7.

[96] Tsivgoulis G, Katsanos AH, Schellinger PD, Köhrmann M, Caso V, Palaiodimou L, et al. Advanced Neuroimaging in Stroke Patient Selection for Mechanical Thrombectomy: A Systematic Review and Meta-Analysis. Stroke 2018;49:3067–70.

[97] Campbell BCV, Khatri P. Stroke. Lancet 2020;396:129–42.

[98] Campbell BCV, Mitchell PJ, Kleinig TJ, Dewey HM, Churilov L, Yassi N, et al. Endovascular Therapy for Ischemic Stroke with Perfusion-Imaging Selection. N Engl J Med 2015;372:1009–18.

[99] Austein F, Riedel C, Kerby T, Meyne J, Binder A, Lindner T, et al. Comparison of Perfusion CT Software to Predict the Final Infarct Volume After Thrombectomy. Stroke 2016;47:2311–7.

[100] Koopman MS, Berkhemer OA, Geuskens RREG, Emmer BJ, van Walderveen MAA, Jenniskens SFM, et al. Comparison of three commonly used CT perfusion software packages in patients with acute ischemic stroke. J NeuroIntervent Surg 2019;11:1249–56.

[101] Rava RA, Snyder KV, Mokin M, Waqas M, Zhang X, Podgorsak AR, et al. Assessment of computed tomography perfusion software in predicting spatial location and volume of infarct in acute ischemic stroke patients: a comparison of Sphere, Vitrea, and RAPID. J NeuroIntervent Surg 2021;13:130–5.

[102] Deutschmann H, Hinteregger N, Wießpeiner U, Kneihsl M, Fandler-Höfler S, Michenthaler M, et al. Automated MRI perfusion-diffusion mismatch estimation may be significantly different in individual patients when using different software packages. Eur Radiol 2021;31:658–65.

[103] Yoo AJ, Chaudhry ZA, Nogueira RG, Lev MH, Schaefer PW, Schwamm LH, et al. Infarct Volume Is a Pivotal Biomarker After Intra-Arterial Stroke Therapy. Stroke 2012;43:1323–30.

[104] Zaidi SF, Aghaebrahim A, Urra X, Jumaa MA, Jankowitz B, Hammer M, et al. Final Infarct Volume Is a Stronger Predictor of Outcome Than Recanalization in Patients With Proximal Middle Cerebral Artery Occlusion Treated With Endovascular Therapy. Stroke 2012;43:3238–44.

[105] Bala F, Ospel J, Mulpur B, Kim BJ, Yoo J, Menon BK, et al. Infarct Growth despite Successful Endovascular Reperfusion in Acute Ischemic Stroke: A Meta-analysis. AJNR Am J Neuroradiol 2021;42:1472–8.

[106] Liu L, Ding J, Leng X, Pu Y, Huang L-A, Xu A, et al. Guidelines for evaluation and management of cerebral collateral circulation in ischaemic stroke 2017. Stroke Vasc Neurol 2018;3:117–30.

[107] Hermier M, Nighoghossian N, Derex L, Adeleine P, Wiart M, Berthezène Y, et al. Hypointense Transcerebral Veins at T2∗-Weighted MRI: A Marker of Hemorrhagic Transformation Risk in Patients Treated with Intravenous Tissue Plasminogen Activator. J Cereb Blood Flow Metab 2003;23:1362–70.

[108] Morita N, Harada M, Uno M, Matsubara S, Matsuda T, Nagahiro S, et al. Ischemic Findings of T2*-Weighted 3-Tesla MRI in Acute Stroke Patients. Cerebrovasc Dis 2008;26:367–75.

[109] Kao H-W, Tsai FY, Hasso AN. Predicting stroke evolution: comparison of susceptibility-weighted MR imaging with MR perfusion. Eur Radiol 2012;22:1397–403.

[110] Zhang X, Zhang S, Chen Q, Ding W, Campbell BCV, Lou M. Ipsilateral Prominent Thalamostriate Vein on Susceptibility-Weighted Imaging Predicts Poor Outcome after Intravenous Thrombolysis in Acute Ischemic Stroke. AJNR Am J Neuroradiol 2017;38:875–81.

[111] Luo Y, Gong Z, Zhou Y, Chang B, Chai C, Liu T, et al. Increased susceptibility of asymmetrically prominent cortical veins correlates with misery perfusion in patients with occlusion of the middle cerebral artery. Eur Radiol 2017;27:2381–90.

[112] Wang Y, Shi T, Chen B, Lin G, Xu Y, Geng Y. Prominent Hypointense Vessel Sign on Susceptibility-Weighted Imaging Is Associated with Clinical Outcome in Acute Ischaemic Stroke. Eur Neurol 2018;79:231–9.

[113] Molina CA. Futile Recanalization in Mechanical Embolectomy Trials: A Call to Improve Selection of Patients for Revascularization. Stroke 2010;41:842–3.

[114] Gilberti N, Gamba M, Premi E, Costa A, Vergani V, Delrio I, et al. Leukoaraiosis is a predictor of futile recanalization in acute ischemic stroke. J Neurol 2017;264:448–52.

[115] Malhotra A, Wu X, Payabvash S, Matouk CC, Forman HP, Gandhi D, et al. Comparative Effectiveness of Endovascular Thrombectomy in Elderly Stroke Patients. Stroke 2019;50:963–9.

[116] Choi K-H, Kim J-H, Kang K-W, Kim J-T, Choi S-M, Lee S-H, et al. Impact of Microbleeds on Outcome Following Recanalization in Patients With Acute Ischemic Stroke. Stroke 2019;50:127–34.

[117] Jahan R, Saver JL, Schwamm LH, Fonarow GC, Liang L, Matsouaka RA, et al. Association Between Time to Treatment With Endovascular Reperfusion Therapy and Outcomes in Patients With Acute Ischemic Stroke Treated in Clinical Practice. JAMA 2019;322:252.

[118] Pedraza MI, de Lera M, Bos D, Calleja AI, Cortijo E, Gómez-Vicente B, et al. Brain Atrophy and the Risk of Futile Endovascular Reperfusion in Acute Ischemic Stroke. Stroke 2020;51:1514–21.

[119] Lee KY, Latour LL, Luby M, Hsia AW, Merino JG. Distal hyperintense vessels on FLAIR: An MRI marker for collateral circulation in acute stroke? Neurology 2009;72:1134-1139

[120] Sanossian N, Saver JL, Alger JR, Kim D, Duckwiler GR, Jahan R, et al. Angiography Reveals That Fluid-Attenuated Inversion Recovery Vascular Hyperintensities Are Due to Slow Flow, Not Thrombus. AJNR Am J Neuroradiol 2009;30:564–8.

[121] on behalf of the THRACE Investigators, Legrand L, Turc G, Edjlali M, Beaumont M, Gautheron V, et al. Benefit from revascularization after thrombectomy according to FLAIR vascular hyperintensities–DWI mismatch. Eur Radiol 2019;29:5567–76.

[122] Lakhan SE, Kirchgessner A, Tepper D, Leonard A. Matrix metalloproteinases and blood-brain barrier disruption in acute ischemic stroke. Front Neurol 2013;3:4-32

[123] Yang C, Hawkins KE, Doré S, Candelario-Jalil E. Neuroinflammatory mechanisms of blood-brain barrier damage in ischemic stroke. Am J Physiol Cell Physiol. 2019;316:C135-C153.

[124] Batra A, Latour LL, Ruetzler CA, Hallenbeck JM, Spatz M, Warach S, et al. Increased Plasma and Tissue MMP Levels are Associated with BCSFB and BBB Disruption Evident on Post-Contrast FLAIR after Experimental Stroke. J Cereb Blood Flow Metab 2010;30:1188–99.

[125] Barr TL, Latour LL, Lee K-Y, Schaewe TJ, Luby M, Chang GS, et al. Blood–Brain Barrier Disruption in Humans Is Independently Associated With Increased Matrix Metalloproteinase-9. Stroke 2010;41:e123-8

[126] Yang CW, Carr JC, Futterer SF, Morasch MD, Yang BP, Shors SM, et al. Contrast-Enhanced MR Angiography of the Carotid and Vertebrobasilar Circulations. AJNR Am J Neuroradiol 2005;26:2095-2101

[127] Korn A, Bender B, Brodoefel H, Hauser T-K, Danz S, Ernemann U, et al. Grading of carotid artery stenosis in the presence of extensive calcifications: dual-energy CT angiography in comparison with contrast-enhanced MR angiography. Clin Neuroradiol 2015;25:33–40.

[128] Grossberg JA, Haussen DC, Cardoso FB, Rebello LC, Bouslama M, Anderson AM, et al. Cervical Carotid Pseudo-Occlusions and False Dissections: Intracranial Occlusions Masquerading as Extracranial Occlusions. Stroke 2017;48:774–7.

[129] Chen Z, Zhang M, Shi F, Gong X, Liebeskind D, Ding X, et al. Pseudo-Occlusion of the Internal Carotid Artery Predicts Poor Outcome After Reperfusion Therapy. Stroke 2018;49:1204–9.

[130] Sohn C-H, Sevick RJ, Frayne R. Contrast-enhanced MR angiography of the intracranial circulation. Magn Reson Imaging Clin N Am 2003;11:599–614.

[131] Ishimaru H, Ochi M, Morikawa M, Takahata H, Matsuoka Y, Koshiishi T, et al. Accuracy of pre- and postcontrast 3D time-of-flight MR angiography in patients with acute ischemic stroke: correlation with catheter angiography. AJNR Am J Neuroradiol 2007;28:923–6.

[132] Sobesky J. Refining the Mismatch Concept in Acute Stroke: Lessons Learned from PET and MRI. J Cereb Blood Flow Metab 2012;32:1416–25.

[133] Albers GW, Thijs VN, Wechsler L, Kemp S, Schlaug G, Skalabrin E, et al. Magnetic resonance imaging profiles predict clinical response to early reperfusion: the diffusion and perfusion imaging evaluation for understanding stroke evolution (DEFUSE) study. Ann Neurol 2006;60:508–17.

[134] Davis SM, Donnan GA, Parsons MW, Levi C, Butcher KS, Peeters A, et al. Effects of alteplase beyond 3 h after stroke in the Echoplanar Imaging Thrombolytic Evaluation Trial (EPITHET): a placebo-controlled randomised trial. Lancet Neurol 2008;7:299–309.

[135] Shih LC, Saver JL, Alger JR, Starkman S, Leary MC, Vinuela F, et al. Perfusion-weighted magnetic resonance imaging thresholds identifying core, irreversibly infarcted tissue. Stroke 2003;34:1425–30.

[136] Olivot J-M, Mlynash M, Thijs VN, Kemp S, Lansberg MG, Wechsler L, et al. Optimal Tmax Threshold for Predicting Penumbral Tissue in Acute Stroke. Stroke 2009;40:469–75.

[137] Zaro-Weber O, Moeller-Hartmann W, Heiss W-D, Sobesky J. MRI perfusion maps in acute stroke validated with 15O-water positron emission tomography. Stroke 2010;41:443–9.

[138] Zaro-Weber O, Fleischer H, Reiblich L, Schuster A, Moeller-Hartmann W, Heiss W. Penumbra detection in acute stroke with perfusion magnetic resonance imaging: Validation with 15 O-positron emission tomography. Ann Neurol 2019;85:875–86.

[139] Eltzschig HK, Eckle T. Ischemia and reperfusion—from mechanism to translation. Nat Med 2011;17:1391–401.

[140] Schilling A, Blankenburg F, Bernarding J, Heidenreich J, Wolf K. Intracerebral pH affects the T2 relaxation time of brain tissue. Neuroradiology 2002;44:968–72.

[141] Horie N, Morikawa M, Nozaki A, Hayashi K, Suyama K, Nagata I. “Brush Sign” on Susceptibility-Weighted MR Imaging Indicates the Severity of Moyamoya Disease. AJNR Am J Neuroradiol 2011;32:1697–702.

[142] Darwish EAF, Abdelhameed-El-Nouby M, Geneidy E. Mapping the ischemic penumbra and predicting stroke progression in acute ischemic stroke: the overlooked role of susceptibility weighted imaging. Insights Imaging 2020;11:6.

[143] Huang X, Liu W, Zhu W, Ni G, Sun W, Ma M, et al. Distal Hyperintense Vessels on Flair: A Prognostic Indicator of Acute Ischemic Stroke. Eur Neurol 2012;68:214–20.

[144] Legrand L, Le Berre A, Seners P, Benzakoun J, Ben Hassen W, Lion S, et al. FLAIR Vascular Hyperintensities as a Surrogate of Collaterals in Acute Stroke: DWI Matters. AJNR Am J Neuroradiol 2023;44:26–32.

[145] Nie X, Pu Y, Zhang Z, Liu X, Duan W, Liu L. Futile Recanalization after Endovascular Therapy in Acute Ischemic Stroke. BioMed Res Int 2018;2018:1–5.

[146] Latour LL, Kang D-W, Ezzeddine MA, Chalela JA, Warach S. Early blood-brain barrier disruption in human focal brain ischemia. Ann Neurol 2004;56:468–77.

[147] Abdullahi W, Tripathi D, Ronaldson PT. Blood-brain barrier dysfunction in ischemic stroke: targeting tight junctions and transporters for vascular protection. Am J Physiol Cell Physiol 2018;315:C343–56.

Annexe n°2 : Publication scientifiques :

1) **Bani-Sadr A**, Eker OF, Cho TH, Ameli R, Berhouma M, Cappucci M, Derex L, Mechtouff L, Meyronet D, Nighoghossian N, Berthezène Y, Hermier M. Early detection of underlying cavernomas in patients with spontaneous acute intracerebral hematomas. AJNR Am J Neuroradiol, 2023 (In press)

2) **Bani-Sadr A**, Kuchcinski G. CT-based radiomics analysis of peri intracerebral hemorrhage edema: A new tool to predict functional outcome. Diag Interv Imaging, 2023 (In press)

3) Dietz M, Jacquet-Francillon N, **Bani-Sadr A**, Collette B, Mure PY, Demède D, Pina-Jomir G, Moreau-Triby C, Grégoire B, Mouriquand P, Janier M Flaus A. Ultrafast cadmium-zinc-telluride-based renal single-photon emission computed tomography: clinical validation. Pediatr Radiol, 2023 (In press)

4) **Bani-Sadr A**, Mechtouff L, De Bourguignon L, Mauffrey A, Boutelier T, Cho TH, Cappucci M, Ameli R, Hermier M, Derex L, Nighoghossian N, Berthezene Y. Brain-Blood Barrier Permeability and Kinetic of Inflammatory Markers in Acute Ischemic Stroke Patients Treated by Thrombectomy. Neurology, 2023 (In press)

5) **Bani-Sadr A**, Escande R, Mechtouff L, Pavie D, Hermier M, Derex L, Cho TH, Eker OF, Nighoghossian N, Berthezène N. Vascular hyperintensities on baseline FLAIR images are associated with functional outcome in stroke patients with successful recanalization after mechanical thrombectomy. Diag Interv Imaging, 2023;104:337-342

6) **Bani-Sadr A**, Pavie D, Mechtouff L, Cappucci M, Hermier M, Ameli R, Derex L, De Bourguignon C, Cho TH, Eker O, Nighoghossian N, Berthezene Y. Brush sign and collateral supply as potential markers of large infarct growth after successful thrombectomy. Eur Radiol, 2023;33:4502-4509

7) Rossi J, Hermier M, Eker OF, Berthezène Y, **Bani-Sadr A**. Imaging of etiologies of spontaneous acute intracerebral hemorrhage: a pictorial review. Clin Imaging, 2023;95:10-23.

8) Rascle L, **Bani-Sadr A**, Amaz C, Mewton N, Buisson M, Hermier M, Ong E, Fontaine J, Derex L, Berthezène Y, Eker OF, Cho TH, Nighoghossian N, Mechtouff L. Does the Brush-Sign Reflect Collateral Status and DWI-ASPECTS in Large Vessel Occlusion? Front Neurol, 2022;13:828256

9) Zumbihl L, Berthezene Y, Hermier M, Barrey C, **Bani-Sadr A**. Isolated atlas-duplication as a manifestation of persistent proatlas: a case report. Surg Radiol Anat, 2022;44:595:598

10) Guery D, Cousyn L, Navarro V, Picard G, Rogemond V, **Bani-Sadr A**, Shor N, Joubert B, Muñiz-Castrillo S, Honnorat J, Rheims S. Long-term evolution and prognostic factors of epilepsy in limbic encephalitis with LGI1 antibodies. J Neurol, 2022;269:5061-5069.

11) Mechtouff L, Sigovan M, Douek P, Costes N, Le Bars D, Mansuy A, Haesebaert J, **Bani-Sadr A**, Tordo J, Feugier P, Millon A, Luong S, Si-Mohamed S, Collet-Benzaquen D, Canet-

Soulas E, Bochaton T, Crola Da Silva C, Paccalet A, Magne D, Berthezene Y, Nighoghossian N. Simultaneous assessment of microcalcifications and morphological criteria of vulnerability in carotid artery plaque using hybrid 18F-NaF PET/MRI. J Nucl Cardiol, 2022;29:1064-1074

12) **Bani-Sadr A**, Ruitton-Allinieu MC, Brisset JC, Ducray F, Joubert B, Picard G, Cotton F. Contribution of diffusion-weighted imaging to distinguish herpetic encephalitis from auto-immune encephalitis at an early stage. J Neuroradiol, 2022;50:288-292

13) **Bani-Sadr A**, Cho TH, Cappucci M, Hermier M, Ameli R, Filip A, Riva R, Derex L, De Bourguignon C, Mechtouff L, Eker OF, Nighoghossian N, Berthezene Y. Assessment of three MR perfusion software packages in predicting final infarct volume after mechanical thrombectomy. J Neurointerv Surg, 2022;15:393-398

15) Mechtouff L, Debs N, Frindel C, **Bani-Sadr A**, Bochaton T, Paccalet A, Crola Da Silva C, Buisson M, Amaz C, Berthezene Y, Eker OF, Bouin M, de Bourguignon C, Mewton N, Ovize M, Bidaux G, Nighoghossian N, Cho TH. Association of Blood Biomarkers of Inflammation With Penumbra Consumption After Mechanical Thrombectomy in Patients With Acute Ischemic Stroke. Neurology, 2022;99:e2063-e2071

15) **Bani-Sadr A**, Aguilera M, Cappucci M, Hermier M, Ameli R, Filip A, Riva R, Tuttle C, Cho TH, Mechtouff L, Nighoghossian N, Eker O, Berthezene Y. Comparison of magnetic resonance angiography techniques to brain digital subtraction arteriography in the setting of mechanical thrombectomy: A non-inferiority study. Rev Neurol, 2022;178:539-545

16) Alhazmi H, **Bani-Sadr A**, Bochaton T, Paccalet A, Da Silva CC, Buisson M, Amaz C, Ameli R, Berthezene Y, Eker OF, Ovize M, Cho TH, Nighoghossian N, Mechtouff L. Large vessel cardioembolic stroke and embolic stroke of undetermined source share a common profile of matrix metalloproteinase-9 level and susceptibility vessel sign length. Eur J Neurol, 2021; 28:1977-1983

17) Fahmi R, Platsch G, **Bani-Sadr A**, Gouttard S, Thobois S, Zuehlsdorff S, Scheiber C. Single-site 123I-FP-CIT reference values from individuals with non-degenerative parkinsonism-comparison with values from healthy volunteers. Eur J Hybrid Imaging, 2020;4:5

18) **Bani-Sadr A**, Ameli R, Di Franco F, Filip A, Hermier M, Berthezene Y. Imagerie des pathologies non traumatiques du cordon médullaire et des espaces périmédullaires. Journal d'Imagerie Diagnostique et Interventionnelle, 2020;3:319-336

19) **Bani-Sadr A**, Eker OF, Berner LP, Ameli R, Hermier M, Barritault M, Meyronet D, Guyotat J, Jouanneau E, Honnorat J, Ducray F, Berthezene Y. Conventional MRI radiomics in patients with suspected early- or pseudo-progression. Neurooncol Adv, 2019;1:vdz019

20) **Bani Sadr A**, Testart N, Tylski P, Scheiber C. Reduced Scan Time in 123I-FP-CIT SPECT Imaging Using a Large-Field Cadmium- Zinc-Telluride Camera. Clin Nucl Med, 2019;44:568-569

21) **Bani- Sadr A**, Berner LP, Barritault M, Chamard L, Bidet CM, Eker OF, Hermier M, Guyotat J, Jouanneau E, Meyronet D, Gouttard S, D'Hombres A, Iziquierdo C, Honnorat J, Berthezène

Y, Ducray F. Combined analysis of MGMT methylation and dynamic-susceptibility-contrast MRI for the distinction between early and pseudo-progression in glioblastoma patients. Rev Neurol, 2019;175:534-543

22) **Bani Sadr A**, Gregoire B, Tordo J, Guyotat J, Boibieux A, Janier M. Potential utility of bone scan in cranial bone flap osteomyelitis. Ann Nucl Med, 2019;33:424-433

23) Kochebina O, Halty A, Taleb J, Kryza D, Janier M, **Bani-Sadr A**, Baudier T, Rit S, Sarrut D. In vivo gadolinium nanoparticle quantification with SPECT/CT. EJNMMI Phys, 2019;6:9

24) Gregoire B, Pina-Jomir G, **Bani-Sadr A**, Moreau-Triby C, Janier M, Scheiber C. Four-Minute Bone SPECT Using Large-Field Cadmium-Zinc-Telluride Camera. Clin Nucl Med, 2018;43:389-395